UNIVERSITÀ DEGLI STUDI DI SALERNO

UNIVERSITÀ DEGLI STUDI DI SALERNO
Dipartimento di Farmacia

PhD Program
in **Drug Discovery and Development**
XXXVIII Cycle – Academic year 2024/2025

PhD Thesis in

Classical and innovative applications of NMR spectroscopy in the metabolomic profiling of biological samples

Candidate

Enza Napolitano

Tutor

Prof. *Anna Maria D'Ursi*

Co-Tutor

Dr. *Marco Tessari*

PhD Program Coordinator: Prof. *Alessandra Tosco*

Scientific publications

Napolitano E, Marino C, Grimaldi M, Buonocore M, D'Ursi AM. Effects of Nicotine on SH-SY5Y Cells: An NMR-Based Metabolomic Study. *Metabolites*. 2025;15(11):752. doi: 10.3390/metabo15110752.

Napolitano E, Marino C, Grimaldi M, Buonocore M, D'Ursi AM. Analyzing nicotine action against amyloid toxicity by NMR-pharmacometabolomics: an exploratory study. *bioRxiv* 2025.09.03.673931; doi: https://doi.org/10.1101/2025.09.03.673931.

Gervasoni J, Marino C, Imarisio A, Santucci L, Napolitano E, Nuzzo T, Yahyavi I, Avenali M, Cicchinelli M, Buongarzone G, Galandra C, Picascia M, Grimaldi M, Pacchetti C, Errico F, D'Ursi AM, Urbani A, Valente EM, Usiello A. Independent serum metabolomics approaches identify disrupted glutamic acid and serine metabolism in Parkinson's disease patients. *NPJ Parkinsons Dis*. 2025;11(1):274. doi: 10.1038/s41531-025-01126-5.

Marino C, Imarisio A, Gasparri C, Napolitano E, Di Maio A, Avenali M, Buongarzone G, Galandra C, Picascia M, Grimaldi M, Errico F, Rondanelli M, D'Ursi AM, Valente EM, Usiello A. 1H-NMR-based metabolomics identifies disrupted betaine metabolism as distinct serum signature of pre-frailty. *npj aging*. 2025; 11(1), 26. https://doi.org/10.1038/s41514-025-00218-z

D'Elia M, Marino C, Celano R, Napolitano E, Colarusso C, Sorrentino R, D'Ursi AM, Rastrelli L. Impact of a Formulation Containing Chaga Extract, Coenzyme Q10, and Alpha-Lipoic Acid on Mitochondrial Dysfunction and Oxidative Stress: NMR Metabolomic Insights into Cellular Energy. *Antioxidants.* 2025; 14(6):753. https://doi.org/10.3390/antiox14060753.

Castaldo G, Marino C, D'Elia M, Grimaldi M, Napolitano E, D'Ursi AM, Rastrelli L. The Effectiveness of the Low-Glycemic and Insulinemic (LOGI) Regimen in Maintaining the Benefits of the VLCKD in Fibromyalgia Patients. *Nutrients*. 2024;16(23):4161. doi: 10.3390/nu16234161.

D'Elia M, Marino C, Celano R, Napolitano E, D'Ursi AM, Russo M, Rastrelli L. Impact of a Withania somnifera and Bacopa monnieri Formulation on SH-SY5Y Human Neuroblastoma Cells Metabolism Through NMR Metabolomic. *Nutrients*. 2024;16(23):4096. doi: 10.3390/nu16234096.

Castaldo G, Marino C, Atteno M, D'Elia M, Pagano I, Grimaldi M, Conte A, Molettieri P, Santoro A, Napolitano E, Puca I, Raimondo M, Parisella C, D'Ursi AM, Rastrelli L. Investigating the Effectiveness of a Carb-Free Oloproteic Diet in Fibromyalgia Treatment. *Nutrients.* 2024;16(11):1620. doi:10.3390/nu16111620.

Buonocore M, Grimaldi M, Santoro A, Covelli V, Marino C, Napolitano E, Novi S, Tecce MF, Ciaglia E, Montella F, Lopardo V, Perugini V, Santin M, D'Ursi AM. Exploiting the Features of Short Peptides to Recognize Specific Cell Surface Markers. *Int J Mol Sci*. 2023;24(21):15610. doi: 10.3390/ijms242115610.

Santoro A, Buonocore M, Grimaldi M, Napolitano E, D'Ursi AM. Monitoring the Conformational Changes of the Aβ(25-35) Peptide in SDS Micelles: A Matter of Time. *Int J Mol Sci*. 2023 Jan 4;24(2):971. doi: 10.3390/ijms24020971.

Abstract

Metabolomics is an *omic* science with rapidly expanding applications, including drug discovery. Within this field, pharmacometabolomics has developed as a branch dedicated to studying drug-induced metabolic effects. It plays a crucial role in hypothesis generation, as demonstrated by its ability to uncover previously unrecognized pathways involved in drug action. A major strength of pharmacometabolomics lies in its use to explore cellular mechanisms of action (MoA), offering an unbiased alternative to traditional hypothesis-driven approaches that typically focus on specific receptors or isolated pathways. In contrast, untargeted metabolomics provides a comprehensive view of treatment-induced metabolic changes and can reveal unexpected or off-target effects.

As part of my PhD research, I investigated the *in vitro* biological MoA of nicotine and Nerve Growth Factor (NGF) using the potential of untargeted metabolomics. Employing SH-SY5Y neuroblastoma cells, I analyzed both the exometabolome (culture medium) and endometabolome (cellular extracts) following treatment with these molecules, which are of potential interest for Alzheimer's disease (AD) therapy.

As a preliminary step, we confirmed that exposure to recombinant amyloid-β peptide Aβ(1–42) reproduced in our model the key metabolic dysregulations characteristic of AD. We then evaluated whether nicotine and NGF could counteract these alterations. To capture the dynamic exchange of metabolites between compartments – essential for interpreting cellular function – we built for the first time a statistical model that combines the quantification matrices of intra- and extracellular metabolites.

Our findings demonstrate that nicotine exerts neuroprotective effects by restoring metabolic imbalances associated with AD pathology. In particular, nicotine reversed the majority of Aβ(1–42)-induced alterations, including disruptions in neurotransmission-related pathways, energy metabolism, and membrane phospholipid turnover. NGF, by contrast, exhibited neuroprotective activity primarily by reducing glutamate and glycine concentrations and functioning as an early modulator of key

biochemical pathways, thereby preventing redox disequilibrium and alterations in energy metabolism.

During my international research period, I further specialized in NMR spectroscopy with focusing on non-hydrogenative parahydrogen-induced hyperpolarization (nhPHIP). At the Magnetic Resonance Research Center of Radboud University, under the supervision of Dr. Marco Tessari, I conducted the first targeted and chiral metabolomic analysis of amino acid content in animal tissues using this approach. This technique enabled the discrimination between D- and L-amino acid enantiomers and revealed amino acid imbalances associated with altered D-aspartate levels. nhPHIP proved particularly valuable for this study, as several amino acids are directly or indirectly involved in neurotransmission. Taken together, the application of nhPHIP in this context highlights the potential of NMR hyperpolarization techniques for targeted metabolomics investigations of amino acid dysregulation.

Table of contents

Scientific publications ..... **I**

Abstract ..... **III**

Chapter I **1**

The evolution of metabolomics **1**

1.1 Introduction **1**

1.1.1 Main techniques in metabolomics ***2***

1.1.2 Different analytical approaches in NMR metabolomics ***3***

1.1.3 Workflow for NMR metabolomics using a profiling approach ***5***

1.1.4 Cellular metabolomics ***6***

1.2 From metabolomics to fluxomics: a dynamic perspective on metabolism **8**

1.3 A modern application in drug sciences: pharmacometabolomics **9**

1.3.1 Metabolomics to study biomolecules molecular mechanism ***11***

1.4 The future direction: hyperpolarization **12**

1.4.1 Parahydrogen ***13***

1.4.2 Parahydrogen Induced Polarization (PHIP) ***15***

1.4.3 SABRE ***15***

1.4.4 nhPHIP ***16***

1.4.5 Hyperpolarization NMR in metabolomics ***17***

1.5 General aims and objectives **18**

Bibliography **20**

Chapter II **25**

Metabolomic approach to investigate nicotine effects in a neurodegenerative cell model **25**

2.1 Nicotine: friend or foe? **25**

2.2 Nicotine in Alzheimer's disease **26**

2.3 The aims of the study **27**

2.4 Results **29**

2.4.1 Impact of nicotine on SH-SY5Y cell viability ***29***

2.4.2 Nicotine impacts on lipid metabolism, mitochondrial function, and amino acid concentrations ***30***

2.4.3 Nicotine protects neuroblastoma cells from Aβ(1–42) toxicity ***35***

2.4.4 Aβ(1–42) disrupts energetic pathways, amino acid metabolism, and membrane stability ***36***

2.4.5 Nicotine reverts AD dysmetabolism, acting on the whole metabolome...41
2.5 Discussion ...45
2.5.1 Nicotine metabolomic impact on SH-SY5Y cells ...45
2.5.2 A proposed mechanism for the nicotine protective role in AD...49
2.6 Conclusions...52
2.7 Materials and Methods...54
2.7.1 Chemicals ...54
2.7.2 Cell Culture ...55
2.7.3 Cell Viability Assay...55
2.7.4 ^{1}H NMR Metabolomics ...56
2.7.4.1 Exposure of SH-SY5Y cells to nicotine and Aβ(1–42) ...56
2.7.4.2 Sample collection and intracellular metabolites extraction ...56
2.7.4.3 NMR Sample Preparation...56
2.7.4.4 NMR Data Acquisition and Processing ...57
2.7.4.5 Statistical analysis...58
Bibliography ...60
Appendix...67
Chapter III ...73
Metabolomic approach to evaluate the protective effect of NGF in AD cellular model...73
3.1 The role of NGF in Alzheimer's disease ...73
3.2 Aim of the study ...75
3.3 Results ...77
3.3.1 NGF protects SH-SY5Y cells from Aβ(1–42) toxicity ...77
3.3.2 NGF modulation of amyloid altered pathways ...78
3.3.3 NGF effects...82
3.4 Discussion ...87
3.4.1 The multifaced action of NGF in precence of Aβ(1–42) ...87
3.4.2 NGF acts as an early metabolic modulator...90
3.5 Conclusions...91
3.6 Materials and methods ...92
3.6.1 Chemicals ...92
3.6.2 Production of CHF6467...92
3.6.3 Cell Culture ...95
3.6.4 Cell Viability Assay...95

3.6.5 ^{1}H NMR Metabolomics *96*
3.6.5.1 Exposure of SH-SY5Y cells to NGF and Aβ(1–42) 96
3.6.5.2 Sample collection and intracellular metabolites extraction 96
3.6.5.3 NMR Sample Preparation 97
3.6.5.4 NMR Data Acquisition and Processing 97
3.6.5.5 Statistical analysis 97
Bibliography **100**
Appendix **103**
Chapter IV **105**
Exploring D-aspartic acid role in the brain by hyperpolarization-NMR **105**
4.1 D-amino acid in mammalian brain **105**
4.2 The time-dependency of D-Asp **106**
4.3 Pharmacological and functional properties of D-Asp **107**
4.4 Aim of the study **109**
4.5 Results **112**
4.5.1 Targeted metabolomic profiling of amino acids in the mouse brain via nhPHIP *112*
4.5.2 Ddo Knock-in *113*
4.5.3 Ddo Knock-out *115*
4.5.3.1 Biochemical pathways altered in Ddo knock-out mice 121
4.5.3.2 Comparative analyses of Ddo knock-out amino acidic dysregulation in the five subregions 122
4.6 Discussion **124**
4.7 Conclusions **128**
4.8 Materials and methods **129**
4.8.1 Mouse models and sample collection *129*
4.8.2 Chemicals *129*
4.8.3 nhPHIP NMR experiments *130*
4.8.3.1 Sample preparation for nhPHIP 130
4.8.3.2 Bubble setup for nhPHIP 131
4.8.3.3 nhPHIP NMR acquisition and processing 131
4.8.3.4 2D ZQ nhPHIP NMR spectra analysis 132
4.8.4 Statistical analysis *132*
Bibliography **134**
General conclusions **139**

Chapter I

The evolution of metabolomics

1.1 Introduction

Metabolomics is an omics science that provides a comprehensive and systematic analysis of multiple metabolite concentrations in a biological sample.

The suffix "-omics", which means "*all constituents considered collectively*", clearly reflects the holistic nature of metabolomics, which aims to study complex biological systems by analyzing their metabolic components at the cellular level.

The term *metabolites* refers to low-molecular-weight compounds (<1500 Da) and includes amino acids, small peptides, lipids, carbohydrates, nucleotides, hormones, organic acids, vitamins, and signalling molecules that can be found in cells, tissues, organs, or biofluids under specific conditions. Their profile reflects the functional state of the biological system, and as a consequence, metabolomics is considered the only approach capable of providing a comprehensive snapshot of the physiological or pathological state of an organism, tissue, or cell system. [1]

Metabolites not only reveal details about metabolic function but also offer predictive insights into health status. They can support early diagnosis or help monitor disease progression in a personalized and targeted way. For example, the detection of specific biomarkers in biofluids related to diabetes, kidney disease, or cardiovascular conditions can reveal molecular signs of dysfunction years before clinical symptoms appear. [2]

Metabolomics offers several benefits compared with other "-omic" strategies, with the most advantageous being its close biological proximity to the phenotype of the system and hence the rapid observation of system perturbations in the metabolome.[3, 4]

Metabolomics has been widely used in recent years across several applications, including assessing responses to diseases and environmental stress, drug discovery, toxicology, nutrition, studying the global effects of genetic manipulation, pathologies, drugs, and natural products. Its broad use is due to the strong connection between the

metabolome and cellular physiology. Compared to other omic sciences, metabolomics is downstream: the transcriptome and proteome represent intermediate stages of gene expression, while the metabolome reflects the final output and helps explain disease phenotypes. [5]

Unlike genomics and proteomics, where thousands of targets are routinely identified, metabolomics has faced quantitative limitations. Until twenty years ago, it lacked electronic databases comparable to *GenBank* or *UniProt*, which are essential for compound identification. The release of the *Human Metabolome Database* (HMDB) in 2007, along with *Kyoto Encyclopedia of Genes and Genomes* (KEGG), the *Small Molecule Pathway Database* (SMPDB), and PubChem, significantly advanced the field. [6-8] These resources support metabolite identification using techniques such as Nuclear Magnetic Resonance (NMR), Gas Chromatography-Mass Spectrometry (GC-MS), and Liquid Chromatography-Mass Spectrometry (LC-MS).

1.1.1 Main techniques in metabolomics

Nuclear Magnetic Resonance (NMR) and Mass Spectrometry (MS) are the most used techniques for studying the metabolomic profile. Each analytical platform has its own advantages and disadvantages. It should be emphasized that a single analytical platform is insufficient to fully identify and quantify all metabolites present in a typical biological sample. As a result, the best metabolomic studies often employ multiple technology platforms. [9]

Table 1.1 summarizes the main advantages and limitations of the two most employed techniques in metabolomics. Shortly, MS offers superior sensitivity, while NMR is inherently reproducible, relatively rapid, and non-destructive. Importantly, NMR enables simultaneous, comprehensive detection of a wide range of metabolites in a single acquisition, without requiring sample manipulation. [10, 11]

Although LC-MS appears to dominate the field of metabolomics, accounting for over 70% of published studies, the number of publications based on NMR methodologies is steadily increasing. According to PubMed, more than 926 papers on NMR-based metabolomics were published in 2021. This trend highlights the growing relevance of NMR within the metabolomics community, supported by expanding applications and significant recent technological advancements. [12]

Table 1.1 *Schematization of the advantages and limitations of NMR spectroscopy compared to MS in metabolomics applications. Adapted from* [11]

	NMR	***MS***
Reproducibility	High reproducibility	Low reproducibility
Sensitivity	Low (≥1 µmol/L)	Very sensitive (>10 nmol/L)
Selectivity	Non-selective	Selective
Sample measurement	Relatively fast in 1D ^{1}H-NMR spectroscopy	Different ionization methods required to maximize the number of metabolites detected
Sample Preparation	Minimal preparation: transfer of the sample to an NMR tube with deuterated solvent	More complex: requires chromatographic separation and/or sample derivatization
Sample retrieval	Can be recovered (non-destructive technique)	Cannot be recovered (destructive technique)
Quantitative analysis	The intensity of the signals is proportional to the concentration of the sample	The intensity of the signals is often not proportional to the concentration of the sample

1.1.2 Different analytical approaches in NMR metabolomics

The metabolomic approach relies on the comprehensive identification of numerous metabolites in a biological sample. Depending on the specific research question, metabolomic analysis can be conducted using two main methods: targeted and untargeted analyses.

- The targeted method focuses on monitoring a pre-selected panel of metabolites, chosen based on known metabolic pathways or previously identified biomarkers linked to the disease or condition being studied. [13] These metabolites must be reliably identified and quantified within the samples. As a hypothesis-driven approach, targeted analysis often follows an untargeted exploration. Sample preparation in targeted studies can adopt optimized techniques to preserve the metabolites of interest while removing other biological components and analytical artifacts. [14]

- Conversely, untargeted metabolomics offers a comprehensive overview of a sample by systematically studying all measurable analytes, including unknown chemicals. [13]

  This goal can be achieved through two main strategies: fingerprinting or profiling.

  a. Fingerprinting involves analyzing spectral data without prior signal assignment or metabolite quantification. The fingerprinting approach primarily aims for sample classification; it discriminates samples based on different biological conditions (e.g., presence or absence of disease, before or after treatment), effectively characterizing a specific health state with a unique metabolic pattern. [15] It has the advantage to provide a rapid, overall assessment of an NMR spectrum, serving as a "fingerprint" of all detectable metabolites – assigned or unassigned – in the biological sample. [16] This is typically done by transforming NMR spectra into data matrices, for example through bucketing, a method that reduces the number of variables and compensates for minor spectral misalignments.
  b. On the other hand, metabolic profiling focuses on quantifying the concentrations of all measurable metabolites in a biological sample. Although the number of metabolites that can be identified and analyzed is constrained by the library used for assignment, profiling provides more valuable biochemical information by allowing the identification of metabolites and the associated modulated pathways linked to specific physiological or pathological conditions. [17]

There is confusion in the scientific literature regarding these terms: "fingerprinting" is often used interchangeably with untargeted metabolomics, while "metabolic profiling" is used as a synonym for targeted metabolomics. However, an untargeted approach can involve either fingerprinting or profiling methods. Conversely, targeted methods, since they focus on specific metabolites, always employ a profiling approach.

Chapters 2 and 3 of the present thesis adopt an untargeted approach through profiling, whereas Chapter 4 focuses on a targeted metabolomic analysis of a specific group of metabolites – amino acids.

1.1.3 Workflow for NMR metabolomics using a profiling approach

The metabolomic research workflow follows these steps:

- Sample collection and preparation
- Data acquisition
- Metabolite identification
- Statistical data analysis
- Biological interpretation of results

Sample collection and preparation are among the most critical phases of metabolomic analysis. For this reason, it is essential to implement standardized operating procedures (SOPs) to minimize sample alteration and ensure reproducibility.[18, 19] While sample preparation in the case of biofluids typically involves only dilution in a deuterated buffer, metabolomic analysis of cells and tissues requires a preliminary extraction step to enable solution-state NMR spectroscopy.[20, 21]

Regarding NMR experiments, a 600 MHz spectrometer is considered the standard for acquiring metabolomic NMR spectra. A 600 MHz spectrometer provides a good compromise between resolution, sensitivity, and cost.[11] 1D NOESY and CPMG (*Carr-Purcell-Meiboom-Gill*) NMR spectra are considered ideal experiments for NMR-based metabolomic analysis, since ^{1}H atoms are found in almost every organic compound and because 1D ^{1}H NMR is a highly automatable, very reliable, and high-speed technique. [11, 22]

Several automated or semi-automated tools have been developed for handling one-dimensional ^{1}H NMR spectra, typically operating through spectral matching against large libraries of reference NMR profiles. Several commercial programs, including Chenomx NMRSuite, [23] FoodScreener, [24, 25] and B.I. QUANT [26] supports both semi-automated NMR data processing and automated or semi-automated small-molecule identification and quantification. On the other hand, Bayesil [27] and MagMet [28] – freely accessible through web servers – can perform fully automated data processing and spectral deconvolution of 1D ^{1}H NMR spectra to identify and quantify metabolites. Like Chenomx NMRSuite, both Bayesil and MagMet are compatible with most NMR instrument models and magnetic field strengths. However, their application is typically limited to the analysis of specific biofluids, such as serum, plasma, or fecal water.

Following the identification and quantification of metabolites, the resulting data are analysed using biostatistical methods, including multivariate analysis (MVA) and

advanced Machine Learning algorithms. This can be performed using platforms such as MetaboAnalyst 6.0 [29] (http://www.metaboanalyst.ca/) or dedicated R packages designed for MVA approaches. [30]

The final and essential step in metabolomic analysis is the biological interpretation of the data. This interpretive phase may involve pathway mapping using curated databases such as KEGG, SMPDB, or Reactome, or may be supported by trans-omic integration tools, including Phenolink, 3-Omics, and OmicsNet, which facilitate the visualization and contextualization of metabolomic findings within broader biological networks. [31-33]

1.1.4 Cellular metabolomics

To date, most metabolomic data have been derived from biofluid analyses, primarily for clinical applications. While this approach provides valuable systemic information, it lacks the resolution necessary to investigate the metabolic dynamics of individual cell types under specific physiological or pathological conditions. Such cellular-level resolution is crucial for a comprehensive understanding of cellular functions and for the development of targeted therapeutics and biomarkers tailored to distinct cellular phenotypes. [1, 34] In this context, cell culture-based metabolomics emerges as a potent tool. Enabling cell-type specificity, it allows for the dissection of metabolic pathways with greater precision, offering insights that are often obscured in whole-organism or biofluid-based analyses.

Additionally, *in vitro* applications of cellular metabolomics offer several advantages over human or animal models: improved control over experimental variables, greater reproducibility, lower costs, more straightforward data interpretation, and the absence of ethical concerns associated with the use of living subjects. [35] In addition, cell culture analysis avoids problems common to other metabolomic applications, such as inter-individual variability across subjects and time points, population heterogeneity, and the influence of confounding factors, including age, sex, health status, and environmental exposure. By focusing on a specific cell type, variability is significantly reduced, facilitating the detection of metabolic changes and enabling more robust correlation of metabolomic data with genomic or proteomic profiles. These datasets, whether used independently or in combination with other omic layers, can contribute to the development of models of biological pathways

and networks, and provide a robust foundation for further investigations using cell culture systems. [34]

The preparation of cell samples for metabolomics analysis follows a strict protocol that includes sampling, quenching, and extraction of metabolites. [36, 37] A crucial aspect is to optimize the number of cultures analyzed to detect even low concentrations of metabolites. It is also critical to carefully consider the composition of the culture medium, as components such as 4-(2-hydroxyethyl)-1-piperazineethanesulfonic acid (HEPES) and complex additives, such as fetal bovine serum (FBS), may contaminate samples and compromise analytical accuracy. [38] HEPES is particularly problematic for NMR-based metabolic profiling, as it is typically present at high concentrations and produces broad, intense resonances that overlap with signals from several metabolites of interest.[37] Therefore, if possible, HEPES should be avoided. To mitigate interference and contamination, cells must be thoroughly separated from the medium by washing with phosphate-buffered saline (PBS), thereby removing residual traces of extracellular components.

Quenching, which instantly blocks cellular metabolism to preserve the real metabolic state, is a fundamental step. A common method involves rapid cooling with liquid nitrogen, often after cell removal by trypsinization. However, trypsin can induce cellular stress and disrupt metabolite levels, compromising data quality. [39] A gentler alternative is to wash the cells with cold PBS or deionized water, followed by the direct addition of liquid nitrogen or frozen methanol. At this point, the cells collected using a cell scraper can either be frozen at −80 °C or immediately processed for metabolite extraction. [38]

Extraction is usually done using mixtures of organic solvents, such as methanol or acetonitrile combined with water or acidified water, to obtain a wide range of chemical compounds, including amino acids, organic acids, nucleotide precursors, sugars, and alcohols. [19, 40] After extraction, the cell extracts are quickly frozen in liquid nitrogen and stored at −80°C until analysis. It is essential to avoid repeated freeze-thaw cycles to prevent metabolite degradation. When necessary, samples should be thawed on ice to allow a gradual increase in temperature and minimize compound alterations.

1.2 From metabolomics to fluxomics: a dynamic perspective on metabolism

Among the most recent advances in the study of cellular metabolism, fluxomics has emerged as a powerful analytical approach. While metabolomics focuses on measuring − through identification and quantification − the largest possible number of metabolites in biological systems, fluxomics aims to obtain information on metabolic fluxes, that is, the rates at which metabolic conversions occur within these systems.

Since reaction rates cannot be measured directly because of the dynamic nature of metabolism, fluxes are deduced indirectly from metabolic intermediates. To achieve this, fluxomics exploits isotopically labelled compounds as tracers to determine the fluxome. The typical workflow involves introducing an isotopically labelled precursor into the biological system, followed by accurate measurement of the extent of label incorporation into downstream metabolites. [41, 42] The most commonly used tracer is ^{13}C, particularly useful for investigating central carbon metabolism. However, isotopes such as ^{15}N can also be employed, especially for studying nitrogen metabolism, amino acid turnover, and transamination reactions. [43] When cells are grown in the presence of a ^{13}C-enriched substrate, labelled carbon atoms propagate through the metabolic network according to pathway structure and activity. The resulting ^{13}C-labelling patterns of metabolic intermediates reflect the underlying intracellular fluxes. Labelling information can be measured by mass spectrometry (MS) or nuclear magnetic resonance (NMR). Eventually, flux quantification is obtained by integrating isotopic labelling data with mathematical models that describe isotope propagation through the metabolic network under investigation. [44]

Fluxomics offers an important advantage over conventional metabolomics by providing a dynamic view of cellular metabolism rather than a static snapshot of metabolite concentrations. While metabolomics shows which metabolites are present and how their levels change, fluxomics determines the actual rates and directions of metabolic reactions, revealing functional pathway activity that cannot be inferred from concentrations alone. However, fluxomics is more complex and costly, requiring labelled substrates, specialised NMR or MS instruments, and complex modelling. Unlike metabolomics, which covers hundreds of metabolites, fluxomics focuses on a limited number of pathways with greater depth. It often requires time-course sampling and strict conditions, making it more demanding.

1.3 A modern application in drug sciences: pharmacometabolomics

Over the past four decades, the prevailing paradigm in drug discovery and development has involved identifying disease-associated genes through DNA analysis and genome sequencing, followed by gene cloning, purification of target proteins, and high-throughput screening to identify potential drug candidates. These leads are subsequently optimized and evaluated in animal models before progressing to human clinical trials. Unfortunately, this paradigm has shown significant limitations. [45] This is evidenced by the lengthy timelines and high costs associated with current drug development programs: only a small fraction of compounds entering the development pipeline reach Phase I clinical trials, and among those, a considerable number ultimately fail during Phase III. One of the significant limitations of the current model is that relatively few diseases have a strong genetic basis – estimated to be less than 10%. Moreover, a substantial proportion of diseases arises from environmental exposures, collectively referred to as the exposome. Additionally, not all disease-associated genes are suitable for high-throughput screening or represent viable targets for pharmacological intervention. [46, 47]

Metabolomics may offer a far more cost-effective and productive route to drug discovery, testing, and development. Considering that the majority of widespread diseases have a strong metabolic basis or a clear metabolic etiology, this reinforces the idea that metabolomics could be a valuable tool in drug discovery. [48, 49]

The application of metabolomics in the pharmaceutical field goes beyond drug discovery, encompassing a wide range of drug-related areas. Pharmacometabolomics is a recent branch of metabolomics; in fact, the term was first used by Clayton in 2006 to refer to "*the prediction of the outcome (e.g., efficacy or toxicity) of a drug or xenobiotic intervention in an individual, based on a mathematical model of 'preintervention' metabolite signatures*". [50]

Pharmacometabolomics has several applications and can be used for:

- Enhancing so-called personalized medicine. The inherent variability of pathologies, combined with pharmacological differences, makes it difficult to predict how an individual patient will respond to a selected therapy, underscoring the need for a more personalized approach to treatment. It is increasingly clear that genetics alone cannot explain all variations in drug response phenotypes, and that other factors, such as environmental exposure, diet, age, gender, ethnicity, disease

subtype, use of other drugs, and the gut microbiome, may contribute to variation in drug response. Pharmacometabolomics, integrating information from pharmacogenomics, enables prediction of a subject's response to a specific treatment to personalize therapy and make it as effective as possible. [51] Pharmacometabolomics involves determining an individual's metabolic status based on environmental, genetic, and gut microbiome influences – the so-called "metabotype" – to define profiles that can inform about treatment outcomes. [52]

- Pharmacokinetic studies of medicinal products – absorption, distribution, metabolism, and excretion (ADME). In fact, metabolomic analyses can be particularly useful for studying how a drug is metabolised in a subject, i.e., the products of xenobiotic-metabolising reactions. [53] In addition, drug absorption, metabolism, and transport to the site of action may be affected by metabolic states and the regulation of intestinal metabolism. Therefore, understanding a patient's metabolomic profile can help predict how the drug behaves before it reaches its biological target. [51]
- Pharmacodynamic studies. Since many emerging targets lack known biochemical function, metabolomics has become essential for understanding the mechanisms of action of new potential drugs or molecules already in use, and for identifying markers of therapeutic efficacy. In fact, metabolomics can help identify therapeutic targets and clarify the mechanism of action of drugs by analyzing the metabolic alterations induced by treatment. This approach relies on using metabolic maps to identify the proteins most affected by drugs, which are then subjected to further analysis. This strategy often combines untargeted metabolomics (which explores the entire metabolic profile without bias) with *in silico* or chemoinformatics approaches to gain a more complete view of induced changes. [54] The pharmacometabolomic approach has recently been employed to uncover new insights into the mechanisms of action of widely used drugs such as statins and sertraline. It has also proven valuable in elucidating the pharmacological activity of compounds with less well-defined mechanisms of action, including some antiprotozoal agents. [55-58]

At the same time, analyzing drug-induced changes at the metabolic level can provide new insights into the toxicity of drug treatments, importantly reducing drug failures. [59] Perhaps the best-known example of these early applications in

toxicology screening is COMET (the Consortium for Metabonomic Toxicity), which brought together five major pharmaceutical companies along with academics from the Imperial College London to use metabolomics as a means of creating an expert system for predicting kidney and liver toxicity of drug-like compounds in rodents. Over a period of 5 years and nearly 150 studies, COMET clearly demonstrated that metabolomics could provide fast, inexpensive, non-invasive approaches to assessing and even predicting liver and kidney toxicity of lead compounds. [60]

1.3.1 Metabolomics to study biomolecules molecular mechanism

As is clear from the previous paragraph, the number of applications of metabolomics in drug discovery and development programs is enormously increasing.

The metabolomics approach has been adopted relatively recently in drug discovery programs. Key areas for its application during the drug development process include: (i) target identification; (ii) clarification of the mechanism of action (MoA); (iii) discovery of markers of therapeutic efficacy (TE); and (iv) markers of physiological response (PR), including monitoring of therapy. [54]

Untargeted Metabolomics is increasingly recognized as a valuable and effective approach for establishing target engagement markers and for gaining insights into MoA. Untargeted strategies are highly advantageous for providing insights not only into MoA but also into potential off-target interactions and adverse effects (AEs). Ultimately, drug repurposing strategies are poised to benefit substantially from a comprehensive understanding of drug-induced metabolic alterations, particularly when integrated with multi-omics, advanced bioinformatics, and pathway-mapping approaches. [5, 54]

Metabolomics, especially when applied in an untargeted manner, offers a broad capacity to uncover unexpected effects. [54, 61] This approach can potentially overcome a fundamental limitation in conventional MoA studies, which are typically driven by specific leading hypotheses and therefore tend to concentrate on a single, potentially biased cellular process. While such hypothesis-driven strategies can yield positive results, they often restrict the scope of investigation and make it difficult to uncover unexpected or off-target biochemical effects.

In this context, pharmacometabolomics offers a powerful strategy for uncovering unexpected molecular effects. [54, 61] This technique enables a comprehensive study of the global impact of a molecule, without restricting the analysis to the stimulation of a specific receptor or the activation of a particular biochemical pathway.

Moreover, clarifying the biochemical pathways affected by a molecule may provide new investigative insights for designing novel molecular entities with enhanced therapeutic activity and fewer side effects.

1.4 The future direction: hyperpolarization

The main limitations of NMR methods are linked to the signal overlaps that occur in the widely used 1D ^{1}H spectra of complex biological mixtures and to their low sensitivity, with a limit of detection in the low micromolar concentration regime. The former is partially overcome by the introduction of a second dimension in the frequency domain using 2D spectra, which recent technologies have made more sensitive, faster, and more qualitative. [62-64] The latter represents the most important issue of all conventional NMR methods and relates to the low energy gap between spin states, leading to a low nuclear polarization – i.e., the polarization of protons in a typical NMR spectrometer (14.1 T, 600 MHz proton Larmor frequency) can be estimated to be 0.0048% at room temperature.

While its relatively lower sensitivity is often considered an Achilles' heel, NMR sensitivity has significantly improved over the past couple of decades. An approach to overcome this problem is to force the distribution of nuclear spin in the lower level of energy, increasing the so-called polarization (P), defined as the ratio between the difference of nuclei in alpha level (N_α) and beta level (N_β), and the total number of nuclei (N):

$$P = \frac{N\alpha - N\beta}{N}$$

So, hyperpolarization NMR methods aim to obtain a transient overpopulation of a nuclear spin state, resulting in large NMR signal enhancements. This can be obtained in different ways.

- The simplest method is the so-called "brute-force" method, in which the sample is frozen at cryogenic temperatures and in a high magnetic field, and the resulting rapid dissolution at room temperature yields a hyperpolarized sample. [65]

- Dissolution Dynamic Nuclear Polarization (d-DNP) is similar to "brute force" but is based on polarization transfer from the unpaired electron of a polarizing agent (PA), typically a free radical, to the nuclear spins of the target molecules. This method requires a dedicated DNP apparatus which provides a suitable magnetic field, low temperatures, and microwave irradiation. d-DNP applications are mainly in ^{13}C detection because ^{13}C hyperpolarization persists longer during transfer between the two magnets, due to their longer T1s. [66, 67]
- Para-hydrogen based hyperpolarization relies on spin order of the *para*-isomer of molecular hydrogen. This spin order can lead to hyperpolarization when the symmetry of the parahydrogen (p-H_2) molecule is broken, either after a hydrogenation reaction or upon formation of a metal complex. [68]

1.4.1 Parahydrogen

The hydrogen molecule consists of two hydrogen atoms linked together and, as a result of the combination of their two protons' spins, four different nuclear spin configurations are obtained. Since the two atoms are identical, the combination gives – outside a magnetic field – two levels of energy:

- The higher represented by the triplet ($\alpha\alpha$, $\beta\beta$, $\alpha\beta+\beta\alpha$) called ortho-hydrogen (o-H_2) and having symmetric nuclear wavefunctions.
- The lower represented by a single state ($\alpha\beta-\beta\alpha$) called parahydrogen (p-H_2) and having an antisymmetric nuclear wavefunction.

Since protons have half-odd-integer spin (I = 1/2), they are fermions and are subject to Pauli's exclusion principle. This means that, under the exchange of two identical particles, the overall molecular wavefunction has to be antisymmetric, restricting the ortho-hydrogen to an antisymmetric rotational state (J = odd) and p-H_2 to symmetric one (J = even) (**Figure 1.1**).

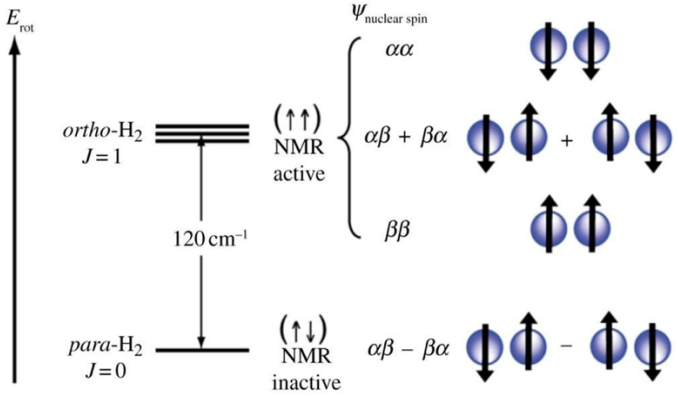

Figure 1.1 *Energy diagram for the lowest spin-rotational states of H_2.*[69]

At room temperature, molecular hydrogen exists as a mixture of ortho e para-hydrogen, in a 3:1 ratio, favouring the ortho form. Due to the forbidden transition between singlet and triplet states, the conversion between *p*-H_2 and o *o*-H_2 is extremely slow at room temperature. However, at low temperature and in the presence of a catalyst (such as ferric oxide and activated carbon), only the J = 0 level is appreciably populated, so that the *p*-H_2 is significantly enhanced.

For example, at the temperature of liquid N_2 (77K), hydrogen spin isomers are present as 50% para and 50% ortho-hydrogen; while at 25 K, the ratio increases to 99:1.

For hyperpolarization experiments, para-enriched H_2 is either permanently added to a target molecule [70] or brought into temporary contact. [71] Hydrogenation at high magnetic fields is usually referred to as a PASADENA experiment. [72, 73] In contrast, hydrogenation at low magnetic fields and subsequent transfer to high field is often called ALTADENA. [70]

Enhanced proton magnetization results from the "singlet order" i.e. the para-/ortho unbalance with respect to thermal hydrogen. This conversion can take place spontaneously or it may be aided by radio-frequency (RF) pulses or variations of the magnetic field (field cycling). Whereas detection of a ^1H signal may be sufficient for *in vitro* analysis, *in vivo* application usually necessitates transfer to a slow-relaxing X-nucleus such as ^{13}C or ^{15}N. [74]

1.4.2 Parahydrogen Induced Polarization (PHIP)

The *p*-H_2-induced polarization (PHIP) consists of a chemical reduction reaction that involves para-enriched hydrogen in its singlet state, facilitated by a rhodium-based catalyst. This means that PHIP has an essential structural requirement: the presence of an unsaturation in the analyte's structure. When parahydrogen is added in a pairwise manner to an asymmetric unsaturated molecule, the symmetry of the hydrogens is broken, and this determines a significantly enhanced nuclear spin polarization. [75]

This insaturation is generally close to a ^{13}C o di ^{15}N labeled nuclei. In such a way, an intramolecular spin transfer passes through spin-spin coupling from nascent parahydrogen protons to significantly longer-lived labeled nuclei. Since the *in vivo* ^{13}C background signal is low, hyperpolarized ^{13}C compounds were quickly shown to be useful as an *in vivo* contrast agent for biomedical imaging applications. [76]

Although PHIP requires specific structural conditions for its application, this limitation can be overcome by incorporating unsaturation into the target molecule, either by using an unsaturated precursor or by introducing a double bond into side chains, as demonstrated for amino acids. [74]

1.4.3 SABRE

In 2009, the PHIP technique, termed signal amplification by reversible exchange (SABRE) was described. [71] In contrast with traditional PHIP methods, SABRE does not involve an irreversible reaction. Still, it employs a reversible interaction between *p*-H_2 and a substrate (e.g., pyridine) and an active iridium-based catalyst (formed from a precatalyst) (**Figure 1.2A**).

At low field, spontaneous polarization transfer occurs between the hydrides originating from *p*-H_2 and the nuclear spins of the analyte that is temporarily associated with the iridium catalyst. Continuous ligand association/dissociation leads to the buildup of hyperpolarization of free analyte in solution, which can be detected by NMR after transferring the sample to a high magnetic field. The addition of a cosubstrate in large excess further increases the analyte's NMR proton signals. [77] SABRE experiments provide hyperpolarized free analyte in solution, whose proton signals can allow analyte identification by a simple chemical shift comparison with an NMR database.

Therefore, the advantage of SABRE over PHIP is that it does not require the presence of a double bond. However, the substrate must possess specific structural features that allow interaction with the catalyst's metal center. Analyte coordination to iridium is required, implying some degree of selectivity, so the hyperpolarization catalyst should be considered a chemosensor.

1.4.4 nhPHIP

Besides SABRE, there is another method called high-field non-hydrogenative PHIP (HF-nhPHIP), which does not require hydrogenation, unlike classical PHIP. HF-nhPHIP – sometimes also called early nhPHIP – uses similar reagents to SABRE for the hyperpolarization process, but differs in some aspects, including the type of signal that is detected.

In nhPHIP, the same iridium complex employed in SABRE is formed through the transient association of *p*-H_2, a dilute analyte, an excess of cosubstrate, and the catalyst (**Figure 1.2B**). In contrast to SABRE, however, the hyperpolarization is not transferred to the free analyte in solution but remains localized on the hydrides derived from *p*-H_2. This process occurs directly at high magnetic field, such as inside the NMR spectrometer.

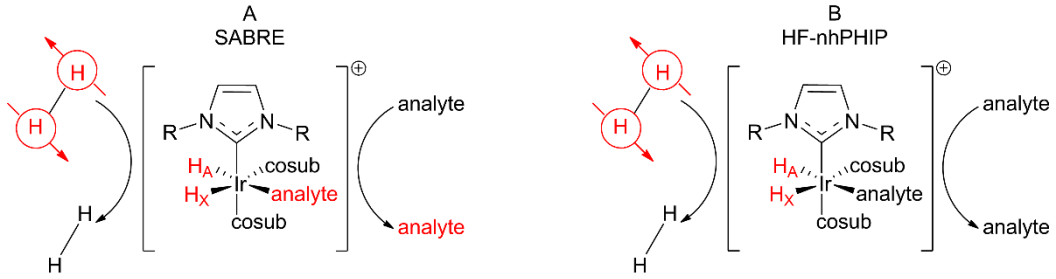

Figure 1.2 *(**A**) Schematic representation of the SABRE experiment at low magnetic field: spontaneous transfer of spin order from hydrides derived from para-enriched hydrogen (p-H_2) to the nuclear spins of the analyte occurs through scalar coupling within the transient complex [Ir(IMes)(H)$_2$(analyte)(cosub)$_2$]Cl. Dissociation of the analyte releases hyperpolarized molecules into solution, enabling enhanced NMR detection. (**B**) Schematic representation of reversible PHIP at high magnetic field: reversible association of p-H_2 and analytes leads to the formation of the asymmetric complex [Ir(IMes)(H)$_2$(analyte)(cosub)$_2$]Cl, resulting in hydride hyperpolarization and up to 1000-fold signal enhancement in NMR. Cosub: cosubstrate. Adapted from* [78]

An asymmetric configuration in which both the analyte and cosubstrate occupy the equatorial plane of the complex is energetically favored. In this geometry, the hydrides derived from *p*-H_2 are chemically non-equivalent, which leads to rapid dephasing of

the singlet spin state into longitudinal spin order. By applying a PASADENA pulse sequence, this spin order is converted into enhanced magnetization. As a result, NMR experiments reveal two hyperpolarized hydride signals for each analyte bound to the iridium complex. Unlike SABRE, nhPHIP does not produce signals from the analyte's own protons. Instead, the hydride signals – whose chemical shifts are highly sensitive to the bound analyte – appear in a typically signal-free region of the ^{1}H spectrum, around -20 ppm. [79]

This improved sensitivity and specificity, combined with minimal background interference, make nhPHIP particularly useful for detecting very dilute components in complex biological mixtures, such as natural extracts and biofluids. [78, 80, 81]

1.4.5 Hyperpolarization NMR in metabolomics

Over the past decade, numerous studies have demonstrated that hyperpolarization techniques can detect metabolites in complex biological matrices derived from both plant and animal sources. [62, 82] Hyperpolarized NMR appears particularly promising in overcoming the sensitivity limitations of conventional NMR-based metabolomics, which often fails to detect metabolites present at very low concentration in biological samples. In the past five years, both d-DNP and parahydrogen-based NMR metabolomics approaches have been reported.

In 2020, Giraudeau's research group successfully incorporated hyperpolarized NMR Metabolomics (via d-DNP) at natural ^{13}C in a metabolomics study, allowing discrimination between red-ripe and mature-green tomato extracts. [83]

More recently, the same research group compared urine samples from patients with chronic kidney disease to those from healthy controls using hyperpolarized ^{13}C NMR metabolomics at natural abundance, achieving detection limits in the sub-millimolar range. When comparing hyperpolarized metabolomics with conventional 1D ^{1}H NMR analysis, they found that several results were consistent across both methods. However, ^{13}C hyperpolarized NMR enabled the identification of two biomarkers that were not detectable by ^{1}H NMR due to peak overlap, taking advantage of the broader spectral dispersion and narrower line widths characteristic of ^{13}C NMR. [84]

Beyond d-DNP, NMR signal enhancement can be achieved for various classes of compounds – including nitrogen- and sulfur-containing heteroaromatics, nitriles, amines, α-amino acids, and oligopeptides – through nhPHIP. [81, 85-88] The selective

nature of nhPHIP-NMR makes it particularly suitable for semi-targeted metabolomics, enabling the detection of low concentrations of these metabolite classes. While such selectivity might initially seem limiting, it actually simplifies the spectral output, helping to highlight biomarkers that are otherwise undetectable by conventional NMR due to spectral crowding or excessive dilution.

A practical example was reported in 2025 by Tessari's research group, who presented the first implementation of parahydrogen-based hyperpolarization in an NMR metabolomics study.[89] The authors used nhPHIP technique to conduct a semi-targeted metabolomics study on urine samples from patients with Pyridoxine-Dependent Epilepsy (PDE) – a condition currently diagnosed through the presence of highly dilute, disease-specific α-amino acid biomarkers. The study demonstrated that 1D and 2D nhPHIP NMR provided better discrimination between PDE patients and healthy controls than conventional ^{1}H NMR. While standard metabolomics identified only one biomarker, the hyperpolarized approach revealed additional disease-specific metabolites uniquely associated with PDE, enhancing diagnostic precision. This study demonstrates that 2D nhPHIP, with its enhanced resolution and signal strength, is a promising tool for highly sensitive NMR-based metabolomics.

1.5 General aims and objectives

My PhD research was primarily centered on metabolomics using NMR, which offers several advantages, including the relative ease of sample preparation, its intrinsically quantitative nature, high reproducibility, and the non-destructive acquisition of the data. More specifically, I focused on modern applications of metabolomics and emerging analytical techniques in the field, represented respectively by pharmacometabolomics and hyperpolarization-enhanced NMR (**Figure 1.3**).

NMR-based metabolomics was used to:

- *Investigate the cellular mechanism of action (MoA) of selected molecular entities*. This strategy emerged in response to a key limitation of conventional studies on MoA, which are often guided by predefined hypotheses and tend to focus narrowly on a single cellular pathway. In contrast, pharmacometabolomics provides a robust and unbiased approach to reveal unexpected molecular effects. [54, 61] When applied with an untargeted approach, this technique allows for a comprehensive assessment of the global biological impact of a compound, without being confined

to the activation of a specific receptor or biochemical cascade. In more detail, I used this approach to study the potential use of two molecules in Alzheimer's disease (AD): the alkaloid nicotine and the growth factor Nerve Growth Factor (NGF).

The metabolomic effects of nicotine and NGF were investigated using a cellular model of SH-SY5Y human neuroblastoma cells. By integrating data from both the exometabolome and endometabolome, I obtained a comprehensive overview of the systemic impact of these two molecules in the presence and absence of the amyloid-β peptide 1–42 (Aβ(1–42)).

- *Apply non-hydrogenative parahydrogen-induced polarization (nhPHIP) for the first time in a metabolomic study on animal tissues.* To investigate the functional role of D-aspartate (D-Asp) in the mature brain, we performed a metabolomic analysis based on nhPHIP-NMR on brain extracts from wild-type mice and mice with genetically modulated expression of the D-aspartate oxidase (*ddo*) gene. Using an iridium-based catalyst, a chiral cosubstrate (*S*-nicotine), and *p*-H_2, this technique enables enhanced sensitivity for detecting the stereochemical configuration of amino acids in metabolomic samples. This work was conducted in collaboration with Prof. Usiello, who provided the animal samples, and Dr. Tessari from the Magnetic Resonance Research Center at Radboud University (The Netherlands), where the spectra were recorded.

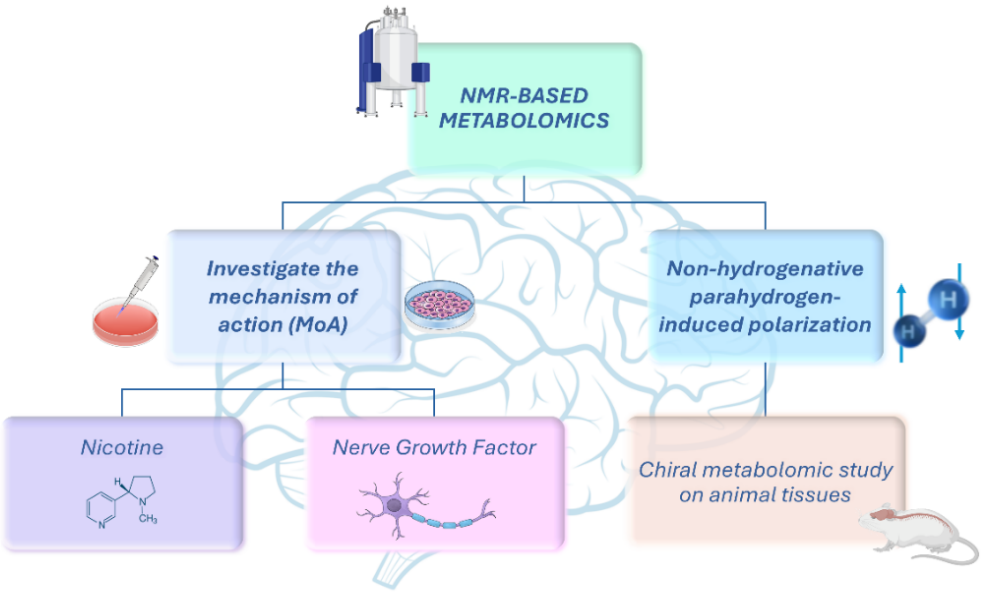

Figure 1.3 *Overview of NMR-based metabolomics applications explored during my PhD and discussed in the following chapters.*

Bibliography

1. Beckonert, O.; Keun, H. C.; Ebbels, T. M. D.; Bundy, J.; Holmes, E.; Lindon, J. C.; Nicholson, J. K., Metabolic profiling, metabolomic and metabonomic procedures for NMR spectroscopy of urine, plasma, serum and tissue extracts. *Nature protocols* **2007,** *2* (11), 2692.
2. Zhang, A.; Sun, H.; Yan, G.; Wang, P.; Wang, X., Metabolomics for biomarker discovery: moving to the clinic. *BioMed research international* **2015,** *2015* (1), 354671.
3. Patti, G. J.; Yanes, O.; Siuzdak, G., Metabolomics: the apogee of the omics trilogy. *Nature reviews Molecular cell biology* **2012,** *13* (4), 263-269.
4. Vignoli, A.; Ghini, V.; Meoni, G.; Licari, C.; Takis, P. G.; Tenori, L.; Turano, P.; Luchinat, C., High-throughput metabolomics by 1D NMR. *Angewandte Chemie International Edition* **2019,** *58* (4), 968-994.
5. Wishart, D. S., Metabolomics for investigating physiological and pathophysiological processes. *Physiological reviews* **2019**.
6. Wishart, D. S.; Tzur, D.; Knox, C.; Eisner, R.; Guo, A. C.; Young, N.; Cheng, D.; Jewell, K.; Arndt, D.; Sawhney, S., HMDB: the human metabolome database. *Nucleic acids research* **2007,** *35* (suppl_1), D521-D526.
7. Kanehisa, M. In *The KEGG database*, 2002; Wiley Online Library: pp 91-103.
8. Frolkis, A.; Knox, C.; Lim, E.; Jewison, T.; Law, V.; Hau, D. D.; Liu, P.; Gautam, B.; Ly, S.; Guo, A. C., SMPDB: the small molecule pathway database. *Nucleic acids research* **2010,** *38* (suppl_1), D480-D487.
9. Bhinderwala, F.; Wase, N.; DiRusso, C.; Powers, R., Combining mass spectrometry and NMR improves metabolite detection and annotation. *Journal of proteome research* **2018,** *17* (11), 4017-4022.
10. Emwas, A.-H. M., The strengths and weaknesses of NMR spectroscopy and mass spectrometry with particular focus on metabolomics research. In *Metabonomics: Methods and protocols*, Springer: 2015; pp 161-193.
11. Emwas, A.-H.; Roy, R.; McKay, R. T.; Tenori, L.; Saccenti, E.; Gowda, G. A. N.; Raftery, D.; Alahmari, F.; Jaremko, L.; Jaremko, M., NMR spectroscopy for metabolomics research. *Metabolites* **2019,** *9* (7), 123.
12. Wishart, D. S.; Cheng, L. L.; Copié, V.; Edison, A. S.; Eghbalnia, H. R.; Hoch, J. C.; Gouveia, G. J.; Pathmasiri, W.; Powers, R.; Schock, T. B., NMR and metabolomics—A roadmap for the future. *Metabolites* **2022,** *12* (8), 678.
13. Roberts, L. D.; Souza, A. L.; Gerszten, R. E.; Clish, C. B., Targeted metabolomics. *Current protocols in molecular biology* **2012,** *98* (1), 30-2.
14. Lelli, V.; Belardo, A.; Timperio, A. M., From targeted quantification to untargeted metabolomics. *Metabolomics—Methodology and Applications in Medical Sciences and Life Sciences* **2021,** *10*.
15. Klupczyńska, A.; Dereziński, P.; Kokot, Z. J., Metabolomics in medical sciences--trends, challenges and perspectives. *Acta poloniae pharmaceutica* **2015,** *72* (4), 629-641.
16. Griffiths, W. J., *Metabolomics, metabonomics and metabolite profiling*. Royal Society of Chemistry: 2008; Vol. 9.
17. Ghini, V.; Meoni, G.; Vignoli, A.; Di Cesare, F.; Tenori, L.; Turano, P.; Luchinat, C., Fingerprinting and profiling in metabolomics of biosamples. *Progress in Nuclear Magnetic Resonance Spectroscopy* **2023,** *138*, 105-135.
18. Álvarez-Sánchez, B.; Priego-Capote, F.; de Castro, M. L., Metabolomics analysis II. Preparation of biological samples prior to detection. *TrAC Trends in Analytical Chemistry* **2010,** *29* (2), 120-127.
19. Smith, L.; Villaret-Cazadamont, J.; Claus, S. P.; Canlet, C.; Guillou, H.; Cabaton, N. J.; Ellero-Simatos, S., Important considerations for sample collection in metabolomics studies with a special focus on applications to liver functions. *Metabolites* **2020,** *10* (3), 104.
20. Snytnikova, O. A.; Khlichkina, A. A.; Sagdeev, R. Z.; Tsentalovich, Y. P., Evaluation of sample preparation protocols for quantitative NMR-based metabolomics. *Metabolomics* **2019,** *15*, 1-9.

21. Lin, C. Y.; Wu, H.; Tjeerdema, R. S.; Viant, M. R., Evaluation of metabolite extraction strategies from tissue samples using NMR metabolomics. *Metabolomics* **2007,** *3* (1), 55-67.
22. Mo, H.; Raftery, D., Pre-SAT180, a simple and effective method for residual water suppression. *Journal of Magnetic Resonance* **2008,** *190* (1), 1-6.
23. Weljie, A. M.; Newton, J.; Mercier, P.; Carlson, E.; Slupsky, C. M., Targeted profiling: quantitative analysis of 1H NMR metabolomics data. *Analytical chemistry* **2006,** *78* (13), 4430-4442.
24. Godelmann, R.; Fang, F.; Humpfer, E.; Schütz, B.; Bansbach, M.; Schäfer, H.; Spraul, M., Targeted and nontargeted wine analysis by 1H NMR spectroscopy combined with multivariate statistical analysis. Differentiation of important parameters: grape variety, geographical origin, year of vintage. *Journal of agricultural and food chemistry* **2013,** *61* (23), 5610-5619.
25. Spraul, M.; Schütz, B.; Humpfer, E.; Mörtter, M.; Schäfer, H.; Koswig, S.; Rinke, P., Mixture analysis by NMR as applied to fruit juice quality control. *Magnetic Resonance in Chemistry* **2009,** *47* (S1), S130-S137.
26. Jiménez, B.; Holmes, E.; Heude, C.; Tolson, R. F.; Harvey, N.; Lodge, S. L.; Chetwynd, A. J.; Cannet, C.; Fang, F.; Pearce, J. T. M., Quantitative lipoprotein subclass and low molecular weight metabolite analysis in human serum and plasma by 1H NMR spectroscopy in a multilaboratory trial. *Analytical chemistry* **2018,** *90* (20), 11962-11971.
27. Ravanbakhsh, S.; Liu, P.; Bjordahl, T. C.; Mandal, R.; Grant, J. R.; Wilson, M.; Eisner, R.; Sinelnikov, I.; Hu, X.; Luchinat, C., Accurate, fully-automated NMR spectral profiling for metabolomics. *PloS one* **2015,** *10* (5), e0124219.
28. Rout, M.; Lipfert, M.; Lee, B. L.; Berjanskii, M.; Assempour, N.; Fresno, R. V.; Cayuela, A. S.; Dong, Y.; Johnson, M.; Shahin, H., MagMet: A fully automated web server for targeted nuclear magnetic resonance metabolomics of plasma and serum. *Magnetic Resonance in Chemistry* **2023,** *61* (12), 681-704.
29. Pang, Z.; Lu, Y.; Zhou, G.; Hui, F.; Xu, L.; Viau, C.; Spigelman, A. F.; MacDonald, P. E.; Wishart, D. S.; Li, S., MetaboAnalyst 6.0: towards a unified platform for metabolomics data processing, analysis and interpretation. *Nucleic acids research* **2024,** *52* (W1), W398-W406.
30. Mair, P.; de Leeuw, J., A general framework for multivariate analysis with optimal scaling: The R package aspect. *Journal of Statistical Software* **2010,** *32*, 1-23.
31. Zhou, G.; Xia, J., OmicsNet: a web-based tool for creation and visual analysis of biological networks in 3D space. *Nucleic acids research* **2018,** *46* (W1), W514-W522.
32. Bayjanov, J. R.; Molenaar, D.; Tzeneva, V.; Siezen, R. J.; van Hijum, S. A. F. T., PhenoLink - a web-tool for linking phenotype to ~omics data for bacteria: application to gene-trait matching for Lactobacillus plantarum strains. *BMC Genomics* **2012,** *13* (1), 170.
33. Kuo, T.-C.; Tian, T.-F.; Tseng, Y. J., 3Omics: a web-based systems biology tool for analysis, integration and visualization of human transcriptomic, proteomic and metabolomic data. *BMC Systems Biology* **2013,** *7* (1), 64.
34. Čuperlović-Culf, M.; Barnett, D. A.; Culf, A. S.; Chute, I., Cell culture metabolomics: applications and future directions. *Drug discovery today* **2010,** *15* (15-16), 610-621.
35. Snijder, B.; Sacher, R.; Rämö, P.; Damm, E.-M.; Liberali, P.; Pelkmans, L., Population context determines cell-to-cell variability in endocytosis and virus infection. *Nature* **2009,** *461* (7263), 520-523.
36. Kapoore, R. V.; Coyle, R.; Staton, C. A.; Brown, N. J.; Vaidyanathan, S., Influence of washing and quenching in profiling the metabolome of adherent mammalian cells: a case study with the metastatic breast cancer cell line MDA-MB-231. *Analyst* **2017,** *142* (11), 2038-2049.
37. Kostidis, S.; Addie, R. D.; Morreau, H.; Mayboroda, O. A.; Giera, M., Quantitative NMR analysis of intra-and extracellular metabolism of mammalian cells: A tutorial. *Analytica chimica acta* **2017,** *980*, 1-24.

38. Lorenz, M. A.; Burant, C. F.; Kennedy, R. T., Reducing time and increasing sensitivity in sample preparation for adherent mammalian cell metabolomics. *Analytical chemistry* **2011,** *83* (9), 3406-3414.
39. Mili, M.; Panthu, B.; Madec, A.-M.; Berger, M.-A.; Rautureau, G. J. P.; Elena-Herrmann, B., Fast and ergonomic extraction of adherent mammalian cells for NMR-based metabolomics studies. *Analytical and bioanalytical chemistry* **2020,** *412* (22), 5453-5463.
40. León, Z.; García-Cañaveras, J. C.; Donato, M. T.; Lahoz, A., Mammalian cell metabolomics: experimental design and sample preparation. *Electrophoresis* **2013,** *34* (19), 2762-2775.
41. Emwas, A.-H.; Szczepski, K.; Al-Younis, I.; Lachowicz, J. I.; Jaremko, M., Fluxomics-new metabolomics approaches to monitor metabolic pathways. *Frontiers in Pharmacology* **2022,** *13*, 805782.
42. Giraudeau, P., NMR-based metabolomics and fluxomics: developments and future prospects. *Analyst* **2020,** *145* (7), 2457-2472.
43. Millard, P.; Cahoreau, E.; Heuillet, M.; Portais, J.-C.; Lippens, G., 15N-NMR-based approach for amino acids-based 13C-metabolic flux analysis of metabolism. *Analytical chemistry* **2017,** *89* (3), 2101-2106.
44. Heux, S.; Bergès, C.; Millard, P.; Portais, J.-C.; Letisse, F., Recent advances in high-throughput 13C-fluxomics. *Current opinion in biotechnology* **2017,** *43*, 104-109.
45. Wishart, D. S., Emerging applications of metabolomics in drug discovery and precision medicine. *Nature reviews Drug discovery* **2016,** *15* (7), 473-484.
46. Maher, B., Personal genomes: The case of the missing heritability. Nature Publishing Group UK London: 2008.
47. Overington, J. P.; Al-Lazikani, B.; Hopkins, A. L., How many drug targets are there? *Nature reviews Drug discovery* **2006,** *5* (12), 993-996.
48. Rappaport, S. M.; Barupal, D. K.; Wishart, D.; Vineis, P.; Scalbert, A., The blood exposome and its role in discovering causes of disease. *Environmental health perspectives* **2014,** *122* (8), 769-774.
49. Calazans, J. A.; Permanyer, I., Levels, trends, and determinants of cause-of-death diversity in a global perspective: 1990–2019. *BMC Public Health* **2023,** *23* (1), 650.
50. Andrew Clayton, T.; Lindon, J. C.; Cloarec, O.; Antti, H.; Charuel, C.; Hanton, G.; Provost, J.-P.; Le Net, J.-L.; Baker, D.; Walley, R. J., Pharmaco-metabonomic phenotyping and personalized drug treatment. *Nature* **2006,** *440* (7087), 1073-1077.
51. Rattray, N. J. W.; Daouk, R. K., Pharmacometabolomics and precision medicine special issue editorial. Springer: 2017; Vol. 13, pp 1-4.
52. Everett, J. R., Pharmacometabonomics in humans: a new tool for personalized medicine. *Pharmacogenomics* **2015,** *16* (7), 737-754.
53. Jian, J.; He, D.; Gao, S.; Tao, X.; Dong, X., Pharmacokinetics in pharmacometabolomics: towards personalized medication. *Pharmaceuticals* **2023,** *16* (11), 1568.
54. Alarcon-Barrera, J. C.; Kostidis, S.; Ondo-Mendez, A.; Giera, M., Recent advances in metabolomics analysis for early drug development. *Drug discovery today* **2022,** *27* (6), 1763-1773.
55. Zhu, H.; Bogdanov, M. B.; Boyle, S. H.; Matson, W.; Sharma, S.; Matson, S.; Churchill, E.; Fiehn, O.; Rush, J. A.; Krishnan, R. R., Pharmacometabolomics of response to sertraline and to placebo in major depressive disorder–possible role for methoxyindole pathway. *PloS one* **2013,** *8* (7), e68283.
56. Elbadawi-Sidhu, M.; Baillie, R. A.; Zhu, H.; Chen, Y.-D. I.; Goodarzi, M. O.; Rotter, J. I.; Krauss, R. M.; Fiehn, O.; Kaddurah-Daouk, R., Pharmacometabolomic signature links simvastatin therapy and insulin resistance. *Metabolomics* **2017,** *13*, 1-13.
57. Vincent, I. M.; Creek, D. J.; Burgess, K.; Woods, D. J.; Burchmore, R. J. S.; Barrett, M. P., Untargeted metabolomics reveals a lack of synergy between nifurtimox and eflornithine against Trypanosoma brucei. *PLoS neglected tropical diseases* **2012,** *6* (5), e1618.

58. Biagini, G. A.; Fisher, N.; Shone, A. E.; Mubaraki, M. A.; Srivastava, A.; Hill, A.; Antoine, T.; Warman, A. J.; Davies, J.; Pidathala, C., Generation of quinolone antimalarials targeting the Plasmodium falciparum mitochondrial respiratory chain for the treatment and prophylaxis of malaria. *Proceedings of the National Academy of Sciences* **2012,** *109* (21), 8298-8303.
59. Beger, R. D.; Flynn, T. J., Pharmacometabolomics in drug safety and drug-exposome interactions. *Metabolomics* **2016,** *12*, 1-11.
60. Lindon, J. C.; Keun, H. C.; Ebbels, T. M. D.; Pearce, J. M. T.; Holmes, E.; Nicholson, J. K., The Consortium for Metabonomic Toxicology (COMET): aims, activities and achievements. *Pharmacogenomics* **2005,** *6* (7), 691-699.
61. Zampieri, M., From the metabolic profiling of drug response to drug mode of action. *Current Opinion in Systems Biology* **2018,** *10*, 26-33.
62. Ribay, V.; Praud, C.; Letertre, M. P. M.; Dumez, J.-N.; Giraudeau, P., Hyperpolarized NMR metabolomics. *Current Opinion in Chemical Biology* **2023,** *74*, 102307.
63. Marchand, J.; Martineau, E.; Guitton, Y.; Dervilly-Pinel, G.; Giraudeau, P., Multidimensional NMR approaches towards highly resolved, sensitive and high-throughput quantitative metabolomics. *Current opinion in biotechnology* **2017,** *43*, 49-55.
64. Martineau, E.; Dumez, J. N.; Giraudeau, P., Fast quantitative 2D NMR for metabolomics and lipidomics: A tutorial. *Magnetic Resonance in Chemistry* **2020,** *58* (5), 390-403.
65. Hirsch, M. L.; Kalechofsky, N.; Belzer, A.; Rosay, M.; Kempf, J. G., Brute-force hyperpolarization for NMR and MRI. *Journal of the American Chemical Society* **2015,** *137* (26), 8428-8434.
66. Ardenkjaer-Larsen, J. H., On the present and future of dissolution-DNP. *Journal of Magnetic Resonance* **2016,** *264*, 3-12.
67. Ardenkjær-Larsen, J. H.; Fridlund, B.; Gram, A.; Hansson, G.; Hansson, L.; Lerche, M. H.; Servin, R.; Thaning, M.; Golman, K., Increase in signal-to-noise ratio of> 10,000 times in liquid-state NMR. *Proceedings of the National Academy of Sciences* **2003,** *100* (18), 10158-10163.
68. Duckett, S. B.; Mewis, R. E., Application of para hydrogen induced polarization techniques in NMR spectroscopy and imaging. *Accounts of chemical research* **2012,** *45* (8), 1247-1257.
69. Chen, Y.-P.; Zhou, H.-C., Characterization of H2 Adsorption Sites: Where Are the Hydrogens Stored in the Materials? In *Nanostructured Materials for Next-Generation Energy Storage and Conversion: Hydrogen Production, Storage, and Utilization*, Springer: 2016; pp 257-290.
70. Pravica, M. G.; Weitekamp, D. P., Net NMR alignment by adiabatic transport of parahydrogen addition products to high magnetic field. *Chemical Physics Letters* **1988,** *145* (4), 255-258.
71. Adams, R. W.; Aguilar, J. A.; Atkinson, K. D.; Cowley, M. J.; Elliott, P. I. P.; Duckett, S. B.; Green, G. G. R.; Khazal, I. G.; López-Serrano, J.; Williamson, D. C., Reversible interactions with para-hydrogen enhance NMR sensitivity by polarization transfer. *Science* **2009,** *323* (5922), 1708-1711.
72. Bowers, C. R.; Weitekamp, D. P., Parahydrogen and synthesis allow dramatically enhanced nuclear alignment. *Journal of the American Chemical Society* **1987,** *109* (18), 5541-5542.
73. Eisenschmid, T. C.; Kirss, R. U.; Deutsch, P. P.; Hommeltoft, S. I.; Eisenberg, R.; Bargon, J.; Lawler, R. G.; Balch, A. L., Para hydrogen induced polarization in hydrogenation reactions. *Journal of the American Chemical Society* **1987,** *109* (26), 8089-8091.
74. Pravdivtsev, A. N.; Buntkowsky, G.; Duckett, S. B.; Koptyug, I. V.; Hövener, J. B., Parahydrogen-Induced Polarization of Amino Acids. *Angewandte Chemie International Edition* **2021,** *60* (44), 23496-23507.

75. Kirss, R. U.; Eisenschmid, T. C.; Eisenberg, R., Para hydrogen induced polarization in hydrogenation reactions catalyzed by ruthenium phosphine complexes. *Journal of the American Chemical Society* **1988,** *110* (25), 8564-8566.
76. Goldman, M.; Jóhannesson, H.; Axelsson, O.; Karlsson, M., Design and implementation of 13C hyper polarization from para-hydrogen, for new MRI contrast agents. *Comptes Rendus Chimie* **2006,** *9* (3-4), 357-363.
77. Eshuis, N.; Hermkens, N.; van Weerdenburg, B. J. A.; Feiters, M. C.; Rutjes, F. P. J. T.; Wijmenga, S. S.; Tessari, M., Toward nanomolar detection by NMR through SABRE hyperpolarization. *Journal of the American Chemical Society* **2014,** *136* (7), 2695-2698.
78. Fraser, R.; Rutjes, F. P. J. T.; Feiters, M. C.; Tessari, M., Analysis of complex mixtures by chemosensing NMR using para-hydrogen-induced hyperpolarization. *Accounts of Chemical Research* **2022,** *55* (13), 1832-1844.
79. Green, R. A.; Adams, R. W.; Duckett, S. B.; Mewis, R. E.; Williamson, D. C.; Green, G. G. R., The theory and practice of hyperpolarization in magnetic resonance using parahydrogen. *Progress in nuclear magnetic resonance spectroscopy* **2012,** *67*, 1-48.
80. Sellies, L.; Reile, I.; Aspers, R. L. E. G.; Feiters, M. C.; Rutjes, F. P. J. T.; Tessari, M., Parahydrogen induced hyperpolarization provides a tool for NMR metabolomics at nanomolar concentrations. *Chemical Communications* **2019,** *55* (50), 7235-7238.
81. Sellies, L.; Aspers, R. L. E. G.; Feiters, M. C.; Rutjes, F. P. J. T.; Tessari, M., Parahydrogen hyperpolarization allows direct NMR detection of α-amino acids in complex (bio) mixtures. *Angewandte Chemie* **2021,** *133* (52), 27160-27165.
82. Dey, A.; Charrier, B.; Ribay, V.; Dumez, J.-N.; Giraudeau, P., Hyperpolarized 1H and 13C NMR spectroscopy in a single experiment for metabolomics. *Analytical Chemistry* **2023,** *95* (46), 16861-16867.
83. Dey, A.; Charrier, B.; Martineau, E.; Deborde, C.; Gandriau, E.; Moing, A.; Jacob, D.; Eshchenko, D.; Schnell, M.; Melzi, R.; Kurzbach, D.; Ceillier, M.; Chappuis, Q.; Cousin, S. F.; Kempf, J. G.; Jannin, S.; Dumez, J.-N.; Giraudeau, P., Hyperpolarized NMR Metabolomics at Natural 13C Abundance. *Analytical Chemistry* **2020,** *92* (22), 14867-14871.
84. Ribay, V.; Charrier, B.; Croyal, M.; Cariou, B.; Hadjadj, S.; Boccard, J.; Cannet, C.; Dumez, J.-N.; Letertre, M. P. M.; Giraudeau, P., Hyperpolarized 13C NMR Metabolomics of Urine Samples at Natural Abundance Applied to Chronic Kidney Disease. *Journal of the American Chemical Society* **2024,** *147* (1), 644-650.
85. Iali, W.; Rayner, P. J.; Alshehri, A.; Holmes, A. J.; Ruddlesden, A. J.; Duckett, S. B., Direct and indirect hyperpolarisation of amines using para hydrogen. *Chemical science* **2018,** *9* (15), 3677-3684.
86. Shchepin, R. V.; Barskiy, D. A.; Coffey, A. M.; Goodson, B. M.; Chekmenev, E. Y., NMR signal amplification by reversible exchange of sulfur-heterocyclic compounds found in petroleum. *ChemistrySelect* **2016,** *1* (10), 2552-2555.
87. Dreisewerd, L.; Aspers, R. L. E. G.; Feiters, M. C.; Rutjes, F. P. J. T.; Tessari, M., Nmr discrimination of d-and l-α-amino acids at submicromolar concentration via parahydrogen-induced hyperpolarization. *Journal of the American Chemical Society* **2023,** *145* (3), 1518-1523.
88. Reimets, N.; Ausmees, K.; Vija, S.; Trummal, A.; Uudsemaa, M.; Reile, I., Parahydrogen hyperpolarized NMR detection of underivatized short oligopeptides. *Analyst* **2023,** *148* (21), 5407-5415.
89. Posthumus, T. B.; Engelke, U. F. H.; Aspers, R. L. E. G.; Merx, J.; Boltje, T. J.; Martens, J.; Wevers, R. A.; Feiters, M. C.; Rutjes, F. P. J. T.; Tessari, M., Semi-Targeted Nuclear Magnetic Resonance Metabolomics via Parahydrogen-Induced Hyperpolarization for Enhanced Sensitivity to Metabolic Composition. *Journal of the American Chemical Society* **2025**.

Chapter II

Metabolomic approach to investigate nicotine effects in a neurodegenerative cell model

2.1 Nicotine: friend or foe?

Nicotine (IUPAC name (S)-3-(1-methyl-2-pyrrolidinyl)pyridine) is a pyridine alkaloid, which represents approximately 95% of the total alkaloids in the leaves of the tobacco plant (*Nicotiana tabacum*). It is the primary psychoactive compound in tobacco smoke and plays a central role in both the initiation and maintenance of dependence. Consequently, nicotine is frequently implicated in the development of smoking-related addiction. It is well-established that smoking cigarettes elevates the risk of various health issues, including but not limited to cancers, [1, 2] atherosclerotic cardiovascular diseases, [3] respiratory diseases, [4] and diabetes. [5] Nevertheless, several studies have shown that nicotine has beneficial effects in certain diseases, possibly due to its anti-inflammatory and antiapoptotic properties. [6-9] It appears that nicotine's role in disease varies greatly depending on the specific condition and the mode of administration. Consequently, the scientific community remains divided on whether this alkaloid should be regarded as beneficial or harmful. [10] However, there is a broad consensus that nicotine positively influences brain function by enhancing several cognitive domains, including attention, learning, and memory. [11] As a result, it has shown potential in alleviating cognitive impairments associated with conditions such as Alzheimer's disease (AD), Parkinson's disease (PD), age-related memory disorders, schizophrenia, autism, and attention deficit hyperactivity disorder (ADHD). [12, 13] The role of nicotine is primarily attributed to its ability to stimulate nicotinic acetylcholine receptors (nAChRs), which are abundant in the brain and play a crucial role in cognitive function.

Nevertheless, nicotine is well known to cross both the blood-brain barrier and the cytoplasmic membrane due to its chemical structure and biophysical properties. Therefore, nicotine could directly affect mitochondrial respiration, cellular processes, and cellular signaling under proper pH conditions. [14] This suggests the existence of

potential alternative mechanisms of action, besides direct receptor stimulation, which remain poorly understood and need further investigation.

Accordingly, nicotine has been shown to affect mitochondrial function both *in vitro* and *in vivo*. Again, the exact mechanisms underlying nicotine's effects on mitochondrial function remain largely unknown. [15, 16] Mitochondrial-mediated energy homeostasis is pivotal for brain function and cognition.[16, 17] Therefore, it may be essential to clarify the impact of nicotine on these organelles to provide additional insights into its action in the brain.

In this context, pharmacometabolomics – thanks to its untargeted nature – represents a powerful tool to explore the mechanism of action of nicotine. [18, 19]

Previous metabolomics studies have examined the effects of nicotine on mouse brains to understand its rewarding properties better, revealing alterations in neurotransmitter levels, energy metabolism, and membrane function.[20] More recently, Uhlig *et al.* employed mass spectrometry-based metabolomics to examine nicotine metabolism in THP-1 monocytes, offering new insights into the physiological responses associated with various nicotine products, including cigarettes and snuff. [21]

Despite these advances, the mechanisms underlying nicotine's impact on cognitive performance remain poorly understood.

2.2 Nicotine in Alzheimer's disease

AD is the primary neurodegenerative disease spreading worldwide, and it is estimated that up to 107 million subjects will be affected by 2050. [22]

One of the main histopathological hallmarks of AD is amyloid plaque deposition in the brain, whose aggregation seems to occur decades before the disease's onset. [23] Amyloid peptide (Aβ) is derived from a large protein called amyloid precursor protein (APP). In the neurons of subjects with AD, APP is cleaved first by β-secretase and then by γ-secretase, resulting in the production of β-amyloid 40 and β-amyloid 42 (Aβ (1-40), Aβ(1–42)). [24] These peptides undergo a conformational transition to aggregate around meningeal and cerebral vessels and grey matter. The extracellular plaques formed disrupt neural function, leading to memory loss and cell death. [25, 26]

Despite several epidemiological studies demonstrating that cigarette smoke is a factor in predisposing people to neurodegenerative diseases such as AD, [27] nicotine has been widely studied for its ability to improve cognitive performance, including

attention, working memory, and episodic memory, both in preclinical models and in human studies. [28] Furthermore, nicotine treatment has been shown to reduce Aβ accumulation in the cortex and hippocampus in rat models. [29] Published studies in humans have reported that intravenous and subcutaneous nicotine administration in AD patients improved several cognitive tasks, such as visual attention and perception, [30, 31] mood and lexical tasks, [32] but not memory. [33]

The mechanism of action responsible for the beneficial effect of nicotine in AD preclinical models and patients is still questioned, although some hypotheses have been proposed: i) nAChRs are significantly reduced in the AD brain, [34] suggesting that nicotine's positive effects may result from the upregulation of these receptors; [35, 36] ii) Nicotine decreases the accumulation of Aβ in the cortex and hippocampus of mice models of AD, preventing the activation of NF-κB and c-Myc by inhibiting the activation of MAP kinases (MAPKs). Thus, inducible nitric oxide synthases (NOS) and NO production activity are downregulated. [37] iii) Furthermore, nicotine binding to α7nAChR prevents Aβ interaction with nicotine receptors, which causes the inhibition of α7nAChR-dependent calcium activation and the acetylcholine release, two processes critically involved in memory and cognitive functions. [38] iv) Enhanced oxidative stress characterized the brain of AD patients, and some studies suggest that the beneficial effects of nicotine in neurodegenerative disease may be, at least partly, due to an antioxidant mechanism; [39] v) The neuroprotective effect of nicotine resides in its antiaggregant properties. Structural studies investigating the interaction of Aβ peptides with nicotine and its derivatives demonstrate that nicotine slows down the aggregation of Aβ (1–42) and Aβ (25–35) peptides. [40, 41]

Once again, the specific mechanisms underlying the protective effects of nicotine – reported across *in vitro*, preclinical, and clinical studies – in AD remain incompletely understood.

2.3 The aims of the study

To address the existing gap in understanding the effects of nicotine on cognitive function and its potential protective role against Aβ(1–42) toxicity, we investigated its mechanism of action through a pharmacometabolomic approach.

In recent years, pharmacometabolomics has emerged as an innovative approach for investigating the molecular mechanisms and toxicity profiles of both approved drugs

and novel molecular entities. [42, 43] Indeed, an intriguing aspect of metabolomics is its untargeted nature, potentially enabling the discovery of unexplored connections among disease, therapeutics, and biological pathways. NMR spectroscopy represents a robust and suitable technique for metabolomic studies, enabling the simultaneous qualitative and quantitative identification of low-molecular-weight compounds in biofluids and other biological matrices. [44-46]

Although several metabolomic studies on nicotine have been conducted, this work represents, to the best of our knowledge, the first comprehensive analysis performed on a human neuron-like cellular system. We employed the SH-SY5Y cell line, an *in vitro* model widely used in neuroscience research, particularly in studies on neurodegenerative diseases and nicotine exposure. [47, 48] SH-SY5Y cells express nAChRs on their cytoplasmic membrane, particularly the α3, α5, and α7 subunits for the alpha component, and β2 and β4 for the beta component (the Human Protein Atlas).

Given the importance of metabolic equilibrium between intracellular and extracellular compartments for proper cellular function, we integrated data from intracellular metabolites (endometabolome) and extracellular metabolites (exometabolome) to gain a deeper understanding of the cells' metabolic behavior. To this end, we built for the first time a statistical model that combines the quantification matrices derived from the analysis of endometabolome and exometabolome spectra.

Figure 2.1 illustrates the workflow followed for this study:

1. We preliminarily analyzed the effect of nicotine alone on SH-SY5Y compared to untreated cells. In this preliminary analysis, we observed that nicotine primarily influences phospholipid and sphingolipid metabolism, as well as mitochondrial function. [49]

Based on these findings, we extended our investigation to a pathological context, specifically AD. To gain new insights into the molecular mechanism underlying the neuroprotective action of nicotine in AD, we analyzed SH-SY5Y neuroblastoma cells treated with nicotine in the presence of Aβ(1–42), the main amyloid peptide that aggregates in AD brain.

2. We first confirmed that our cellular model could reproduce the metabolic alterations typical of AD. [50-53]
3. Then, we analyzed the effect of nicotine in the presence of Aβ(1–42). Interestingly, our data show a rebalancing of the metabolic state of SH-SY5Y

cells pretreated with nicotine and incubated with Aβ(1–42) toward that of healthy control cells. A careful analysis of our data to understand how nicotine may impact different sides of cellular metabolism suggests significant effects of the alkaloid on (i) amino acid metabolism, particularly those involved in neurotransmission, (ii) energy metabolism, and (iii) membrane phospholipid metabolism.

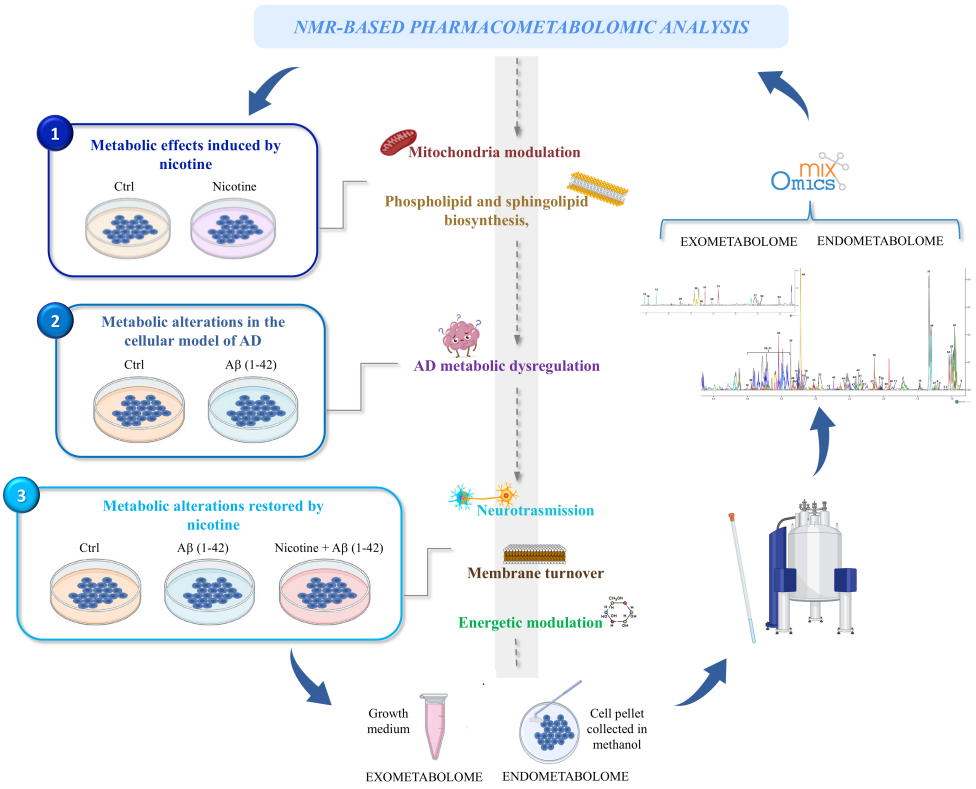

Figure 2.1 *Experimental workflow. NMR Metabolomics was the approach used to evaluate the mechanism of action of nicotine in absence and in presence of a pathological insult, i.e. amyloid peptide (Aβ(1–42)).*

2.4 Results

2.4.1 Impact of nicotine on SH-SY5Y cell viability

Initially, we performed a viability test to determine the effect of nicotine on SH-SY5Y cell survival. Since metabolomic analysis results depend heavily on treatment conditions, we deemed this preliminary step essential. The viability test helps us identify the optimal nicotine concentration and exposure duration for sample preparation in metabolomics analysis. The bar graph in **Figure 2.2A** shows that nicotine significantly reduces cell viability at concentrations above 1.30 mM, with an IC_{50} of 5.58 ± 0.34 mM (**Figure 2.2B**).

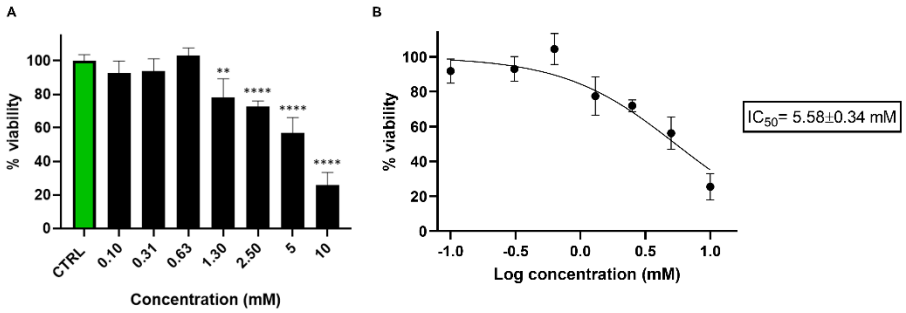

Figure 2.2 *(**A**) Bar graph showing the percentage of viable SH-SY5Y cells 24 hours after treatment with nicotine (0.10–10 mM). Cell viability was assessed using the CCK-8 assay and expressed as the percentage of viable cells in treated cultures relative to untreated controls (CTRL). Data are presented as mean ± standard deviation (SD) from three independent experiments. Statistical analysis was performed using one-way ANOVA followed by Dunnett's multiple comparisons test, using GraphPad Prism 8.0 software (San Diego, CA, USA). Statistical significance was set $p < 0.05$. Asterisks indicate significance levels compared to CTRL: $p < 0.01$ (**), and $p < 0.0001$ (****). (**B**) Nicotine IC_{50} was calculated using GraphPad Prism 8.0 software by nonlinear regression of dose-response inhibition.*

2.4.2 Nicotine impacts on lipid metabolism, mitochondrial function, and amino acid concentrations

^{1}H-NMR spectroscopy was employed to investigate the metabolomic profiles of cellular extracts and growth medium, representing the endometabolome and exometabolome, respectively. SH-SY5Y cells were treated with 100 µM nicotine for 24 h prior to sample collection for metabolomic analysis. This concentration was selected based on cell viability assays, which confirmed that it does not compromise SH-SY5Y cell viability. It was therefore considered appropriate for investigating potential metabolomic alterations induced by nicotine under non-cytotoxic conditions. **Figures 2.3A** and **B** show representative 1D ^{1}H NOESY NMR spectra of the cellular endo- and exo-metabolome, respectively. [54]

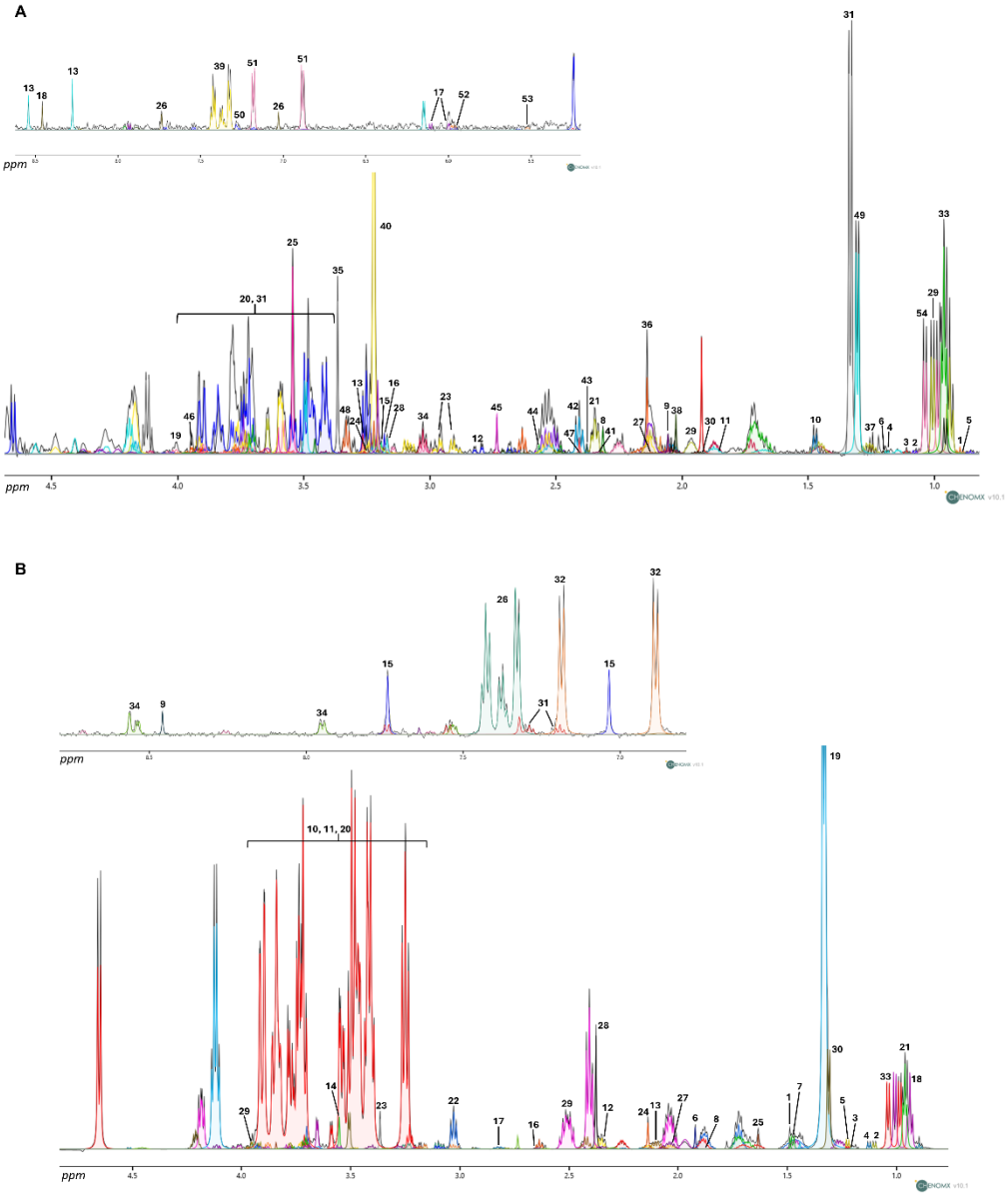

Figure 2.3 *(**A**) Representative 1D ^{1}H NOESY spectrum illustrating the polar cellular extracts (endometabolome) obtained from SH-SY5Y cells treated with nicotine. A total of 54 metabolites were identified in the endometabolome: 1: 2-Hydroxybutyric acid; 2: 2-Methyl-3-ketovaleric acid; 3: 2-Oxobutyrate; 4: 3-Hydroxybutyrate; 5: 3-Methyl-2-oxovalerate; 6: 5,6-Dihydrothymine; 7: Acetate; 8: Acetoacetate; 9: Acetylcysteine; 10: Alanine; 11: Arginine; 12: Aspartate; 13: ATP; 14: Betaine; 15: Carnitine; 16: Choline; 17: Citicoline; 18: Formate; 19: Fructose; 20: Glucose; 21: Glutamate; 22: Glutamine; 23: Glutathione; 24: Glycerophosphocholine; 25: Glycine; 26: Histidine; 27: Homocysteine; 28: Isobutyryl-L-carnitine; 29: Isoleucine; 30: Isovalerate; 31: Lactate; 32: Lactose; 33: Leucine; 34: Lysine; 35: Methanol; 36: Methionine; 37: Methylmalonate; 38: N-Acetyl-L-aspartic acid; 39: Phenylalanine; 40: Phosphorylcholine; 41: Proline; 42: Pyroglutamate; 43: Pyruvate; 44: Riboflavin; 45: Sarcosine; 46: Serine; 47: Succinate; 48: Taurine; 49: Threonine; 50: Tryptophan; 51: Tyrosine; 52: UDP-glucose; 53: UDP-N-Acetylglucosamine; 54: Valine. (**B**) Representative 1D ^{1}H NOESY spectrum of growth medium (exometabolome) obtained from SH-SY5Y cells treated with nicotine. A total of 34 metabolites were identified in the exometabolome: 1: 2-Aminoisobutyric acid; 2: 2-Methyl-3-ketovaleric acid; 3: 3-Hydroxybutyrate; 4: 3-Methyl-2-oxovalerate; 5: 5,6-Dihydrothymine; 6: Acetate; 7: Alanine;*

8: Arginine; 9: Formate; 10: Fructose; 11: Glucose; 12: Glutamate; 13:Glutamine; 14: Glycine; 15: Histidine; 16: Homocysteine; 17: Homocystine; 18: Isoleucine; 19: Lactate; 20: Lactose; 21: Leucine; 22: Lysine; 23: Methanol; 24: Methionine; 25: N-Methyl-a-aminoisobutyric acid; 26: Phenylalanine; 27: Proline; 28: Pyroglutamate; 29: Serine; 30: Threonine; 31: Tryptophan; 32: Tyrosine; 33: Valine; 34: Nicotine. Spectra were acquired at 600 MHz. The different colours denote individual metabolites identified. The figure of spectra has been directly exported from Chenomx NMR Suite v10.1 software.

^{1}H chemical shift assignment, conducted with Chenomx NMR-Suite (Chenomx NMR suite, v10.1, Edmonton, AB, Canada), detects the presence of 54 metabolites in the endometabolome and 34 in the exometabolome. The metabolites were quantified using NMRProcFlow, [55] with the internal standard trimethylsilyl propanoic acid (TSP-d_4) added to the sample as a reference compound.

After normalization by sum, Log transformation, and Pareto scaling, the concentration data matrices were analyzed using both univariate and multivariate approaches.

As shown in the Volcano plot, the cellular medium of SH-SY5Y cells treated with nicotine exhibits a lower concentration of 3-hydroxybutyrate (**Figure 2.4A**). On the other hand, the intracellular compartment reports higher concentrations of glycine, L-aspartyl-L-phenylalanine, sarcosine, and phosphorylcholine (PC), while lower concentrations of lactose and proline (**Figure 2.4B**). A comprehensive overview of the relative concentrations of all metabolites is shown in the heatmaps (**Figures 2.5A, 2.5B**).

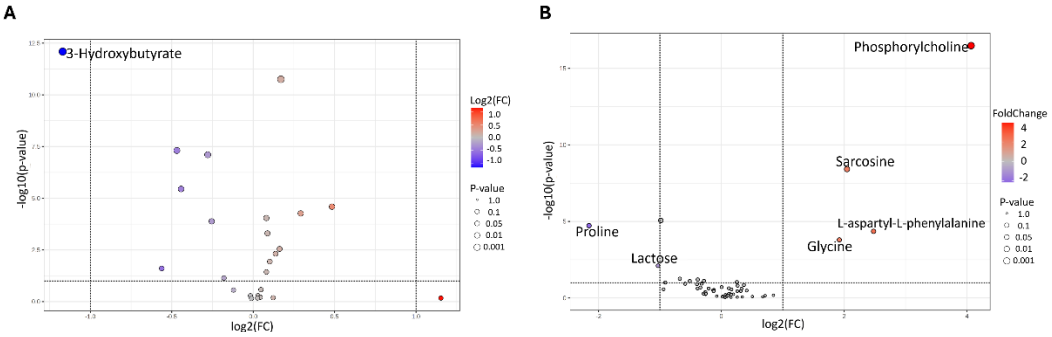

Figure 2.4 *Volcano plot analysis of metabolic changes in the exo- (**A**) and endo-metabolome (**B**) of SH-SY5Y cells treated with nicotine vs untreated cells. Each point on the volcano plot was based on p-value and fold-change value, set at 0.05 and 2.0, respectively. Red points identify up-regulated metabolites, whereas blue points identify down-regulated metabolites.*

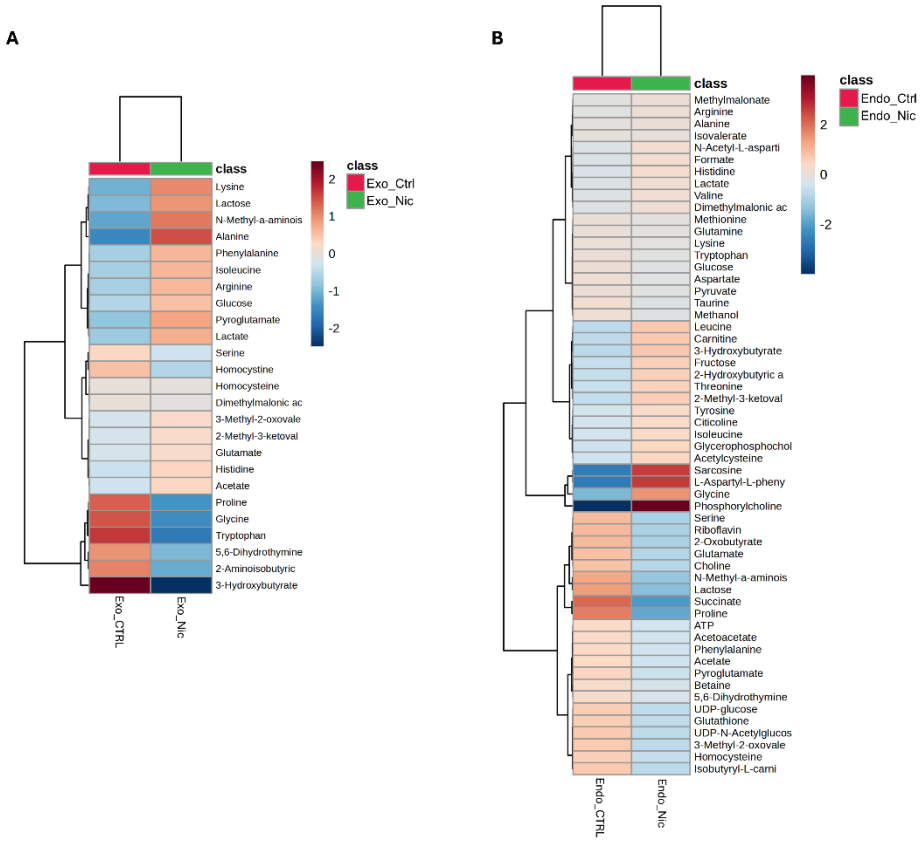

Figure 2.5 *Heatmaps of changed metabolites in SH-SY5Y cells treated with nicotine, for exo- (**A**) and endometabolome (**B**). The color of each section corresponds to a concentration value of each metabolite calculated by a normalized concentration matrix (red, up-regulated; blue, down-regulated).*

Considering the dynamic interchange between intracellular and extracellular compartments, and following an initial exploration of these compartments separately, we performed a supervised, integrated analysis using the sparse Partial Least Squares Discriminant Analysis (sPLS-DA) approach.

Figure 2.6A shows a sPLS-DA score plot representing the metabolomic profile of the combined cellular compartments of SH-SY5Y cells treated with nicotine and control cells exposed to the vehicle. The Cartesian space, described by the first and second principal components (PC1; PC2), explains 22% and 25% of the dataset variance, consistent with a net metabolomic difference between the endo- and exo-metabolome of treated and untreated cells. The model's validity was evaluated using a cross-validation approach, based on Q^2 parameter (0.58 and 0.55 Q^2 indices on PC1 and PC2, respectively). Furthermore, the separation model area was validated by calculating the Mahalanobis distance, maximum distance, and centroids (**Figure S1**).

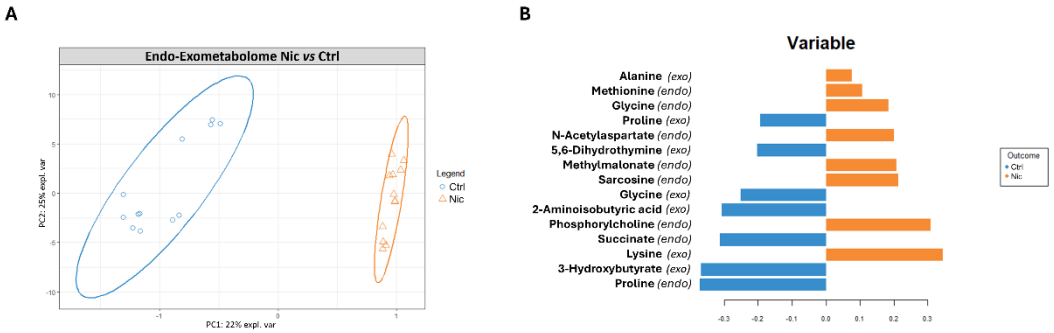

Figure 2.6 *(**A**) sPLS-DA score scatter plots related to the metabolomic profile of combined cellular compartments related to SH-SY5Y treated with nicotine for 24 h (Nic) vs. control cells (Ctrl). The cluster analyses are reported in the Cartesian space described by the principal components PC1:22% and PC2:25%. sPLS-DA was evaluated using cross-validation (CV) analysis. CV tests performed according to the sPLS-DA statistical protocol show a significant cluster separation (0.98 and 0.79 accuracy values on PC1 and PC2, with positive 0.58 and 0.55 Q^2 indices, respectively). (**B**) Loadings barplot related to the combined matrices of endo- and exo-metabolome. The variables responsible for metabolomic profile differences are ordered according to values of increasing importance from bottom to top. Colors indicate the cluster where the median is maximum for each metabolite (orange: nicotine; blue: control).*

The bar plot (**Figure 2.6B**), reporting the discriminating metabolites classified by their loading values, indicates that nicotine-exposed cells exhibit, in the extracellular environment, higher concentrations of alanine and lysine and lower concentrations of proline, 5,6-dihydrothymine, glycine, 2-aminoisobutyric acid, and 3-hydroxybutyrate. Conversely, in response to nicotine treatment, the intracellular compartment shows increased concentrations of methionine, glycine, N-acetylaspartate (NAA), sarcosine, PC, and reduced concentrations of succinate and proline.

To identify the biochemical pathways affected by nicotine action, in agreement with the observed metabolite modifications, we performed an Enrichment pathway analysis of intracellular metabolites (**Figure 2.7, Table S1**).

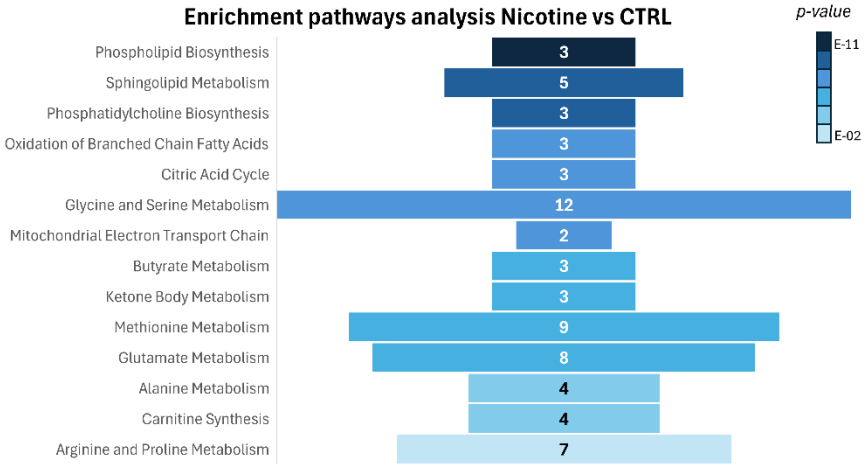

Figure 2.7 *Enrichment pathways analysis, showing the biochemical pathway affected by nicotine treatment: the discriminative pathways are ranked according to p-value and number of hits reported in the bars.*

Consistent with a significant increase in PC concentration, enrichment analysis reveals effects on biochemical pathways related to phospholipid biosynthesis, specifically *sphingolipid* and *phosphatidylcholine biosynthesis*, highlighting a role for nicotine in inducing an important lipid remodelling, modifying lipid metabolism and altering cell membrane structure. On the other hand, evident effects are observable in amino acid metabolism (*methionine, arginine, and proline metabolism; glycine and serine metabolism; glutamate and alanine metabolism*) and mitochondrial activity, particularly in the *mitochondrial electron transport chain*, *oxidation of branched-chain fatty acids*, and *citric acid metabolism*.

2.4.3 Nicotine protects neuroblastoma cells from Aβ(1–42) toxicity

Before evaluating the protective effect of nicotine against Aβ(1–42) recombinant protein toxicity, the impact of Aβ(1–42) on SH-SY5Y cell viability was assessed, revealing an IC_{50} value of 46.75 ± 4.01 μM, as determined by dose–response analysis (**Figure S2**).

To estimate the protective effect of nicotine on SH-SY5Y neuroblastoma cells a viability assay was performed. We confirmed the protective effect of nicotine against Aβ(1–42) toxicity, as reported in the literature. [56, 57] **Figure 2.8** shows that SH-SY5Y neuroblastoma cells treated with Aβ(1–42) (25 μM) have 70.12 ± 3.07% survival. The

presence of 1mM and 100µM nicotine preserved cell viability up to 90.75 ± 3.14% and 93.75 ± 1.22%, respectively.

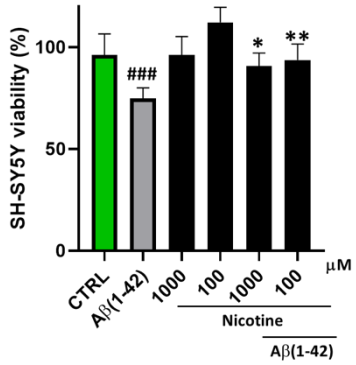

Figure 2.8 *Neuroprotective effect of nicotine against Aβ(1–42)-induced cytotoxicity. Cell viability was examined by the CCK-8 assay. SH-SY5Y cells were exposed to nicotine (1 mM and 100 µM) for 24 h before administration of Aβ (1- 42) recombinant monomer 25 µM for an additional 48 h. The viability variations were calculated as the percentage of viable cells in treated cultures compared to untreated ones (CTRL). Results are shown as mean ± standard deviation (SD) from three independent experiments.* $^{###}$ *denote respectively p < 0.001 vs. Ctrl; *, ** denote respectively p < 0.05 and p < 0.01 vs. Aβ(1–42).*

2.4.4 Aβ(1–42) disrupts energetic pathways, amino acid metabolism, and membrane stability

To evaluate the effects of Aβ(1–42) on SH-SY5Y cells, we analyzed the metabolic profiles of cells exposed to Aβ(1–42) compared with those of control cells treated with the vehicle alone (CTRL). ^{1}H NMR spectra of intracellular extracts (endometabolome) and extracellular media (exometabolome) were collected (**Figures 2.9A, B**), and the ^{1}H resonance assignment resulted in a metabolite matrix including, for each sample, the intracellular and extracellular metabolite concentrations.

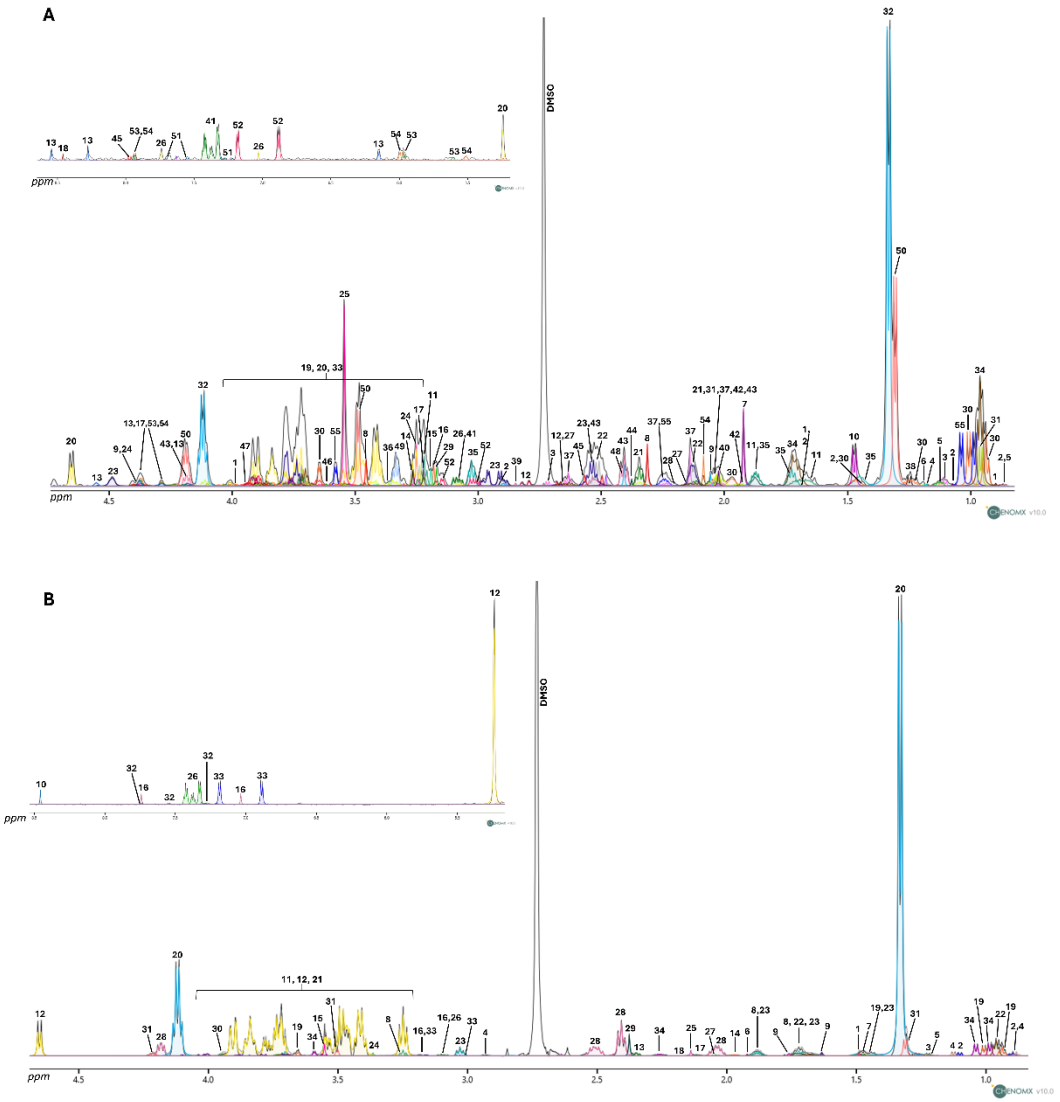

Figure 2.9 *(**A**) Representative 1D ^{1}H NOESY spectrum of the polar cellular extracts of SH-SY5Y cells (endometabolome). A total of 55 metabolites were identified in the endometabolome: 1: 2-Hydroxybutyrate; 2:2-Methyl-3-ketovaleric acid; 3: 2-Oxobutyrate; 4: 3-Hydroxybutyrate; 5: 3-Methyl-2-oxovalerate; 6: 5,6-Dihydrothymine; 7: Acetate; 8: Acetoacetate; 9: Acetylcysteine; 10: Alanine; 11: Arginine; 12: Aspartate; 13: ATP; 14: Betaine; 15: Carnitine; 16: Choline; 17: Citicoline; 18: Formate; 19: Fructose; 20: Glucose; 21: Glutamate; 22: Glutamine; 23: Glutathione; 24: Glycerophosphocholine; 25: Glycine; 26: Histidine; 27: Homocysteine; 28: Homocystine; 29: Isobutyryl-L-carnitine; 30: Isoleucine; 31: Isovalerate; 32: Lactate; 33: Lactose; 34: Leucine; 35: Lysine; 36: Methanol; 37: Methionine; 38: Methylmalonate; 39: N,N-Dimethylformamide; 40: N-Acetyl-L-aspartic acid; 41: Phenylalanine; 42: Proline; 43: Pyroglutamate; 44: Pyruvate; 45: Riboflavin; 46: Sarcosine; 47: Serine; 48: Succinate; 49: Taurine; 50: Threonine; 51: Tryptophan; 52: Tyrosine; 53: UDP-glucose; 54: UDP-N-Acetylglucosamine; 55: Valine. (**B**) Representative 1D ^{1}H NOESY spectrum of and conditioned growth medium (exometabolome). A total of 34 metabolites were identified in the exometabolome: 1: 2-Aminoisobutyric acid; 2: 2-Methyl-3-ketovaleric acid; 3: 3-Hydroxybutyrate; 4: 3-Methyl-2-oxovalerate; 5: 5,6-Dihydrothymine; 6: Acetate; 7: Alanine; 8: Arginine; 9: Dimethylallylpyrophosphate; 10: Formate; 11: Fructose; 12: Glucose; 13: Glutamate; 14: Glutamine; 15: Glycine; 16: Histidine; 17: Homocysteine; 18: Homocystine; 19: Isoleucine; 20: Lactate; 21: Lactose; 22: Leucine; 23: Lysine; 24: Methanol; 25: Methionine; 26: Phenylalanine; 27: Proline; 28: Pyroglutamate; 29: Pyruvate; 30: Serine; 31: Threonine; 32: Tryptophan; 33: Tyrosine; 34: Valine. The*

spectra are acquired at 600 MHz and T = 310 K. The continuous black lines represent the experimental spectra, whereas the individual metabolites - identified with the Chenomx NMR Suite v10.1 software - are denoted by different colors. The figure of spectra has been directly exported from Chenomx NMR Suite v10.1 software.

Figures 2.10A and **2.10B** show the Volcano Plots for the endo- and exometabolome of cells incubated with Aβ(1–42). The quantification of the metabolite concentration reveals an increase in pyruvate, succinate, isobutyryl-carnitine, and homocysteine and a reduction of pyroglutamate, taurine, and carnitine in the endometabolome. Moreover, an increase in threonine and a decrease in fructose were observed in the exometabolome.

Based on univariate statistical analysis, sarcosine appears to increase and serine to decrease in both endo- and exo-metabolomes of SH-SY5Y cells incubated with Aβ(1–42); conversely, tryptophan concentration increases in the intracellular compartment and decreases in the extracellular compartment.

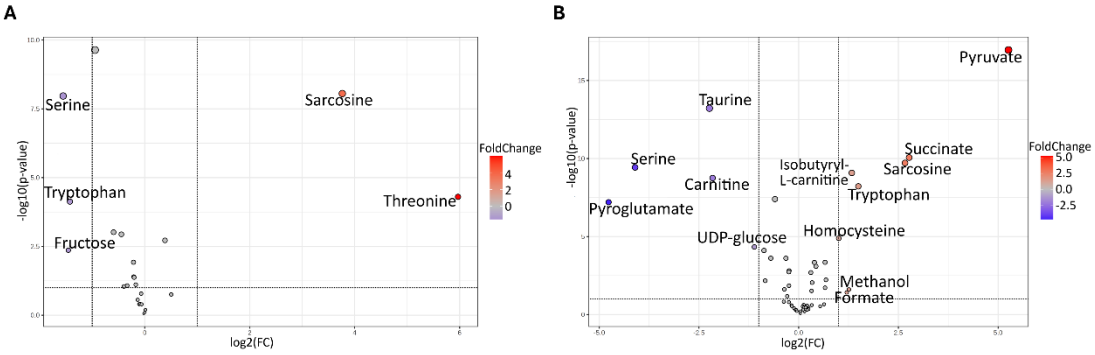

Figure 2.10 *Volcano plot analysis of metabolic changes in the exo (**A**) and endometabolome (**B**) of SH-SY5Y cells incubated with Aβ(1–42) vs. control cells. Each point on the volcano plot was based on p-value and fold-change values, set at 0.05 and 2.0, respectively. Red points identify up-regulated metabolites, whereas blue points identify down-regulated metabolites.*

Volcano plot results were confirmed by heatmap analysis, which indicated, using a specific color code, the downregulation (in blue) and upregulation (in red) of all metabolites detected in the spectra (**Figures 2.11A, B**).

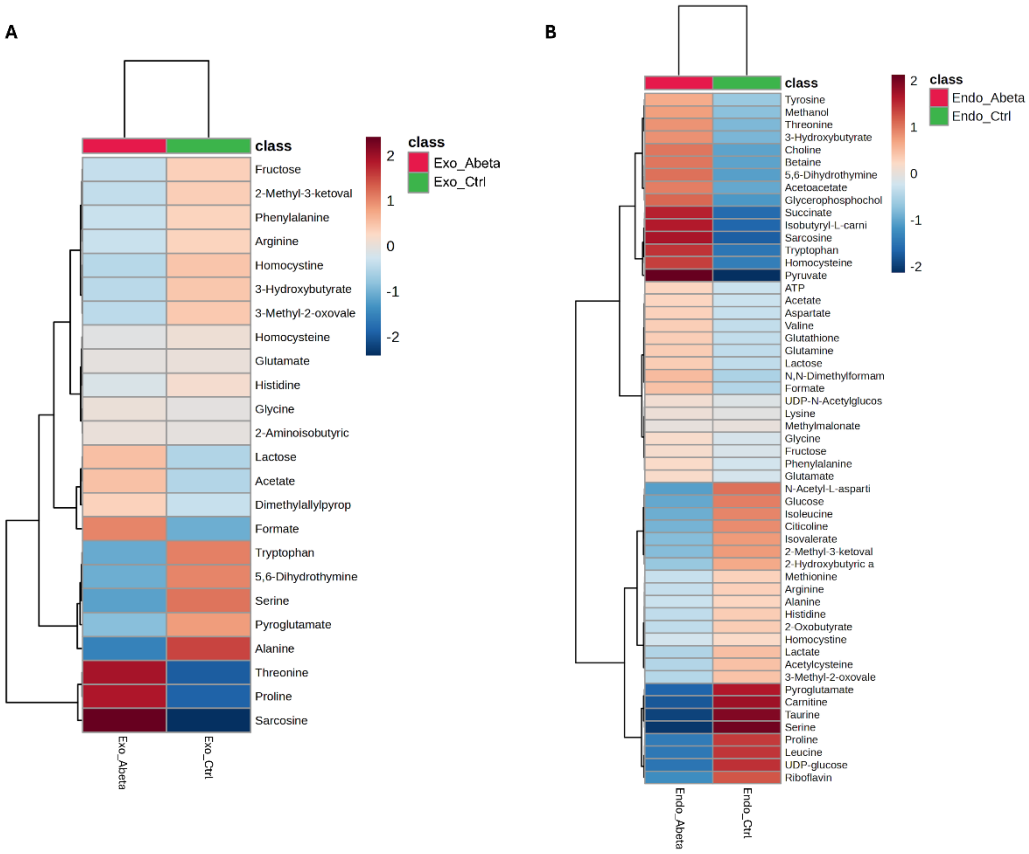

Figure 2.11 *Heatmaps of changed metabolites in SH-SY5Y cells treated with Aβ(1–42), for exo- (**A**) and endometabolome (**B**). The color of each section corresponds to a concentration value of each metabolite calculated by a normalized concentration matrix (red, up-regulated; blue, down-regulated).*

Using a combined approach to analyze the metabolomic profiles of intra- and extracellular compartments, we derived an sPLS-DA score plot representing the metabolomic profiles of the cell compartments of SH-SY5Y cultures incubated with Aβ(1–42) *vs.* untreated controls (**Figure 2.12A**). The Cartesian space is described by the first and second main components (PC1; PC2), which explain 40% and 16% of the dataset's variance, respectively. The model's validity was evaluated using a cross-validation approach, using the Q^2 parameter (0.80 and 0.90 on PC1 and PC2, respectively). Furthermore, the separation model area was validated by calculating the Mahalanobis distance, maximum distance, and centroids (**Figure S3**). The separation of clusters indicates that Aβ(1–42) perturbs both exometabolome and endometabolome of the cell cultures.

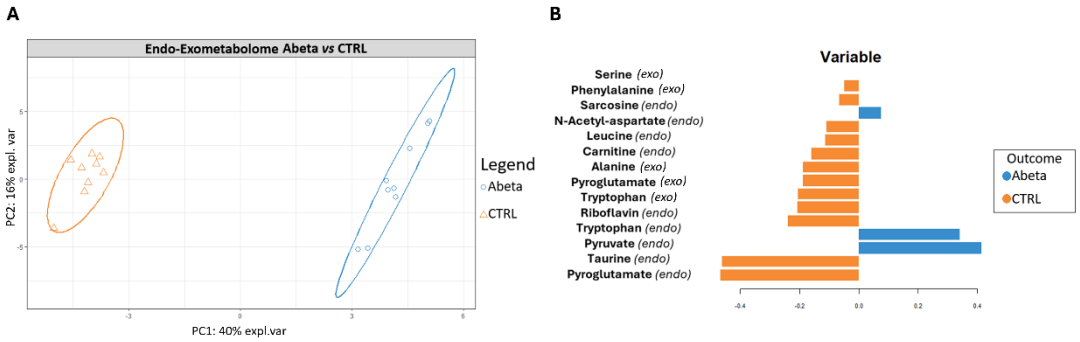

Figure 2.12 *(**A**) sPLS-DA score scatter plots related to the combined matrices of endo and exometabolome of SH-SY5Y cells treated with Aβ(1–42) (Abeta) vs. control cells (CTRL). The cluster analyses are reported in the Cartesian space described by the principal components PC1:40% and PC2:16%. sPLS-DA was evaluated using cross-validation (CV) analysis. CV tests performed according to the sPLS-DA statistical protocol show a significant cluster separation (1.0 accuracy values on PC1 and PC2, with positive 0.80 and 0.90 Q^2 indices, respectively). (**B**) Loadings barplot related to the combined matrices of endo and exometabolome. The variables responsible for metabolomic profile differences are ordered according to values of increasing importance from bottom to top. Colours indicate the cluster where the median is maximum for each metabolite (blue: Abeta; orange: CTRL).*

The variables' loadings were calculated to identify the metabolites responsible for cluster separation. The bar plot, shown in **Figure 2.12B**, reports the discriminating metabolites, classified by their loading values, and the clusters with the highest concentration of each metabolite. The data indicated a reduction in the concentrations of taurine, riboflavin, carnitine, leucine, and N-acetylAspartate (NAA) in the endo-metabolome of cells treated with Aβ(1–42); on the contrary, an increase in the pyruvate and sarcosine concentrations was observed with respect to control cells. Furthermore, the exometabolome of cells incubated with Aβ(1–42) shows lower alanine and phenylalanine concentrations than those of untreated cells. The combined analysis also showed an influence of Aβ(1–42) in reducing the concentrations of pyroglutamate and serine in both cellular compartments. In contrast, tryptophan concentration is reduced in exometabolome and increased in endometabolome (**Figure 2.12B**).

Pathway analysis of the endometabolome's quantified metabolites showed an impact of Aβ(1–42) on membrane lipid metabolism, specifically in *Phosphatidylethanolamine biosynthesis and sphingolipid metabolism.* Enrichment Pathways also points to energetic metabolic dysregulation, mainly linked to the *citric acid cycle, ketone body metabolism, pyruvate metabolism, glycolysis*, and the *urea cycle*. In addition, dysregulation of several amino acid pathways, including *glutamate*

metabolism, glycine and serine metabolism, and *methionine metabolism*, has been reported. (**Figure 2.13, Table S2**)

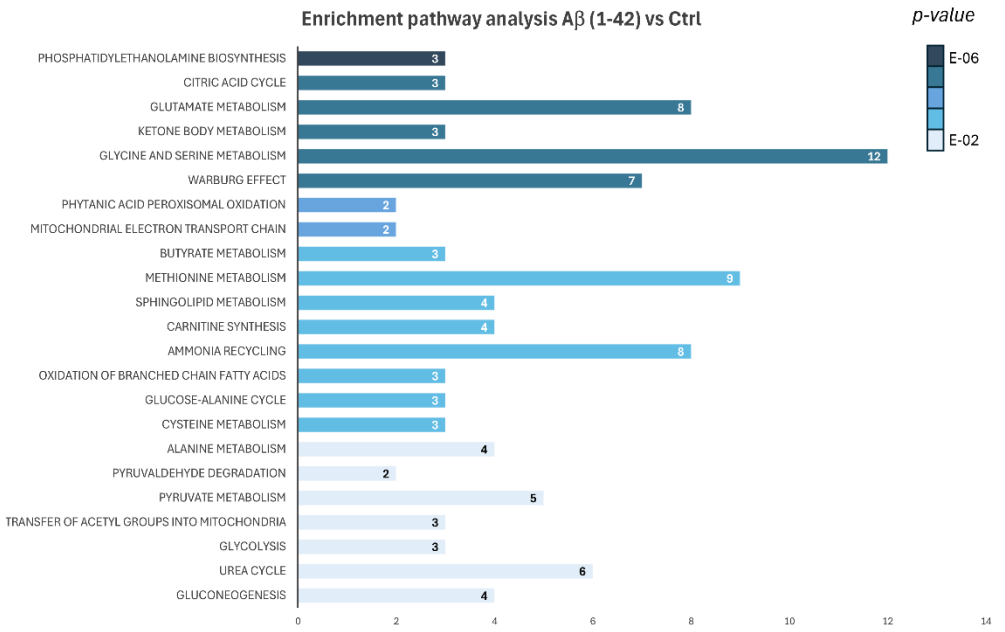

Figure 2.13 *Enrichment pathways analysis showing the biochemical pathway affected by Aβ(1–42) treatment: the discriminative pathways are ranked according to p-value and number of hits reported in the bars.*

2.4.5 Nicotine reverts AD dysmetabolism, acting on the whole metabolome

To evaluate the potential of nicotine to modulate dysmetabolism caused by Aβ(1–42), we treated SH-SY5Y cells with nicotine for 24 hours before exposure to Aβ(1–42). Metabolite concentrations in the intra- and extracellular compartments, derived from quantitative analysis of ^{1}H NMR spectra, were analyzed using multivariate statistical analysis (MVA). To examine the impact of nicotine on Aβ(1–42)-induced alterations on SH-SY5Y metabolism, we conducted a comparative study of the endo and exometabolome profiles of three distinct cell groups: (i) cells treated with nicotine and then incubated with Aβ(1–42) (Abeta_Nic); (ii) cells incubated with Aβ(1–42) alone (Abeta); and (iii) untreated cells (CTRL).

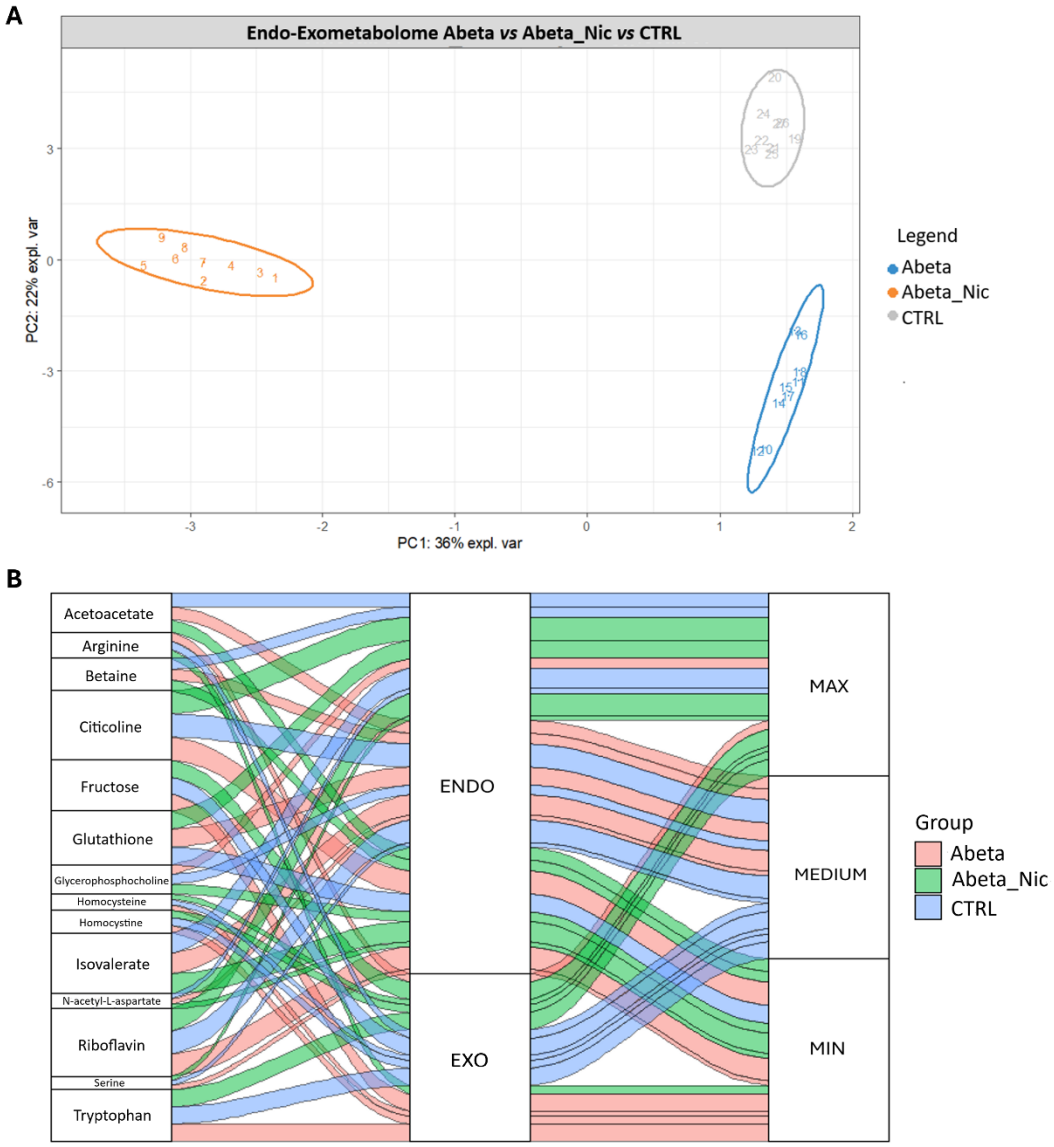

Figure 2.14 *(**A**) sPLS-DA score scatter plots related to the combined matrices of endo and exometabolome of SH-SY5Y cells treated with Aβ(1–42) in blue (Abeta) vs. cells pretreated with nicotine before being incubated with Aβ(1–42) in orange (Abeta_Nic) vs. control cells in grey (CTRL). The cluster analyses are reported in the Cartesian space described by the principal components PC1:36% and PC2:22%. sPLS-DA was evaluated using cross-validation (CV) analysis. CV tests performed according to the sPLS-DA statistical protocol show a significant cluster separation (0.60 and 1.0 accuracy values on PC1 and PC2, with positive 0.77 and 0.95 Q^2 indices, respectively). (**B**) Alluvial plot reporting metabolites discriminating clusters analyzed in sPLS-DA and classified according to loading value. The first column reports the discriminating metabolites, the second column is the cellular compartment, and the third column is the concentration change. The maximum concentrations in the comparison between the three clusters are indicated as "Max", the intermediate as "Medium", and the minimum as "Min". The lines connect the metabolite, the cell compartment in which it is discriminated, and the column representing quantitative variation. Each line is reported in pink if the metabolite has the variation in the clusters of cells incubated with Aβ(1–42); in green if the variation is typical of cells pretreated with nicotine before being incubated with Aβ(1–42) and in blue if the variation is typical of control cells.*

The combined omic analysis using sPLS-DA shows a clear separation of the three metabolomic profiles. This indicates that the effect of nicotine on cells incubated with Aβ(1–42) differs from that in control cells, which represent the healthy cellular phenotype (**Figure 2.14A**). The model's validity was assessed via cross-validation using Q^2 (0.77 and 0.95 Q^2 indices on PC1 and PC2, respectively) and calculating Mahalanobis distance, maximum distance, and centroids (**Figure S3**).

The alluvial plot shown in **Figure 2.14B** reveals that the endometabolome of cells pretreated with nicotine in the absence of Aβ(1–42) has high concentrations of citilcoline, glutathione, riboflavin, and serine. In contrast, the endometabolome of this group of cells includes minimal concentrations of acetoacetate, betaine, glycerophoshocholine, isovalerate, and N-acetylaspartate. Furthermore, the exometabolome of SH-SY5Y cells incubated with nicotine and Aβ(1–42) shows the highest concentrations of fructose, homocysteine, and tryptophan, while low concentration of arginine compared to the same cells incubated with Aβ(1–42) in the absence of nicotine or compared to the untreated cells.

Heatmaps (**Figures 2.15A, B**) based on average concentrations of the cytoplasmic and extracellular metabolite concentrations of the three groups of cells under investigation show that the metabolomic profile of the cells treated with Aβ(1–42) in the presence of nicotine is very similar to that of the control cells. Indeed, the exometabolome and endometabolome of neuroblastoma cells treated with nicotine and Aβ(1–42) cluster with the control cells' metabolomic profile. This suggests that nicotine induces metabolic changes towards a phenotype more similar to healthy controls rather than the pathological AD condition, represented by cells exposed only to Aβ(1–42).

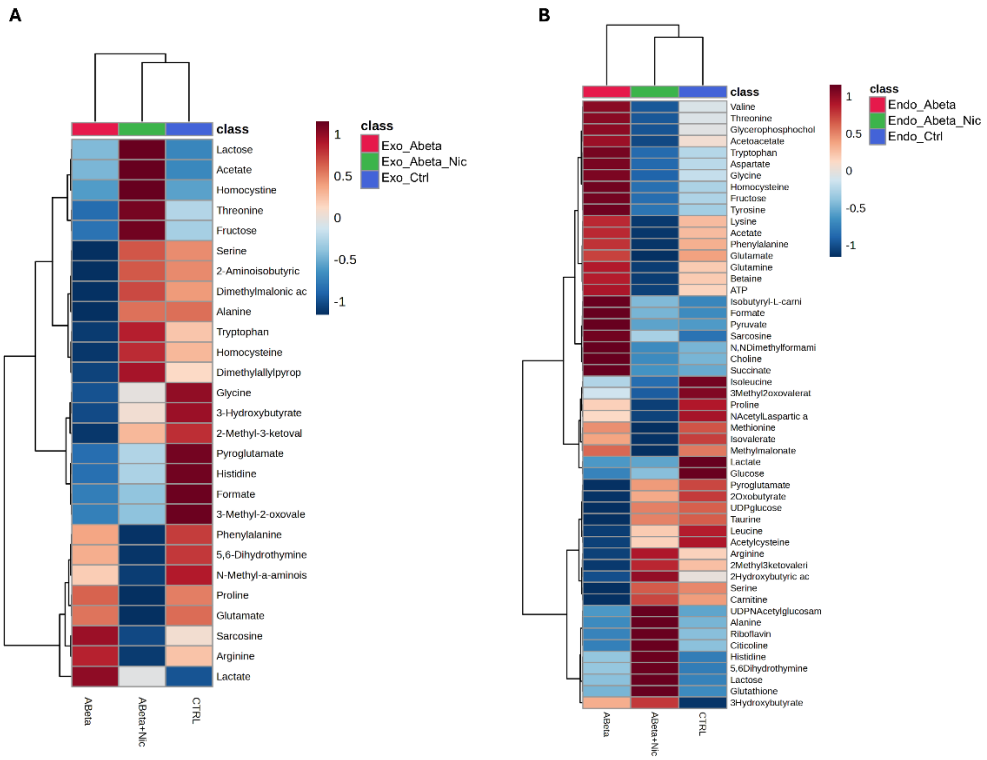

Figure 2.15 *Heatmaps showing changed metabolites in i) SH-SY5Y cells treated with Aβ(1–42), ii) SH-SY5Y cells treated with both Aβ(1–42) and nicotine, and iii) untreated SH-SY5Y cells, for exo- (**A**) and endometabolome (**B**). The color of each section corresponds to a concentration value of each metabolite calculated by a normalized concentration matrix (red, up-regulated; blue, down-regulated).*

Figure 2.16 reports the results of the Enrichment pathway analysis performed on the data matrix containing the endometabolites relative to the cells i) pretreated with nicotine before being incubated with Aβ(1–42) ii) incubated only with Aβ(1–42) to evaluate the biochemical pathways regulated by nicotine in the AD cellular model. Accordingly, it is evident that there is a dysregulation of *betaine metabolism, methionine metabolism, homocysteine degradation,* and *folate metabolism*. Moreover, alterations in several energy pathways, such as *amino sugar metabolism, the citric acid cycle, ketone body metabolism, glycolysis, pyruvate metabolism,* and the *Urea cycle*, have been shown. Enrichment analysis revealed modulation of amino acid pathways most involved in neurotransmission, including *glutamate metabolism, glycine and serine metabolism,* and *phenylalanine and tyrosine metabolism*. Moreover, the Enrichment analysis confirmed effects on pathways of membrane phospholipid and sphingolipid biosynthesis and revealed an antioxidant action of nicotine, identifying dysregulation of *glutathione metabolism* (**Figure 2.16, Table S2**).

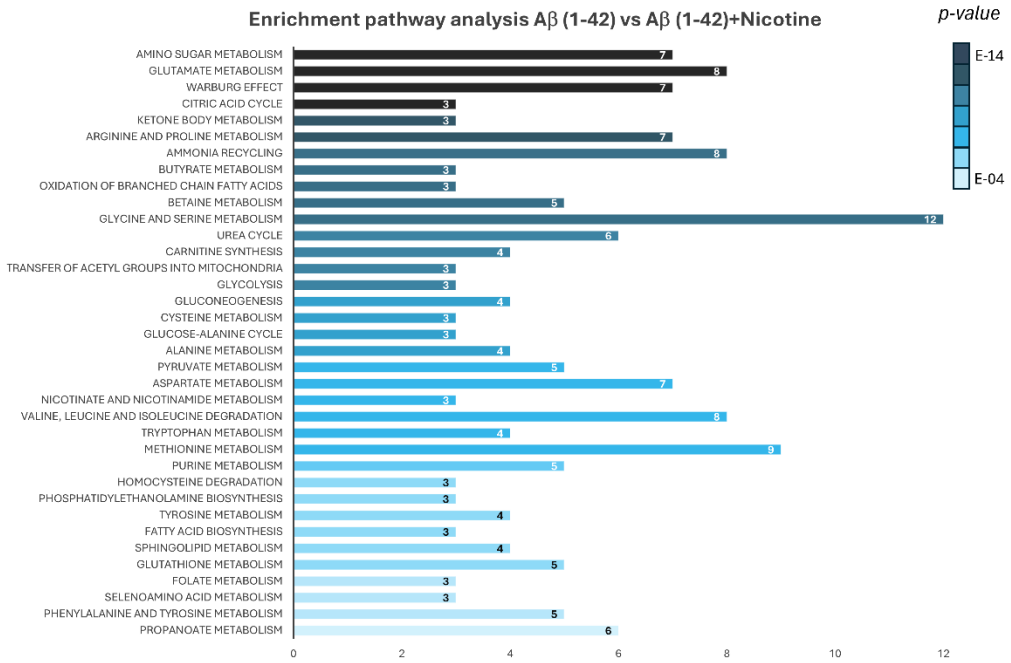

Figure 2.16 *Enrichment pathways analysis: the discriminative pathways are ranked according to p-value and number of hits reported in the bars.*

2.5 Discussion

2.5.1 Nicotine metabolomic impact on SH-SY5Y cells

Nicotine, the primary alkaloid in *Nicotiana tabacum*, is considered the main psychoactive component of tobacco smoke. However, it is widely accepted that nicotine enhances brain function and cognitive performance. Accordingly, some research indicates that this effect is partly because of nicotine's influence on mitochondrial activity, although the complete mechanism has not been fully clarified. [10, 15, 28, 58]

Studies on the metabolomics impact of nicotine on mice's brains have already been published. [20] To deepen the knowledge on the nicotine's mechanism of action on brain function, we decided to perform NMR metabolomic analysis using an *in vitro* system of SH-SY5Y cells. These human neuroblastoma cells are frequently used in neuroscience research and are among the most widely used cell lines for studying nicotine-related mechanisms, primarily because they express nicotinic acetylcholine receptors (nAChRs) on their cell membrane. [47, 59-62]

Our analysis emphasises the significant impact of nicotine on altering lipid metabolism and cell membrane structure. Specifically, treating SH-SY5Y cells with

nicotine increases intracellular PC levels (**Figure 2.6B**). Consequently, the metabolic pathways most affected by nicotine are *phospholipid biosynthesis, sphingolipids biosynthesis*, *and phosphatidylcholine biosynthesis* (**Figure 2.7, Table S1**).

Given the predominant role of phosphatidylcholine in animal cell membranes, its precursor, PC, represents a robust biomarker of phospholipid synthesis – a process essential for neural membrane assembly and dendritic extension during brain development. Consistent with this role, previous studies employing ^{31}P NMR spectroscopy have demonstrated a pronounced increase in PC levels throughout neuronal maturation, indicative of enhanced membrane biogenesis and remodeling. These dynamic processes are fundamental for the establishment of synaptic connectivity and the initiation of neuronal electrical activity. [63] This interpretation is further supported by recent findings showing that increased availability of phospholipid precursors promotes neuronal membrane expansion and synaptogenesis. [64] The ability of nicotine to modulate phospholipid metabolism aligns with recent lipidomic studies demonstrating its neuroprotective effects. For instance, in SH-SY5Y cells exposed to 6-hydroxydopamine (6-OHDA) to model Parkinson's disease, nicotine was shown to normalize lipid metabolism via α7 nAChR-mediated signaling and anti-inflammatory pathways. These findings underscore nicotine's capacity to reprogram lipid metabolism under neurodegenerative conditions. [65] Moreover, our observations are consistent with previous *in vivo* studies examining the metabolomic profile of mouse brain tissues in response to nicotine exposure. [20, 66] The effect of nicotine on membranes is supported by proteomics data, indicating that nicotine predominantly influences proteins that play crucial roles in membrane function, such as receptors and proteins involved in transmembrane signaling. [67] Despite future validation being needed to confirm this hypothesis, collectively, these data support the notion that upregulation of phospholipid synthesis – facilitating membrane remodeling – is likely to enhance synaptic connectivity and neural plasticity, mechanisms that may underlie the cognitive-enhancing effects attributed to nicotine.

In accordance with data previously collected in preclinical studies, [20] the treatment of SH-SY5Y cells with nicotine affects several biochemical pathways related to amino acid metabolism, specifically those involving methionine, arginine, proline, glycine, serine, glutamate, and alanine (**Figures 2.6B, 2.7**). The effect of nicotine on amino acid metabolism was already described in preclinical studies. However, the

interpretation of this effect is challenging, [20] and several hypotheses have been proposed regarding whether alterations in amino acid concentration are related to changes in energetic metabolism and/or synaptic neurotransmission. Notably, the observed increases in glycine and sarcosine following nicotine administration may reflect neuroprotective mechanisms (**Figures 2.4B, 2.6B**). Indeed, glycine modulates excitatory neurotransmission by potentiating glutamate action at N-methyl-D-aspartate (NMDA) receptors. [68] Specifically, glycine serves as a co-agonist of NMDA receptors, meaning its binding is essential for full receptor activation. [69] Furthermore, sarcosine increases synaptic glycine levels and enhances NMDA receptor function – critical for learning, memory, and synaptic plasticity. [70, 71] Moreover, sarcosine has demonstrated neuroprotective potential by reducing glutamate-induced toxicity in SH-SY5Y cells, suggesting protective effects in models of excitotoxic damage. [72]

Several pieces of evidence have demonstrated nicotine's ability to influence mitochondrial activity. [15] It has been proposed that nicotine may exert its effects by binding to nicotinic acetylcholine receptors (nAChRs) located on the outer mitochondrial membrane (OMM), whose presence has been identified on isolated mitochondria from mouse liver. These receptors may serve as binding sites for nicotine and contribute to the modulation of mitochondrial signaling and function. [73]

Independently of the precise site of action, our findings confirm that nicotine treatment modulates multiple biochemical pathways associated with mitochondrial function.

Among these, the most significantly affected are *oxidation of branched-chain fatty acids, citric acid metabolism, mitochondrial electron transport chain* stand out as the most significantly affected pathways (**Figure 2.7, Table S1**). Moreover, nicotine administration was associated with a reduction in intracellular succinate levels (**Figure 2.6B**). Previous studies in rodents have demonstrated that both acute and chronic nicotine exposure elicit marked hyperactivities of mitochondrial dehydrogenases, specifically malate dehydrogenase (MDH) and succinate dehydrogenase (SDH), within the brain. [74] The observed decrease in intracellular succinate in human cells may therefore reflect a comparable nicotine-induced enhancement of SDH activity.

Being the biological space where ATP is produced through oxidative phosphorylation (OXPHOS), mitochondria are organelles with a pivotal role in human cells, often referred to as the cell's powerhouses. Studies conducted by Cormier *et al.*

on mitochondria isolated from rat forebrain revealed that nicotine binds to complex I and inhibits its NADH-ubiquinone reductase activity, as demonstrated by *in vitro* oxygen consumption binding assays. This interaction impairs the electron flow from NADH to complex I, resulting in reduced mitochondrial oxygen consumption. [75] Additionally, Wang *et al*. reported that in the rat brain, chronic nicotine administration modulates the expression of several genes encoding subunits of protein complexes involved in the mitochondrial respiratory chain. [76] Our findings confirm that nicotine can also modulate the electron transport chain in human neuronal-like cells, supporting the notion that mitochondria are a key target of nicotine's action. However, further investigation is required to clarify the underlying mechanisms of nicotine's effects on human mitochondrial function.

Additional evidence for nicotine's action at the mitochondrial level is provided by the observed increase in N-acetylaspartate (NAA) concentration (**Figure 2.6B**). NAA is widely regarded as a biomarker of neuronal integrity, with reduced levels typically reflecting neuronal loss or impaired neuronal function. [77] In our study, NAA was found to increase in response to nicotine treatment, a change that may indicate improved neuronal viability and mitochondrial activity. Consistent with this observation, elevated NAA concentrations have been reported in the brains of smokers, suggesting that nicotine exposure may contribute, at least in part, to this effect. [78]

Collectively, these findings indicate that nicotine modulates key mitochondrial processes related to energy metabolism and cellular function in neuronal-like cells, consistent with observations from both *in vivo* animal models and human studies. Interestingly, our results about nicotine effect on mitochondria are consistent with previous analyses using other omics approaches: Navarrete-Perea *et al*. found that proteome changes in SH-SY5Y cells exposed to nicotine mainly involve mitochondria.[67]

While our findings provide valuable insights into the effects of nicotine on neuron-like cells, several limitations must be acknowledged. SH-SY5Y cells, derived from human neuroblastoma, exhibit an immature neuronal phenotype, which may not fully recapitulate the responses of mature neurons *in vivo.* [79] Additionally, their use in monoculture fails to capture the complex interactions with glial cells, which are critical for neuronal function and homeostasis. [80] Moreover, this study was conducted under

non-pathological conditions, limiting its applicability to disease models where neuronal metabolism is altered.

Despite these limitations, SH-SY5Y cells remain a useful tool for early-stage mechanistic studies. Future studies should aim to validate these findings in more physiologically relevant systems, including differentiated neurons, co-culture models, or *in vivo* approaches, particularly in the context of neurodegenerative diseases, such as AD and PD.

2.5.2 A proposed mechanism for the nicotine protective role in AD

Recently, a renewed interest emerged in the investigation of nicotine as a compound endowed with biological activity in controlling AD symptoms. In particular, nicotine appears to control neuroinflammation and apoptosis, and to reduce the misfolding of amyloid proteins. [14, 29, 37, 40, 41, 81, 82]

SH-SY5Y cells are recognized as a functional cellular model for studying neurogenerative diseases such as AD and PD. [83, 84] This cell line has proven to be a valuable model for studying the metabolic changes associated with AD when treated with the amyloid peptide Aβ(1–42). [50, 51]

To extend the results obtained in SH-SY5Y cells exposed only to nicotine (presented in the previous paragraph) and to gain insights into the hitherto unknown role of nicotine in protecting from the neurotoxic action of Aβ(1–42) amyloid peptide, we performed an NMR-based metabolomics investigation of SH-SY5Y neuroblastoma cells exposed to nicotine before being treated with Aβ(1–42).

Previous metabolomic analyses of SH-SY5Y cells treated with Aβ(1–42) demonstrated that this model mimics AD-related alterations observed in patient biofluids, including increased oxidative stress and inflammation, along with detrimental effects on neurotransmission and lipid metabolism. [51, 85] This effect is particularly evident in altered phosphatidylcholine and lipo-phosphatidylcholine concentrations and coincides with data also derived from CSF and plasma analysis of AD patients. [50]

Our NMR-based metabolomic investigation employed for the first time a combined endo- and exometabolomic approach focused on SH-SY5Y cells treated with Aβ(1–42). In agreement with evidence from previous experiments on AD cellular models and AD patient biofluids, our observations indicated abnormally low NAA levels

compatible with altered glutamatergic neurotransmission. [51, 86, 87] Changes in NAA could affect glutamate neurotransmission, as NAA may function as a neurotransmitter by modulating metabotropic glutamate receptors. [88] Furthermore, we observed that Aβ(1–42) induces increased sarcosine and decreased serine and pyroglutamate concentrations in both extracellular and intracellular compartments. In contrast, tryptophan concentration is up-regulated in the cells and down-regulated in the extracellular environment (**Figure 2.12B**). Enrichment analysis indicated in correspondence with these metabolic signatures an alteration in *glycine and serine metabolism,* an imbalance of *sphingolipid and phospholipid metabolism,* and most energetic pathways, such as the *ketone body* and *pyruvate metabolism, citric acid,* and *urea cycle* (**Figure 2.13**). [89-91]

The benefits of nicotine in reducing Aβ(1–42) toxicity. As previously reported, a great deal of data has proved the benefits of nicotine in reducing Aβ(1–42) toxicity. Interestingly, in line with these data, our pharmacometabolomic study indicates a rebalance in the metabolic state of SH-SY5Y cells pretreated with nicotine before incubation with Aβ(1–42) toward the metabolic state of healthy control cells (**Figures 2.15A, B**). A careful analysis of our data to understand how nicotine may impact different sides of cellular metabolism suggests significant effects of the alkaloid on (i) amino acid metabolism, particularly those involved with neurotransmission, (ii) energy metabolism (iii) membrane phospholipid metabolism.

Nicotine treatment affects amino acid metabolism, particularly those involved in neurotransmission. Nicotine is effective in i) reducing glutamate concentration in the extracellular and intracellular compartments. Upregulation of excitotoxic glutamate transmission is a typical signature of neurodegenerative disease. [92, 93] We demonstrated that the neuroprotective action of nicotine can be exerted through the down-regulation of glutamate pathways (**Figures 2.15A,B, 16**). ii) increasing Serine concentration. Dietary supplementation with L-serine has been shown to restore synaptic plasticity and memory deficits, suggesting it is a potential therapy for AD. [94] On the other hand L-serine deficiency and deficiency of its downstream products is associated with severe neurological deficits (**Figure 2.14B**). [95] iii) Increasing Arginine excretion, consistent with a rebalancing of the *urea cycle*, which is altered in AD patients (**Figures 2.14B, 2.16**). [91] *iv)* reducing intracellular aromatic amino acids – phenylalanine and tryptophan – thus reverting an AD pathology signature, consisting

of abnormally high concentrations of aromatic amino acids in the brain [96] (**Figures 2.15B, 2.16**).

Nicotine treatment affects energetic metabolism. Nicotine in SH-SY5Y cells treated with Aβ(1–42) induces reduced levels of acetoacetate, increased concentrations of 3-hydroxybutyrate, and rebalance of *pyruvate metabolism* and *TCA* (**Figures 2.14B, 2.15B, 2.16**). High pyruvate concentrations observed in Aβ(1–42)-treated cells are consistent with a downregulation of TCA and hypoglycemia condition (**Figures 2.10B, 2.12B, 2.13**), as observed in the brains of AD patients. [89, 90] Accordingly, the intracellular concentration of glucose was shown to be reduced by Aβ(1–42) treatment (**Figure 2.11B**). This hypoglycaemic state is reversed in the presence of nicotine, as shown by increased conversion of acetoacetate to 3-hydroxybutyrate. Thus, nicotine may protect cells from hypoglycemia by favoring the use of ketone bodies as an alternative fuel source (**Figure 2.16**). [97]

Elevated homocysteine levels have been recognized as a contributing factor to the development of cognitive decline, dementia, and AD in elderly individuals since they induce mitochondrial dysfunction. [98, 99] Nicotine pretreatment reduces intracellular homocysteine and betaine concentrations and increases glutathione levels (**Figures 2.14B, 2.15B**). Indeed, a decrease in betaine induces upregulation of glutathione production, which modulates homocysteine concentrations. [100, 101] Therefore, nicotine affects the *folate pathway, betaine metabolism, homocysteine degradation,* and *glutathione metabolism* (**Figure 2.16**); all these effects are compatible with a final antioxidant effect of nicotine.

Furthermore, nicotine restores riboflavin physiological concentrations (**Figure 2.16**). Because of riboflavin deficiency found in AD patients, therapies based on flavin mononucleotide (FMN) supplementation have an effect in containing AD symptoms. [102] Our results confirm the low riboflavin concentrations in the Aβ(1–42) pretreated cell model and show the efficacy of nicotine in rebalancing FMN physiological concentrations (**Figures 2.12B, 2.14B**).

Nicotine treatment affects membrane phospholipid metabolism. Nicotine pre-treatment significantly up-regulates *phosphoethanolamine biosynthesis* while decreasing glycerophosphocholine, a degradative product of phosphatidylcholine (**Figures 2.14B, 2.16**). [103, 104] Moreover, nicotine treatment increases citicoline concentration (**Figure 2.14B**), an essential intermediate in the biosynthetic pathway of

phosphatidylcholine in cell membranes. [105] Several studies have reported a dysregulation of phospholipid metabolism in AD, particularly a reduction of phosphatidylcholine and phosphoethanolamine production. [106, 107] We demonstrate that nicotine restores phospholipid metabolism, which is significantly impaired in AD. (**Figure 2.16**)

2.6 Conclusions

In conclusion, our results demonstrate that nicotine significantly alters the metabolic profile of SH-SY5Y neuron-like cells, primarily through two distinct mechanisms, as illustrated in **Figure 2.17**:

i) Regulation of membrane dynamics and plasticity. Nicotine treatment leads to elevated levels of intracellular phosphorylcholine (PC), accompanied by significant modulation of *phospholipid biosynthesis, sphingolipid metabolism, and phosphatidylcholine biosynthesis*. These alterations suggest enhanced membrane remodeling and synaptic plasticity, which may contribute to nicotine's cognitive-enhancing effects.

ii) Modulation of mitochondrial bioenergetics and homeostasis. Nicotine exposure affects several biochemical pathways related to mitochondrial function, including *branched-chain fatty acid oxidation, citric acid cycle activity*, and the *mitochondrial electron transport chain*. Consistent with these changes, we observed an increase in intracellular NAA levels – a metabolite widely recognized as a marker of mitochondrial activity and neuronal viability. These findings reinforce previous evidence and highlight mitochondria as a central target of nicotine's cellular mechanism of action.

The identification of specific metabolic pathways affected by nicotine opens potential avenues for therapeutic intervention in neurodegenerative disorders or cognitive impairments, where mitochondrial dysfunction and altered membrane dynamics are commonly implicated.

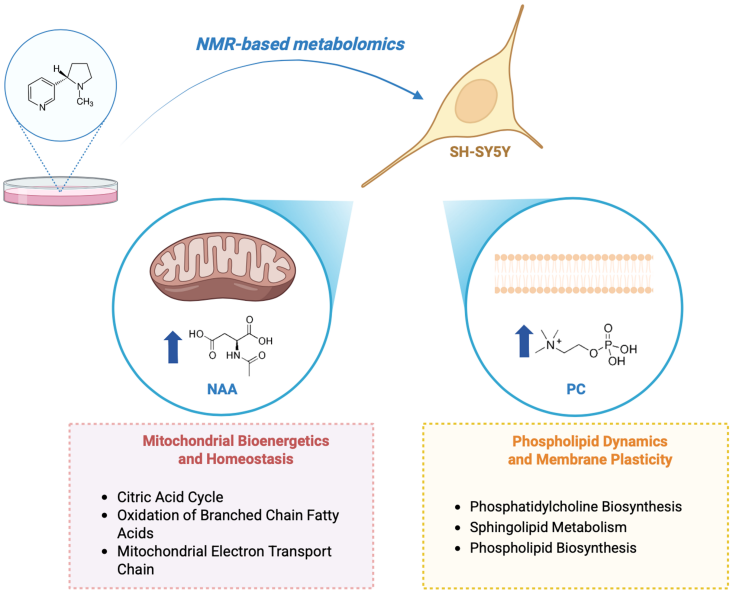

Figure 2.17 *Schematic representation of nicotine-induced effects on SH-SY5Y neuron-like cells, illustrating key metabolic and functional changes. Figure created using BioRender, https://www.biorender.com/.*

Regarding the pathological cellular model, as shown in **Figure 2.18**, nicotine pre-treatment of SH-SY5Y cells exposed to Aβ(1–42) peptide induces i) glutamate reduction where excessive glutamate can lead to excitotoxicity, neuronal damage, and disease progression; ii) serine increasing, where low serine levels are linked to neurological disorders, cognitive decline or mood disorders; iii) improvement of mitochondrial function, counteracting hyperhomocysteinemia associated with neurodegeneration and fighting hypoglycemia with the ketone body consumption shift; iv) rebalance in membrane phospholipid metabolism, restoring the synthesis of phospho- and sphingolipids necessary for membrane integrity.

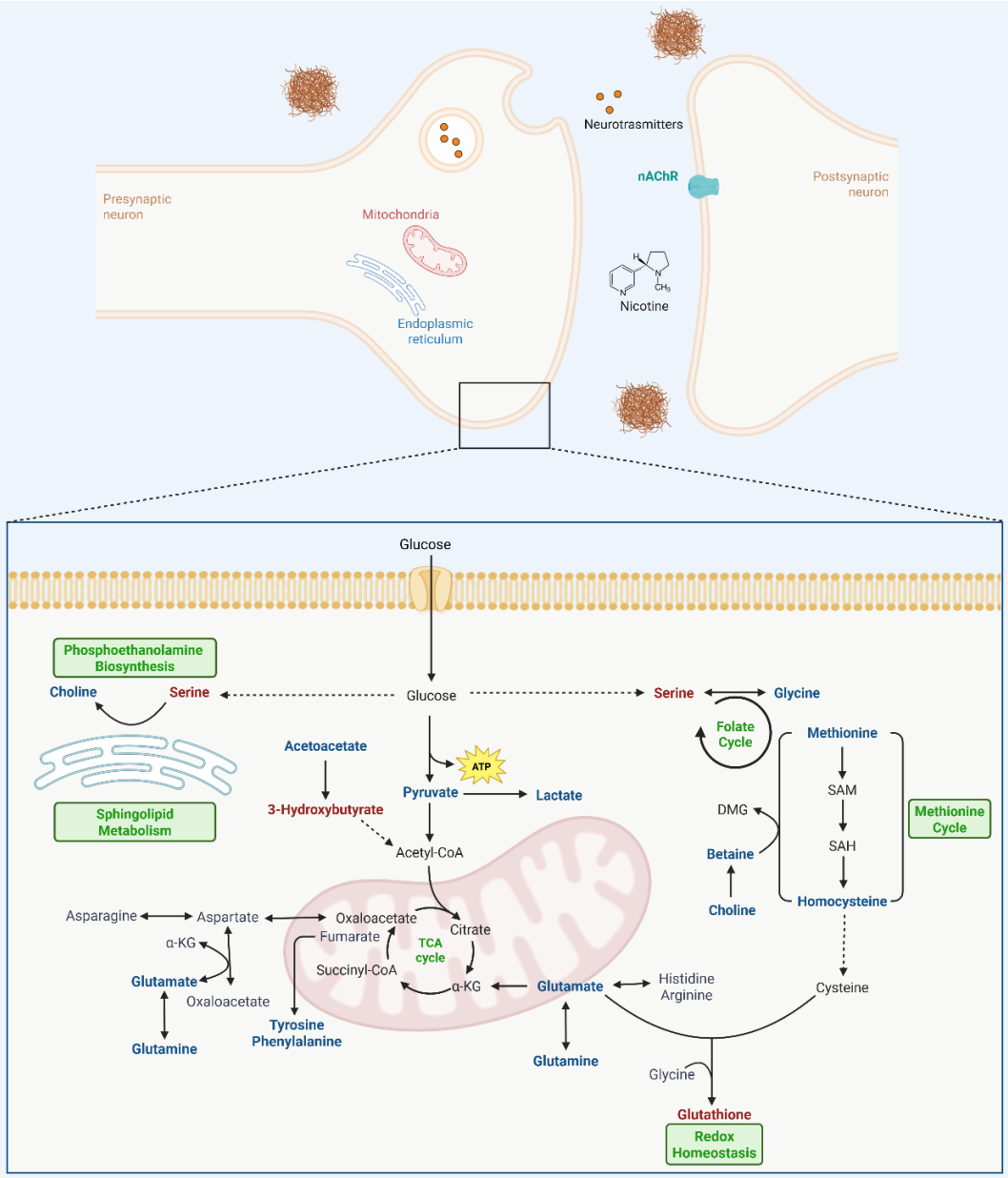

Figure 2.18 *Overview of the metabolic effects of nicotine on Alzheimer's disease. Up-regulated metabolites in Aβ(1–42)-nicotine cells are indicated in red; downregulated ones in blue; dysregulated pathways are labelled in green. Figure created using BioRender, https://www.biorender.com/.*

2.7 Materials and Methods

2.7.1 Chemicals

Dulbecco's Modified Eagle's Medium (DMEM), L-glutamine, penicillin and streptomycin, fetal bovine serum (FBS), CCK-8, and (-)-nicotine (≥99%) were purchased from Sigma-Aldrich (St. Louis, MI, USA). Aβ(1–42) was obtained after transformation of E. coli BL21(DE3)-pLysS cells with PetSac plasmid, provided by the research group of Walsh, as previously reported. [108]

2.7.2 Cell Culture

The human neuroblastoma line SH-SY5Y was purchased from American Type Culture Collection (ATCC, Rockville, MD, USA). Cells were cultured in Dulbecco's Modified Eagle Medium (DMEM, 4500 mg/mL glucose) supplemented with 10% (v/v) FBS, 2 mM L-glutamine, 100 U/mL penicillin, and 0.1 mg/mL streptomycin. Cells were maintained in a humidified incubator at 37 °C with 5% CO_2 and passaged every 2 days.

2.7.3 Cell Viability Assay

Cell viability was established by measuring mitochondrial metabolic activity with Cell Counting Kit-8 (CCK-8 Cat. CK04, Dojindo Laboratories, Rockville, MD, USA). This assay evaluates the viability of cells considering the ability of dehydrogenases' cells to reduce the tetrazolium salt WST-8 (2-(2-methoxy-4-nitrophenyl)-3-(4-nitrophenyl)-5-(2,4-disulfophenyl)-2H-tetrazolium, monosodic salt) in an orange-colored formazan dye, which is soluble in the tissue culture medium. The quantity of formazan dye generated by intracellular dehydrogenase activity is directly proportional to the number of living cells.

Briefly, to evaluate nicotine EC_{50}, SH-SY5Y cells (8×10^3 per well) were seeded into 96-well plates and incubated for 24 hours. Next, nicotine (0.10 – 10 mM) was added and incubated for a further 24 hours.

To evaluate nicotine's ability to protect SH-SY5Y cells from Aβ(1–42) toxicity, 8×10^3 cells/well were plated in 96-well plates for 24 h, then nicotine at 1 mM or 100 μM was added for 24 h. Next, Aβ(1–42) peptide 25 μM was added for 48 h.

At the end of each treatment, the CCK-8 reagent was diluted in cell medium (10%) and incubated for 1 hour. Absorbance was measured at 450 nm with a microplate reader (Multiskan Go, Thermo Scientific, Waltham, MA, USA). Cell viability was expressed as a percentage relative to untreated cells cultured in medium only with vehicle, which was set to 100%, whereas 10% DMSO was used as a positive control and set to 0% viability. Data are presented as mean ± standard deviation (SD) from three independent experiments, performed in triplicate. Statistical analysis was performed using one-way ANOVA followed by Dunnett's multiple-comparison test in GraphPad Prism version 8.0 (GraphPad Software, San Diego, CA, USA). Statistical

significance was set at $p < 0.05$. EC_{50} was calculated using GraphPad Prism 8.0 software by nonlinear regression of dose-response inhibition.

2.7.4 ^{1}H NMR Metabolomics

2.7.4.1 Exposure of SH-SY5Y cells to nicotine and Aβ(1–42)

To prepare metabolomic samples, cells were plated in 60 mm culture dishes and allowed to adhere overnight. Then, 100 μM nicotine was added for 24 hours. For the control group, cells were treated only with the vehicle for the same duration.

For the nicotine – Aβ(1–42) co-administration, cells were pretreated with nicotine (100 μM), and after 24 h Aβ(1–42) was added for an additional 48 hours at a sub-toxic concentration (5 μM). Cells exposed only to Aβ(1–42) peptide at the same concentration and incubation time were used for the comparison. For the control group, cells were treated only with the vehicle.

2.7.4.2 Sample collection and intracellular metabolites extraction

After treatments, both culture media and cell pellet were collected for the metabolomics analysis targeting the exometabolome and endometabolome, respectively. Specifically, the medium was transferred to microcentrifuge tubes and centrifuged at 1000× g for 10 min. The same procedure was applied to cell-free medium incubated under identical conditions. The resulting supernatants were transferred to fresh microcentrifuge tubes and stored at −80 °C until NMR analysis. After media removal, cell dishes were washed with cold PBS (pH 7.4) to remove media residues and cells were collected by scraping in methanol. To extract intracellular metabolites from cell pellet, homogenization was followed by biphasic extraction method using methanol, chloroform, and water in a 1:1:1 ratio. [109] Samples were centrifuged at 6000 rpm for 10 min at 4 °C to separate the polar and apolar phases. Polar extracts from cell pellet were dried under vacuum with a SP-Genevac EZ-2 4.0 concentrator while lipophilic extracts were dried with nitrogen flow for later analysis. All extracts were stored at −80 °C before NMR testing.

2.7.4.3 NMR Sample Preparation

Lyophilized cell extracts were reconstituted in 200 μL of buffer (50 mM Na_2HPO_4, 1 mM trimethylsilyl propionic-2,2,3,3-d_4 acid sodium salt (TSP-d_4), 10% of D_2O).

TSP-d_4 was used as an internal standard for the alignment and quantification of NMR signals. For growth media analysis, 100 µL of cell medium was mixed with 100 µL of the same buffer used for the lyophilized extracts. The resulting samples were transferred into 3 mm NMR tubes for ^{1}H NMR acquisition.

2.7.4.4 NMR Data Acquisition and Processing

1D ^{1}H NMR spectra were recorded on a Bruker Ascend™ 600 MHz spectrometer equipped with a 5 mm triple resonance Z gradient TXI probe (Bruker Co, Rheinstetten, Germany) at 298 K. One-dimensional NOESY NMR spectra were recorded with 20 k points, 12 ppm spectral width, 1.36s acquisition time, 5 s relaxation delay, 10 ms of mixing time and 128 scans. [54] Topspin version 3.0 (Bruker Biospin) was used for spectrometer control and data processing. Spectra analysis followed an untargeted metabolomic approach, with each metabolite identified prior to statistical testing using Chenomx NMR-Suite v10.1 (Chenomx NMR suite, v10.1, Edmonton, AB, Canada). Quantitative analysis of the 1D-NMR spectra was performed with NMRProcFlow ver 1.4.10. [55] In more details, the FID 1D NMR spectra have been uploaded to the software, and before integration, several processing steps were carried out. First, ppm calibration was performed to align chemical shifts using the internal reference TSP-d4, set at 0.00 ppm. Next, baseline correction was applied to the NMR spectra, using global correction in soft mode and considering the noisy ppm range of 10.5-10.2 ppm. Lastly, where necessary, spectra alignment was performed using the Least Squares algorithm, with a maximum relative shift of 0.1 ppm. After processing, metabolites were quantified by selecting ppm ranges for each metabolite peak in less crowded regions of the spectrum to avoid contamination from nearby peaks. All data required for quantification were exported to a spreadsheet using the "qHNMR" template. This template organises information across five tabs: the sample table, the bucket table, the data table (which reports integration values without correction parameters), the signal-to-noise ratio matrix, and the quantification table, which shows corrected integration values for each bucket (columns) and spectrum (rows). This last table includes essential data for accurate quantification, such as sample volume (mL), sample mass (mg), the number of protons corresponding to each metabolite peak, and the metabolites' molecular weights. The resulting quantification data matrix produced by NMRProcFlow was used for statistical analysis.

2.7.4.5 Statistical analysis

The resulting quantification matrix was normalised to the sum of quantified metabolites, log-transformed, Pareto-scaled, and analysed using the open-source tool Metaboanalyst 6.0 and the MixOmics R package. [110, 111] This normalisation method was chosen because, with an equal number of cells across the experimental groups, differences in signal intensity are assumed to reflect biological variability rather than sample quantity. Furthermore, because the number of variables was significantly higher than the number of samples, especially after combining the endo- and exometabolome matrices, probabilistic quotient normalisation could not be applied. Pareto scaling was also applied to reduce the relative influence of high values while preserving the data structure. Moreover, the quantification matrix was logarithmically transformed to reduce data skewness and variability caused by outliers. [112] Univariate analysis was performed separately on the exometabolome and endometabolome of the groups, using a T-Test and Fold Change, and the results were displayed in a Volcano plot. [113]

To enhance data accuracy and gain biological insights, multivariate statistical analysis (MVA) was first applied to the exometabolome and endometabolome concentration matrices, followed by analysis of the combined data sets.

To analyze the combined endo- and exometabolome, we employed the mixOmics R package using a P-integration approach. This method integrates multiple datasets measured on the same type of variables – metabolites in our case – and enhances statistical power by accounting for batch effects prior to applying standard multivariate techniques such as supervised Sparse Partial Least Squares (or Projection to Latent Space-sPLS). To further improve the accuracy of the combined analysis and reduce variability between matrices, batch effects were additionally corrected using the *limma* R package. [114]

MVA was conducted on combined matrices of endo- and exo-metabolites using the sPLS. [115] This method is a linear and multivariate visualisation technique for integrable datasets that addresses limitations of Principal Component Analysis and Canonical correspondence analysis (CCA). [116] In this integrated approach, sPLS analysis is effective when the total number of variables in the combined matrices exceeds the number of samples analysed, as demonstrated in this study. The sPLS was conducted with an LASSO penalty on the loading vectors to reduce the number of original

variables used to construct the latent variables. [117] A sample plot illustrates the clustering of samples' metabolomic profiles. In the graph, each sample appears as a point located based on its projection onto the selected latent components of the data. Leave-one-out cross-validation is conducted to validate the model, using R^2, Q^2, and accuracy metrics. [118] Furthermore, sPLS models were additionally validated using distance matrices derived from the centroid method, maximum distance, and Mahalanobis distance. [119]

Variable correlations are displayed using a circular correlation plot, where all vectors are plotted inside a unit circle with a radius of 1. Each vector's position reflects its correlation with the components; stronger associations produce vectors that extend further from the center. Additionally, variables with vectors close to each other are highly correlated. [110] The contribution of each variable is shown in a bar graph. The contribution graph based on loadings for variable separation has been color-coded to show the maximum value between two, indicating the clusters where the metabolite has the highest concentration. To comprehensively depict the quantitative changes in metabolites, we created heatmaps using normalised data, average group concentrations, and Euclidean distance. [120] The enrichment pathway tool was used to conduct pathway analysis with Metaboanalyst 6.0. KEGG pathways were selected based on lower false discovery rates (FDR), with p-values less than 0.05, and a hit value (the number of metabolites in the pathway) greater than 1. [121]

Bibliography

1. Jassem, E.; Szymanowska, A.; Siemińska, A.; Jassem, J., Smoking and lung cancer. *Advances in Respiratory Medicine* **2009,** *77* (5), 469-473.
2. Scherübl, H., Smoking tobacco and cancer risk. *Deutsche Medizinische Wochenschrift (1946)* **2021,** *146* (6), 412-417.
3. Kondo, T.; Nakano, Y.; Adachi, S.; Murohara, T., Effects of tobacco smoking on cardiovascular disease. *Circulation Journal* **2019,** *83* (10), 1980-1985.
4. Pietinalho, A.; Pelkonen, A.; Rytilä, P., Linkage between smoking and asthma. *Allergy* **2009,** *64* (12), 1722-1727.
5. Durlach, V.; Vergès, B.; Al-Salameh, A.; Bahougne, T.; Benzerouk, F.; Berlin, I.; Clair, C.; Mansourati, J.; Rouland, A.; Thomas, D., Smoking and diabetes interplay: a comprehensive review and joint statement. *Diabetes & metabolism* **2022,** *48* (6), 101370.
6. Copeland, R. L.; Das, J. R.; Kanaan, Y. M.; Taylor, R. E.; Tizabi, Y., Antiapoptotic effects of nicotine in its protection against salsolinol-induced cytotoxicity. *Neurotoxicity research* **2007,** *12*, 61-69.
7. De Jonge, W. J.; Ulloa, L., The alpha7 nicotinic acetylcholine receptor as a pharmacological target for inflammation. *British journal of pharmacology* **2007,** *151* (7), 915-929.
8. Picciotto, M. R.; Addy, N. A.; Mineur, Y. S.; Brunzell, D. H., It is not "either/or": activation and desensitization of nicotinic acetylcholine receptors both contribute to behaviors related to nicotine addiction and mood. *Progress in neurobiology* **2008,** *84* (4), 329-342.
9. Quik, M.; Perez, X. A.; Bordia, T., Nicotine as a potential neuroprotective agent for Parkinson's disease. *Movement disorders* **2012,** *27* (8), 947-957.
10. Wang, Q.; Du, W.; Wang, H.; Geng, P.; Sun, Y.; Zhang, J.; Wang, W.; Jin, X., Nicotine's effect on cognition, a friend or foe? *Progress in Neuro-Psychopharmacology and Biological Psychiatry* **2023,** *124*, 110723.
11. Majdi, A.; Sadigh-Eteghad, S.; Gjedde, A., Effects of transdermal nicotine delivery on cognitive outcomes: A meta-analysis. *Acta Neurologica Scandinavica* **2021,** *144* (2), 179-191.
12. Echeverria, V.; Mendoza, C.; Iarkov, A., Nicotinic acetylcholine receptors and learning and memory deficits in Neuroinflammatory diseases. *Frontiers in Neuroscience* **2023,** *17*, 1179611.
13. Heishman, S. J.; Kleykamp, B. A.; Singleton, E. G., Meta-analysis of the acute effects of nicotine and smoking on human performance. *Psychopharmacology* **2010,** *210*, 453-469.
14. Zhang, W.; Lin, H.; Zou, M.; Yuan, Q.; Huang, Z.; Pan, X.; Zhang, W., Nicotine in inflammatory diseases: anti-inflammatory and pro-inflammatory effects. *Frontiers in immunology* **2022,** *13*, 826889.
15. Malińska, D.; Więckowski, M. R.; Michalska, B.; Drabik, K.; Prill, M.; Patalas-Krawczyk, P.; Walczak, J.; Szymański, J.; Mathis, C.; Van der Toorn, M., Mitochondria as a possible target for nicotine action. *Journal of bioenergetics and biomembranes* **2019,** *51*, 259-276.
16. Picard, M.; McEwen, B. S., Mitochondria impact brain function and cognition. *Proceedings of the National Academy of Sciences* **2014,** *111* (1), 7-8.
17. Anitha, A.; Thanseem, I.; Iype, M.; Thomas, S. V., Mitochondrial dysfunction in cognitive neurodevelopmental disorders: cause or effect? *Mitochondrion* **2023,** *69*, 18-32.
18. Shah, N. J.; Sureshkumar, S.; Shewade, D. G., Metabolomics: a tool ahead for understanding molecular mechanisms of drugs and diseases. *Indian Journal of Clinical Biochemistry* **2015,** *30* (3), 247-254.
19. Phapale, P., Pharmaco-metabolomics opportunities in drug development and clinical research. *Analytical Science Advances* **2021,** *2* (11-12), 611-616.
20. Li, H.; Chen, B.; Shao, X.; Hu, Z.; Deng, Y.; Zhu, R.; Li, Y.; Zhang, B.; Hou, J.; Du, C., 1 H-Nuclear magnetic resonance-based metabolomic analysis of brain in mice with nicotine treatment. *BMC neuroscience* **2014,** *15*, 1-11.

21. Uhlig, S.; Olderbø, B. P.; Samuelsen, J. T.; Uvsløkk, S.; Ivanova, L.; Vanderstraeten, C.; Grutle, L. A.; Rangel-Huerta, O. D., Mass spectrometry-based metabolomics study of nicotine exposure in THP-1 monocytes. *Scientific Reports* **2024,** *14* (1), 14957.
22. Calabrò, M.; Rinaldi, C.; Santoro, G.; Crisafulli, C., The biological pathways of Alzheimer disease: A review. *AIMS neuroscience* **2020,** *8* (1), 86.
23. Oxtoby, N. P.; Young, A. L.; Cash, D. M.; Benzinger, T. L. S.; Fagan, A. M.; Morris, J. C.; Bateman, R. J.; Fox, N. C.; Schott, J. M.; Alexander, D. C., Data-driven models of dominantly-inherited Alzheimer's disease progression. *Brain* **2018,** *141* (5), 1529-1544.
24. De Strooper, B.; Vassar, R.; Golde, T., The secretases: enzymes with therapeutic potential in Alzheimer disease. *Nature reviews neurology* **2010,** *6* (2), 99-107.
25. Soto, C.; Castano, E. M.; Frangione, B.; Inestrosa, N. C., The α-Helical to β-Strand Transition in the Amino-terminal Fragment of the Amyloid β-Peptide Modulates Amyloid Formation∗. *Journal of Biological Chemistry* **1995,** *270* (7), 3063-3067.
26. Tomaselli, S.; Esposito, V.; Vangone, P.; van Nuland, N. A. J.; Bonvin, A. M. J. J.; Guerrini, R.; Tancredi, T.; Temussi, P. A.; Picone, D., The α-to-β conformational transition of Alzheimer's Aβ-(1–42) peptide in aqueous media is reversible: a step by step conformational analysis suggests the location of β conformation seeding. *ChemBioChem* **2006,** *7* (2), 257-267.
27. Mihailescu, S.; Drucker-Colín, R., Nicotine, brain nicotinic receptors, and neuropsychiatric disorders. *Archives of medical research* **2000,** *31* (2), 131-144.
28. Valentine, G.; Sofuoglu, M., Cognitive effects of nicotine: recent progress. *Current neuropharmacology* **2018,** *16* (4), 403-414.
29. Utsuki, T.; Shoaib, M.; Holloway, H. W.; Ingram, D. K.; Wallace, W. C.; Haroutunian, V.; Sambamurti, K.; Lahiri, D. K.; Greig, N. H., Nicotine lowers the secretion of the Alzheimer's amyloid β-protein precursor that contains amyloid β-peptide in rat. *Journal of Alzheimer's Disease* **2002,** *4* (5), 405-415.
30. Jones, G. M. M.; Sahakian, B. J.; Levy, R.; Warburton, D. M.; Gray, J. A., Effects of acute subcutaneous nicotine on attention, information processing and short-term memory in Alzheimer's disease. *Psychopharmacology* **1992,** *108*, 485-494.
31. Newhouse, P. A.; Sunderland, T.; Narang, P. K.; Mellow, A. M.; Fertig, J. B.; Lawlor, B. A.; Murphy, D. L., Neuroendocrine, physiologic, and behavioral responses following intravenous nicotine in nonsmoking healthy volunteers and in patients with Alzheimer's disease. *Psychoneuroendocrinology* **1990,** *15* (5-6), 471-484.
32. Gentry, M. V.; Hammersley, J. J.; Hale, C. R.; Nuwer, P. K.; Meliska, C. J., Nicotine patches improve mood and response speed in a lexical decision task. *Addictive Behaviors* **2000,** *25* (4), 549-557.
33. Sahakian, B.; Jones, G.; Levy, R.; Gray, J.; Warburton, D. J. T. B. J. o. P., The effects of nicotine on attention, information processing, and short-term memory in patients with dementia of the Alzheimer type. **1989,** *154* (6), 797-800.
34. Martin-Ruiz, C. M.; Court, J. A.; Molnar, E.; Lee, M.; Gotti, C.; Mamalaki, A.; Tsouloufis, T.; Tzartos, S.; Ballard, C.; Perry, R. H., α4 but not α3 and α7 nicotinic acetylcholine receptor subunits are lost from the temporal cortex in Alzheimer's disease. *Journal of neurochemistry* **1999,** *73* (4), 1635-1640.
35. Kihara, T.; Shimohama, S.; Sawada, H.; Kimura, J.; Kume, T.; Kochiyama, H.; Maeda, T.; Akaike, A., Nicotinic receptor stimulation protects neurons against β-amyloid toxicity. *Annals of Neurology: Official Journal of the American Neurological Association and the Child Neurology Society* **1997,** *42* (2), 159-163.
36. Zamani, M. R.; Allen, Y. S.; Owen, G. P.; Gray, J. A., Nicotine modulates the neurotoxic effect of β-amyloid protein (25–35) in hippocampal cultures. *Neuroreport* **1997,** *8* (2), 513-517.
37. Liu, Q.; Zhang, J.; Zhu, H.; Qin, C.; Chen, Q.; Zhao, B., Dissecting the signaling pathway of nicotine-mediated neuroprotection in a mouse Alzheimer disease model. *The FASEB Journal* **2007,** *21* (1), 61-73.

38. Wang, H.-Y.; Lee, D. H. S.; D'Andrea, M. R.; Peterson, P. A.; Shank, R. P.; Reitz, A. B., β-Amyloid1–42 binds to α7 nicotinic acetylcholine receptor with high affinity: implications for Alzheimer's disease pathology. *Journal of Biological Chemistry* **2000,** *275* (8), 5626-5632.
39. Linert, W.; Bridge, M. H.; Huber, M.; Bjugstad, K. B.; Grossman, S.; Arendash, G. W., In vitro and in vivo studies investigating possible antioxidant actions of nicotine: relevance to Parkinson's and Alzheimer's diseases. *Biochimica et Biophysica Acta (BBA)-Molecular Basis of Disease* **1999,** *1454* (2), 143-152.
40. Salomon, A. R.; Marcinowski, K. J.; Friedland, R. P.; Zagorski, M. G., Nicotine inhibits amyloid formation by the β-peptide. *Biochemistry* **1996,** *35* (42), 13568-13578.
41. Campiglia, P.; Esposito, C.; Scrima, M.; Gomez-Monterrey, I.; Bertamino, A.; Grieco, P.; Novellino, E.; D'Ursi, A. M., Conformational Stability of Aβ-(25–35) in the Presence of Thiazolidine Derivatives. *Chemical Biology & Drug Design* **2007,** *69* (2), 111-118.
42. Alarcon-Barrera, J. C.; Kostidis, S.; Ondo-Mendez, A.; Giera, M., Recent advances in metabolomics analysis for early drug development. *Drug discovery today* **2022,** *27* (6), 1763-1773.
43. Pang, H.; Hu, Z., Metabolomics in drug research and development: the recent advances in technologies and applications. *Acta Pharmaceutica Sinica B* **2023,** *13* (8), 3238-3251.
44. Brennan, L., NMR-based metabolomics: From sample preparation to applications in nutrition research. *Progress in Nuclear Magnetic Resonance Spectroscopy* **2014,** *83*, 42-49.
45. Moco, S., Studying metabolism by NMR-based metabolomics. *Frontiers in molecular biosciences* **2022,** *9*, 882487.
46. Wishart, D. S., NMR metabolomics: A look ahead. *Journal of Magnetic Resonance* **2019,** *306*, 155-161.
47. Cui, W.-Y.; Wang, J.; Wei, J.; Cao, J.; Chang, S. L.; Gu, J.; Li, M. D., Modulation of innate immune-related pathways in nicotine-treated SH-SY5Y cells. *Amino acids* **2012,** *43* (3), 1157-1169.
48. Takahashi, T.; Yoshida, T.; Harada, K.; Miyagi, T.; Hashimoto, K.; Hide, I.; Tanaka, S.; Irifune, M.; Sakai, N., Component of nicotine-induced intracellular calcium elevation mediated through α3-and α5-containing nicotinic acetylcholine receptors are regulated by cyclic AMP in SH-SY 5Y cells. *PLoS One* **2020,** *15* (11), e0242349.
49. Napolitano, E.; Marino, C.; Grimaldi, M.; Buonocore, M.; D'Ursi, A. M., Effects of Nicotine on SH-SY5Y Cells: An NMR-Based Metabolomic Study. *Metabolites* **2025,** *15* (11), 752.
50. Davani, L.; Fu, X.; De Simone, A.; Li, P.; Montanari, S.; Lämmerhofer, M.; Andrisano, V., Aβ1-42 peptide toxicity on neuronal cells: A lipidomic study. *Journal of Pharmaceutical and Biomedical Analysis* **2022,** *219*, 114876.
51. Phelan, M. M.; Caamaño-Gutiérrez, E.; Gant, M. S.; Grosman, R. X.; Madine, J., Using an NMR metabolomics approach to investigate the pathogenicity of amyloid-beta and alpha-synuclein. *Metabolomics* **2017,** *13*, 1-13.
52. Vignoli, A.; Tenori, L., NMR-based metabolomics in Alzheimer's disease research: a review. *Frontiers in Molecular Biosciences* **2023,** *10*, 1308500.
53. Wilkins, J. M.; Trushina, E., Application of metabolomics in Alzheimer's disease. *Frontiers in neurology* **2018,** *8*, 719.
54. McKay, R. T., How the 1D-NOESY suppresses solvent signal in metabonomics NMR spectroscopy: an examination of the pulse sequence components and evolution. *Concepts in Magnetic Resonance Part A* **2011,** *38* (5), 197-220.
55. Jacob, D.; Deborde, C.; Lefebvre, M.; Maucourt, M.; Moing, A., NMRProcFlow: a graphical and interactive tool dedicated to 1D spectra processing for NMR-based metabolomics. *Metabolomics* **2017,** *13* (4), 36.
56. Arias, E.; Gallego-Sandín, S.; Villarroya, M.; García, A. G.; López, M. G., Unequal neuroprotection afforded by the acetylcholinesterase inhibitors galantamine, donepezil, and

rivastigmine in SH-SY5Y neuroblastoma cells: role of nicotinic receptors. *The Journal of pharmacology and experimental therapeutics* **2005,** *315* (3), 1346-1353.
57. Liu, Q.; Zhao, B., Nicotine attenuates β-amyloid peptide-induced neurotoxicity, free radical and calcium accumulation in hippocampal neuronal cultures. *British journal of pharmacology* **2004,** *141* (4), 746-754.
58. Rezvani, A. H.; Levin, E. D., Cognitive effects of nicotine. *Biological psychiatry* **2001,** *49* (3), 258-267.
59. Takahashi, T.; Yoshida, T.; Harada, K.; Miyagi, T.; Hashimoto, K.; Hide, I.; Tanaka, S.; Irifune, M.; Sakai, N., Component of nicotine-induced intracellular calcium elevation mediated through α3- and α5-containing nicotinic acetylcholine receptors are regulated by cyclic AMP in SH-SY 5Y cells. *PLOS ONE* **2020,** *15* (11), e0242349.
60. Gould, J.; Reeve, H. L.; Vaughan, P. F.; Peers, C., Nicotinic acetylcholine receptors in human neuroblastoma (SH-SY5Y) cells. *Neuroscience letters* **1992,** *145* (2), 201-4.
61. Wang, F.; Gerzanich, V.; Wells, G. B.; Anand, R.; Peng, X.; Keyser, K.; Lindstrom, J., Assembly of human neuronal nicotinic receptor α5 subunits with α3, β2, and β4 subunits. *Journal of Biological Chemistry* **1996,** *271* (30), 17656-17665.
62. Kormelink, P. J. G.; Luyten, W. H. M. L., Cloning and sequence of full-length cDNAs encoding the human neuronal nicotinic acetylcholine receptor (nAChR) subunits β3 and β4 and expression of seven nAChR subunits in the human neuroblastoma cell line SH-SY5Y and/or IMR-32. *FEBS letters* **1997,** *400* (3), 309-314.
63. Pettegrew, J. W.; Panchalingam, K.; Withers, G.; McKeag, D.; Strychor, S., Changes in brain energy and phospholipid metabolism during development and aging in the Fischer 344 rat. *Journal of Neuropathology & Experimental Neurology* **1990,** *49* (3), 237-249.
64. Cansev, M., Synaptogenesis: Modulation by availability of membrane phospholipid precursors. *Neuromolecular medicine* **2016,** *18* (3), 426-440.
65. Yang, J.; Li, Y.; Wang, H.; Li, X.; Chen, H.; Hou, H.; Hu, Q., Nicotine Attenuates Pathogenesis of Parkinson's Disease via α7-nAChR-Mediated Lipid Metabolic Reprogramming and Anti-inflammatory Signaling. *Molecular Neurobiology* **2025**, 1-16.
66. Guo, L.-L.; Zhang, C.; Huang, Y.-J.; Liu, X.-Y.; Liu, D.-S.; Long, T.; Sun, J.-H.; Liu, S.-F.; Li, Z.-H.; Wang, J.-Z., Effects of nicotine exposure on endogenous metabolites in mouse brain based on metabolomics and mass spectrometry imaging. *Se pu= Chinese journal of chromatography* **2025,** *43* (4), 363-371.
67. Navarrete-Perea, J.; Gygi, S. P.; Paulo, J. A., Temporal proteomic changes induced by nicotine in human cells: a quantitative proteomics approach. *Journal of proteomics* **2021,** *241*, 104244.
68. López-Corcuera, B.; Geerlings, A.; Aragón, C., Glycine neurotransmitter transporters: an update. *Molecular membrane biology* **2001,** *18* (1), 13-20.
69. Cummings, K. A.; Popescu, G. K., Glycine-dependent activation of NMDA receptors. *The Journal of general physiology* **2015,** *145* (6), 513-27.
70. Zhang, H. X.; Hyrc, K.; Thio, L. L., The glycine transport inhibitor sarcosine is an NMDA receptor co-agonist that differs from glycine. **2009,** *587* (13), 3207-3220.
71. Chayrov, R.; Volkova, T.; Perlovich, G.; Zeng, L.; Li, Z.; Štícha, M.; Liu, R.; Stankova, I., Synthesis, neuroprotective effect and physicochemical studies of novel peptide and nootropic analogues of alzheimer disease drug. *Pharmaceuticals* **2022,** *15* (9), 1108.
72. Tanas, A.; Tozlu, Ö.; Gezmiş, T.; Hacimüftüoğlu, A.; Abd El-Aty, A. M.; Ceylan, O.; Mardinoğlu, A.; Türkez, H., In Vitro and In Vivo Neuroprotective Effects of Sarcosine. *BioMed research international* **2022,** *2022*, 5467498.
73. Gergalova, G.; Lykhmus, O.; Kalashnyk, O.; Koval, L.; Chernyshov, V.; Kryukova, E.; Tsetlin, V.; Komisarenko, S.; Skok, M., Mitochondria express α7 nicotinic acetylcholine receptors to regulate Ca2+ accumulation and cytochrome c release: study on isolated mitochondria. *PloS one* **2012,** *7* (2), e31361.
74. Turégano, L.; Martínez-Rodríguez, R.; Alvarez, M. I.; Gragera, R. R.; Gómez de Segura, A.; De Miguel, E.; Toledano, A., Histochemical study of acute and chronic intraperitoneal nicotine effects on several glycolytic and Krebs cycle dehydrogenase activities

in the frontoparietal cortex and subcortical nuclei of the rat brain. *Journal of Neuroscience Research* **2001,** *64* (6), 626-635.
75. Cormier, A.; Morin, C.; Zini, R.; Tillement, J.-P.; Lagrue, G., In vitro effects of nicotine on mitochondrial respiration and superoxide anion generation. *Brain research* **2001,** *900* (1), 72-79.
76. Wang, J.; Kim, J.-M.; Donovan, D. M.; Becker, K. G.; Li, M. D., Significant modulation of mitochondrial electron transport system by nicotine in various rat brain regions. *Mitochondrion* **2009,** *9* (3), 186-195.
77. Moffett, J. R.; Ross, B.; Arun, P.; Madhavarao, C. N.; Namboodiri, A. M., N-Acetylaspartate in the CNS: from neurodiagnostics to neurobiology. *Prog Neurobiol* **2007,** *81* (2), 89-131.
78. O'Neill, J.; Diaz, M. P.; Alger, J. R.; Pochon, J.-B.; Ghahremani, D.; Dean, A. C.; Tyndale, R. F.; Petersen, N.; Marohnic, S.; Karaiskaki, A., Smoking, tobacco dependence, and neurometabolites in the dorsal anterior cingulate cortex. *Molecular Psychiatry* **2023,** *28* (11), 4756-4765.
79. Kovalevich, J.; Langford, D., Considerations for the use of SH-SY5Y neuroblastoma cells in neurobiology. *Methods in molecular biology (Clifton, N.J.)* **2013,** *1078*, 9-21.
80. Demmings, M. D.; da Silva Chagas, L.; Traetta, M. E.; Rodrigues, R. S.; Acutain, M. F.; Barykin, E.; Datusalia, A. K.; German-Castelan, L.; Mattera, V. S.; Mazengenya, P.; Skoug, C.; Umemori, H., (Re)building the nervous system: A review of neuron-glia interactions from development to disease. *Journal of neurochemistry* **2025,** *169* (1), e16258.
81. Mugayar, A. A.; da Silva Guimarães, G.; de Oliveira, P. H. T.; Miranda, R. L.; Dos Santos, A. A., Apoptosis in the neuroprotective effect of α7 nicotinic receptor in neurodegenerative models. *Journal of Neuroscience Research* **2023,** *101* (12), 1795-1802.
82. Piao, W.-H.; Campagnolo, D.; Dayao, C.; Lukas, R. J.; Wu, J.; Shi, F.-D., Nicotine and inflammatory neurological disorders. *Acta Pharmacologica Sinica* **2009,** *30* (6), 715-722.
83. Fontana, I. C.; Zimmer, A. R.; Rocha, A. S.; Gosmann, G.; Souza, D. O.; Lourenco, M. V.; Ferreira, S. T.; Zimmer, E. R., Amyloid-β oligomers in cellular models of Alzheimer's disease. *Journal of neurochemistry* **2020,** *155* (4), 348-369.
84. Vestuto, V.; Amodio, G.; Pepe, G.; Basilicata, M. G.; Belvedere, R.; Napolitano, E.; Guarnieri, D.; Pagliara, V.; Paladino, S.; Rodriquez, M., Cocoa extract provides protection against 6-OHDA toxicity in SH-SY5Y dopaminergic neurons by targeting PERK. *Biomedicines* **2022,** *10* (8), 2009.
85. Rojas-Gutierrez, E.; Muñoz-Arenas, G.; Treviño, S.; Espinosa, B.; Chavez, R.; Rojas, K.; Flores, G.; Díaz, A.; Guevara, J., Alzheimer's disease and metabolic syndrome: A link from oxidative stress and inflammation to neurodegeneration. *Synapse* **2017,** *71* (10), e21990.
86. Jimenez-Jimenez, F. J.; Molina, J. A.; Gomez, P.; Vargas, C.; De Bustos, F.; Benito-Leon, J.; Tallon-Barranco, A.; Ortí-Pareja, M.; Gasalla, T.; Arenas, J., Neurotransmitter amino acids in cerebrospinal fluid of patients with Alzheimer's disease. *Journal of neural transmission* **1998,** *105*, 269-277.
87. Pomara, N.; Singh, R.; Deptula, D.; Chou, J. C.; Schwartz, M. B.; LeWitt, P. A., Glutamate and other CSF amino acids in Alzheimer's disease. *Am J Psychiatry* **1992,** *149* (2), 251-4.
88. Yan, H. D.; Ishihara, K.; Serikawa, T.; Sasa, M., Activation by N-acetyl-L-aspartate of acutely dissociated hippocampal neurons in rats via metabotropic glutamate receptors. *Epilepsia* **2003,** *44* (9), 1153-1159.
89. Cunnane, S.; Nugent, S.; Roy, M.; Courchesne-Loyer, A.; Croteau, E.; Tremblay, S.; Castellano, A.; Pifferi, F.; Bocti, C.; Paquet, N., Brain fuel metabolism, aging, and Alzheimer's disease. *Nutrition* **2011,** *27* (1), 3-20.
90. L Ferreira, I.; Resende, R.; Ferreiro, E.; C Rego, A.; F Pereira, C., Multiple defects in energy metabolism in Alzheimer's disease. *Current drug targets* **2010,** *11* (10), 1193-1206.
91. Polis, B.; Samson, A. O., A new perspective on Alzheimer's disease as a brain expression of a complex metabolic disorder. *Alzheimer's Disease [Internet]* **2019**.

92. Walton, H. S.; Dodd, P. R., Glutamate–glutamine cycling in Alzheimer's disease. *Neurochemistry international* **2007,** *50* (7-8), 1052-1066.
93. Wang, R.; Reddy, P. H., Role of glutamate and NMDA receptors in Alzheimer's disease. *Journal of Alzheimer's Disease* **2017,** *57* (4), 1041-1048.
94. Le Douce, J.; Maugard, M.; Veran, J.; Matos, M.; Jégo, P.; Vigneron, P.-A.; Faivre, E.; Toussay, X.; Vandenberghe, M.; Balbastre, Y., Impairment of glycolysis-derived l-serine production in astrocytes contributes to cognitive deficits in Alzheimer's disease. *Cell metabolism* **2020,** *31* (3), 503-517.
95. Phone Myint, S. M. M.; Sun, L. Y., L-serine: neurological implications and therapeutic potential. *Biomedicines* **2023,** *11* (8), 2117.
96. Griffin, J. W. D.; Bradshaw, P. C., Amino acid catabolism in Alzheimer's disease brain: friend or foe? *Oxidative medicine and cellular longevity* **2017,** *2017* (1), 5472792.
97. Zhang, J.; Cao, Q.; Li, S.; Lu, X.; Zhao, Y.; Guan, J.-S.; Chen, J.-C.; Wu, Q.; Chen, G.-Q., 3-Hydroxybutyrate methyl ester as a potential drug against Alzheimer's disease via mitochondria protection mechanism. *Biomaterials* **2013,** *34* (30), 7552-7562.
98. Smith, A. D.; Refsum, H.; Bottiglieri, T.; Fenech, M.; Hooshmand, B.; McCaddon, A.; Miller, J. W.; Rosenberg, I. H.; Obeid, R., Homocysteine and dementia: an international consensus statement. SAGE Publications Sage UK: London, England: 2018; Vol. 62, pp 561-570.
99. Petras, M.; Tatarkova, Z.; Kovalska, M.; Mokra, D.; Dobrota, D.; Lehotsky, J.; Drgova, A., Hyperhomocysteinemia as a risk factor for the neuronal system disorders. *J Physiol Pharmacol* **2014,** *65* (1), 15-23.
100. Arumugam, M. K.; Paal, M. C.; Donohue, T. M.; Ganesan, M.; Osna, N. A.; Kharbanda, K. K., Beneficial effects of betaine: a comprehensive review. *Biology* **2021,** *10* (6), 456.
101. Khodayar, M. J.; Kalantari, H.; Khorsandi, L.; Rashno, M.; Zeidooni, L., Betaine protects mice against acetaminophen hepatotoxicity possibly via mitochondrial complex II and glutathione availability. *Biomedicine & Pharmacotherapy* **2018,** *103*, 1436-1445.
102. Ekundayo, B. E.; Adewale, O. B.; Obafemi, B. A.; Afolabi, O. B.; Obafemi, T. O., Management of Alzheimer's disease and related neurotoxic pathologies: Role of thiamine, pyridoxine and cobalamin. *European Journal of Pharmacology* **2024**, 176958.
103. Fernández-Murray, J. P.; McMaster, C. R., Glycerophosphocholine catabolism as a new route for choline formation for phosphatidylcholine synthesis by the Kennedy pathway. *Journal of Biological Chemistry* **2005,** *280* (46), 38290-38296.
104. Morash, S. C.; Cook, H. W.; Spence, M. W., Phosphatidylcholine metabolism in cultured cells: catabolism via glycerophosphocholine. *Biochimica et biophysica acta* **1988,** *961* (2), 194-202.
105. Adibhatla, R. M.; Hatcher, J. F.; Dempsey, R. J., Effects of citicoline on phospholipid and glutathione levels in transient cerebral ischemia. *Stroke* **2001,** *32* (10), 2376-2381.
106. Wong, M. W.; Braidy, N.; Poljak, A.; Pickford, R.; Thambisetty, M.; Sachdev, P. S., Dysregulation of lipids in Alzheimer's disease and their role as potential biomarkers. *Alzheimer's & Dementia* **2017,** *13* (7), 810-827.
107. Zhu, L.; Zhong, M.; Elder, G. A.; Sano, M.; Holtzman, D. M.; Gandy, S.; Cardozo, C.; Haroutunian, V.; Robakis, N. K.; Cai, D., Phospholipid dysregulation contributes to ApoE4-associated cognitive deficits in Alzheimer's disease pathogenesis. *Proceedings of the National Academy of Sciences* **2015,** *112* (38), 11965-11970.
108. Santoro, A.; Grimaldi, M.; Buonocore, M.; Stillitano, I.; D'Ursi, A. M., Exploring the early stages of the amyloid Aβ (1–42) peptide aggregation process: An NMR study. *Pharmaceuticals* **2021,** *14* (8), 732.
109. Beckonert, O.; Keun, H. C.; Ebbels, T. M. D.; Bundy, J.; Holmes, E.; Lindon, J. C.; Nicholson, J. K., Metabolic profiling, metabolomic and metabonomic procedures for NMR spectroscopy of urine, plasma, serum and tissue extracts. *Nature protocols* **2007,** *2* (11), 2692.

110. Rohart, F.; Gautier, B.; Singh, A.; Lê Cao, K.-A., mixOmics: An R package for 'omics feature selection and multiple data integration. *PLoS computational biology* **2017,** *13* (11), e1005752.
111. Pang, Z.; Lu, Y.; Zhou, G.; Hui, F.; Xu, L.; Viau, C.; Spigelman, A. F.; MacDonald, P. E.; Wishart, D. S.; Li, S., MetaboAnalyst 6.0: towards a unified platform for metabolomics data processing, analysis and interpretation. *Nucleic acids research* **2024,** *52* (W1), W398-W406.
112. Sun, J.; Xia, Y., Pretreating and normalizing metabolomics data for statistical analysis. *Genes & Diseases* **2024,** *11* (3), 100979.
113. Kumar, N.; Hoque, M. A.; Sugimoto, M. J. B. b., Robust volcano plot: identification of differential metabolites in the presence of outliers. **2018,** *19*, 1-11.
114. Ritchie, M. E.; Phipson, B.; Wu, D. I.; Hu, Y.; Law, C. W.; Shi, W.; Smyth, G. K., limma powers differential expression analyses for RNA-sequencing and microarray studies. *Nucleic acids research* **2015,** *43* (7), e47-e47.
115. Abdi, H., Partial least squares regression and projection on latent structure regression (PLS Regression). *Wiley interdisciplinary reviews: computational statistics* **2010,** *2* (1), 97-106.
116. Lê Cao, K.-A.; Welham, Z. M., *Multivariate data integration using R: methods and applications with the mixOmics package*. Chapman and Hall/CRC: 2021.
117. Lê Cao, K.-A.; Rossouw, D.; Robert-Granié, C.; Besse, P., A sparse PLS for variable selection when integrating omics data. *Statistical applications in genetics and molecular biology* **2008,** *7* (1).
118. Wong, T.-T., Performance evaluation of classification algorithms by k-fold and leave-one-out cross validation. *Pattern recognition* **2015,** *48* (9), 2839-2846.
119. Chevallier, S.; Bertrand, D.; Kohler, A.; Courcoux, P., Application of PLS-DA in multivariate image analysis. *Journal of Chemometrics: A Journal of the Chemometrics Society* **2006,** *20* (5), 221-229.
120. Tiessen, A.; Cubedo-Ruiz, E. A.; Winkler, R., Improved representation of biological information by using correlation as distance function for heatmap cluster analysis. *American Journal of Plant Sciences* **2017,** *8* (3), 502-516.
121. Pang, Z.; Lu, Y.; Zhou, G.; Hui, F.; Xu, L.; Viau, C.; Spigelman, Aliya F.; MacDonald, Patrick E.; Wishart, David S.; Li, S.; Xia, J., MetaboAnalyst 6.0: towards a unified platform for metabolomics data processing, analysis and interpretation. *Nucleic Acids Research* **2024,** *52* (W1), W398-W406.

Appendix

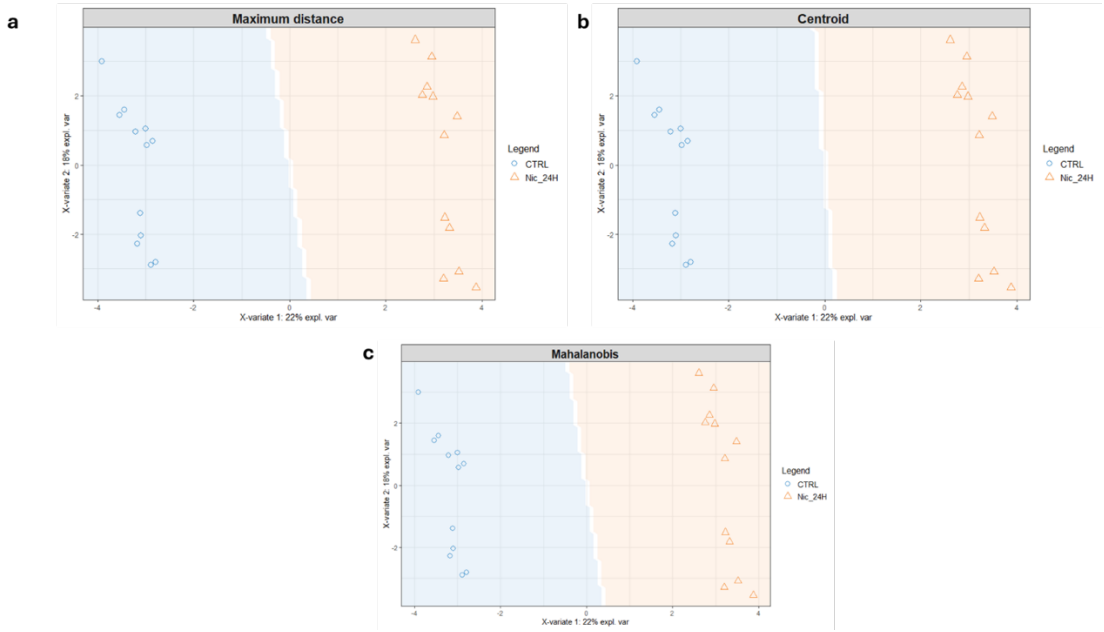

Figure S1. *Sample prediction area plot created using Maximum distance, Centroid and Mahalanobis showing the distribution of samples in validation areas related to Nicotine-24H vs. CTRL (**a,b,c**).*

Table S1. *Pathway Enrichment analysis discriminates between the analysed clusters. The number of hits corresponds to the number of metabolites detected in the spectrum that participate in the biochemical pathways and are explicit in the column "metabolites". Raw p represents the significance validation index reporting the p-value; Holm Bonferroni represents the adjustment of the p-value for the number of analysed samples (Holm p.); the FDR index calculates the number of False Discovery Rates. Biochemical pathways with hits>2 and Raw.p, Holm p, FDR <0.05 were considered significant.*

Pathways Nic vs. Ctrl	Hits	Raw p	Holm p	FDR	Metabolites
Phospholipid Biosynthesis	3	1,31E-11	1,12E-09	1,12E-09	Phosphorylcholine; Choline; Citilcoline
Sphingolipid Metabolism	5	3,26E-10	2,77E-08	1,36E-08	Uridine diphosphate glucose; Phosphorylcholine; Serine; Glucose; ATP
Phosphatidylcholine Biosynthesis	3	4,75E-10	3,99E-08	1,36E-08	Phosphorylcholine; Choline; ATP
Oxidation of Branched Chain Fatty Acids	3	1,83E-05	0.0014267	0.00017477	Succinic acid; Adenosine triphosphate; Carnitine
Citric Acid Cycle	3	6,47E-05	0.0049849	0.00050665	Pyruvic acid; Succinic acid; Adenosine triphosphate
Glycine and Serine Metabolism	12	6,48E-05	0.0049849	0.00050665	2-Ketobutyric acid; Betaine; Glycine; Glutamic acid; L-Threonine; Serine; Pyruvic acid; Sarcosine; L-Arginine; Adenosine triphosphate; Methionine; Homocysteine

Mitochondrial Electron Transport Chain	2	8,79E-05	0.0007028 2	9,44E-01	Succinic acid; Adenosine triphosphate
Butyrate Metabolism	3	3,58E-04	0.026458	0.0023652	Acetoacetic acid; Succinic acid; Adenosine triphosphate
Ketone Body Metabolism	3	5,68E-04	0.041449	0.0034879	3-Hydroxybutyric acid; Acetoacetic acid; Succinic acid
Methionine Metabolism	9	7,64E-04	6,34E-03	1,64E-02	2-Ketobutyric acid; Betaine; Glycine; Serine; Sarcosine; ATP; Methionine; Homocysteine; Choline
Glutamate Metabolism	8	8,34E-04	0.060073	0.0047836	Glutathione; Glutamic acid; Glycine; L-Aspartic acid; Pyruvic acid; Succinic acid; Adenosine triphosphate; Glutamine
Alanine Metabolism	4	4,61E-03	0.32736	0.024016	Glycine; Glutamic acid Pyruvic acid; Adenosine triphosphate
Carnitine Synthesis	4	4,69E-03	3,85E-01	8,07E-02	L- Carnitine; Glycine; Lysine; Succinic acid
Arginine and Proline Metabolism	7	4,52E-02	0.0003662	6,48E-01	Glutamic acid; Proline; L-Aspartic acid; Succinic acid; L-Arginine; Adenosine triphosphate; Glycine

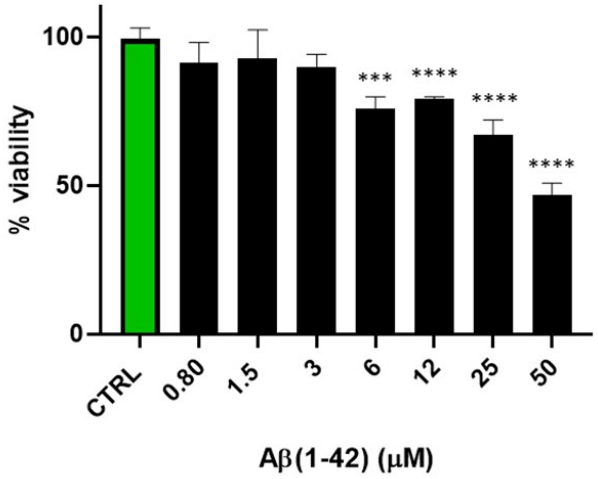

Figure S2. *Aβ(1–42) effect on SH-SY5Y cells viability after 48h, examined by the CCK-8 assay. The viability variations were calculated as the percentage of viable cells in treated cultures compared to untreated ones (CTRL). Results are shown as mean ± standard deviation (SD) from three independent experiments. ***, **** denote respectively $p < 0.001$ and $p < 0.0001$ vs. CTRL.*

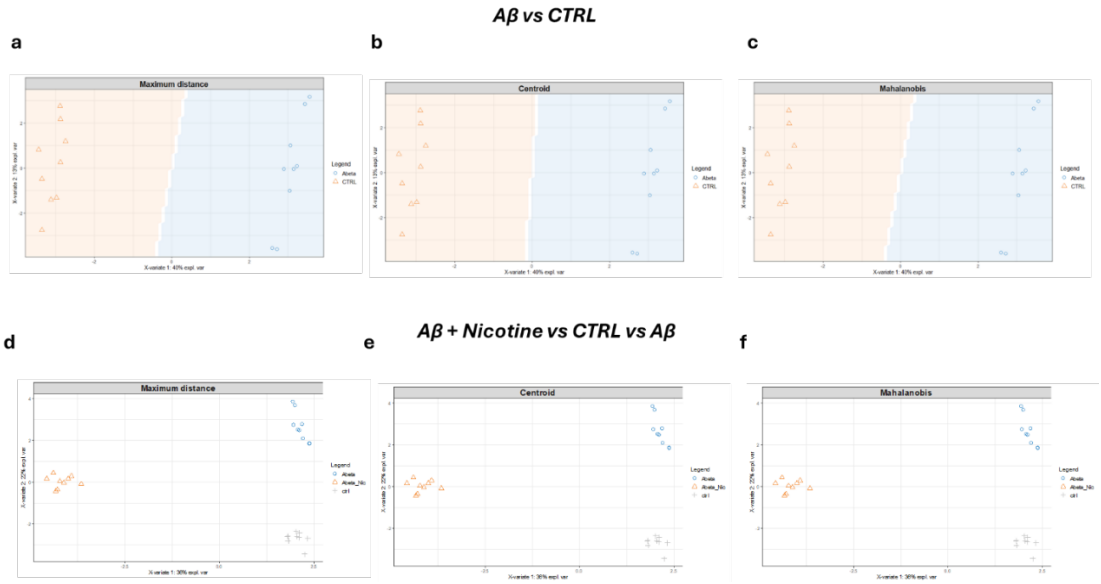

Figure S3. *Sample prediction area plot created using Maximum distance, Centroid and Mahalanobis showing the distribution of samples in validation areas related to Aβ vs. CTRL* ***(a,b,c)*** *and Aβ+Nicotine vs. CTRL vs. Aβ* ***(e,f,g)****.*

Table S2. *Pathway Enrichment analysis discriminates between the analysed clusters. The number of hits corresponds to the number of metabolites detected in the spectrum that participate in the biochemical pathways and are explicit in the column "metabolites". Raw p represents the significance validation index reporting the p-value; Holm Bonferroni represents the adjustment of the p-value for the number of analysed samples (Holm p.); the FDR index calculates the number of False Discovery Rates. Biochemical pathways with hits>2 and Raw.p, Holm p, FDR <0.05 were considered significant.*

Pathways Aβ vs. CTRL	Hits	Raw p	Holm p	FDR	Metabolites
Phosphatidylethanol amine Biosynthesis	3	4,58E-06	3,94E-04	3,94E-04	Choline; Serine; ATP
Citric Acid Cycle	3	1,23E-05	9,90E-03	1,32E-03	Pyruvic acid; Succinic acid; Adenosine triphosphate
Glutamate Metabolism	8	1,36E-05	1,16E-03	5,85E-04	Glycine; Glutathione; Glutamic acid; L-Aspartic acid; Pyruvic acid; Succinic acid; Adenosine triphosphate; Glutamine
Ketone Body Metabolism	3	2,78E-05	2,33E-03	6,36E-05	3-Hydroxybutyric acid; Acetoacetic acid; Succinic acid
Glycine and Serine Metabolism	12	2,96E-05	2,45E-03	6,36E-05	3-Hydroxybutyric acid; Acetoacetic acid; Succinic acid
Warburg Effect	7	6,06E-05	4,97E-03	1,04E-03	2-Ketobutyric acid; Betaine; Glycine; Glutamic acid; L-Threonine; Serine; Pyruvic acid; Sarcosine; L-Arginine; Adenosine triphosphate; Methionine; Homocysteine
Mitochondrial Electron Transport Chain	2	1,22E-04	9,90E-03	1,32E-03	Succinic acid; Adenosine triphosphate
Phytanic Acid Peroxisomal Oxidation	2	1,22E-04	9,90E-03	1,32E-03	Succinic acid; Adenosine triphosphate
Butyrate Metabolism	3	1,10E-03	8,56E-02	1,05E-02	Acetoacetic acid; Succinic acid; Adenosine triphosphate

Methionine Metabolism	9	1,64E-03	1,26E-01	1,41E-02	2-Ketobutyric acid; Betaine; Choline; Glycine; Serine; Sarcosine; Adenosine triphosphate; Methionine; Homocysteine
Sphingolipid Metabolism	4	2,03E-03	1,54E-01	1,59E-02	D-Glucose; Serine; Uridine diphosphate glucose; Adenosine triphosphate
Carnitine Synthesis	4	2,48E-03	1,86E-02	1,78E-02	L-Carnitine; Glycine; Lysine; Succinic acid
Ammonia Recycling	8	3,08E-03	2,28E-02	2,04E-02	Glycine; Glutamic acid; Histidine; Serine; L-Aspartic acid; Pyruvic acid; Adenosine triphosphate; Glutamine
Oxidation of Branched Chain Fatty Acids	3	3,98E-03	2,91E-02	2,45E-02	L-Carnitine; Succinic acid; Adenosine triphosphate
Glucose-Alanine Cycle	3	7,58E-03	5,46E-02	4,35E-02	D-Glucose; Glutamic acid; Pyruvic acid
Cysteine Metabolism	3	8,51E-03	6,04E-03	4,58E-02	D-Glucose; Glutamic acid; Pyruvic acid
Alanine Metabolism	4	1,07E-02	7,49E-03	5,39E-02	Glycine; Glutamic acid; Pyruvic acid; Adenosine triphosphate
Pyruvaldehyde Degradation	2	1,13E-02	7,79E-03	5,39E-02	Glutathione; Pyruvic acid
Pyruvate Metabolism	5	1,61E-02	0.00010966	7,30E-02	Acetic acid; Glutathione; Lactic acid; Pyruvic acid; Adenosine triphosphate
Glycolysis	3	1,90E-02	0.00012722	7,78E-02	D-Glucose; Pyruvic acid; Adenosine triphosphate
Transfer of Acetyl Groups into Mitochondria	3	1,90E-02	0.00012722	7,78E-02	D-Glucose; Pyruvic acid; Adenosine triphosphate
Urea Cycle	6	2,34E-02	0.0001519	8,83E-02	Glutamic acid; L-Aspartic acid; Pyruvic acid; L-Arginine; Adenosine triphosphate; Glutamine
Gluconeogenesis	4	2,36E-02	0.0001519	8,83E-02	D-Glucose; Lactic acid; Pyruvic acid; Adenosine triphosphate

Pathways Aβ+Nicotine vs. Aβ	**Hits**	**Raw p**	**Holm p**	**FDR**	**Metabolites**
Amino Sugar Metabolism	7	3,07E-14	2,64E-12	1,44E-12	Acetic acid; Glutamic acid; Pyruvic acid; Pyrophosphate; Adenosine triphosphate; Glutamine; D-Fructose
Glutamate Metabolism	8	3,62E-14	3,08E-12	1,44E-12	Glycine; Glutathione; Glutamic acid; Pyruvic acid; Succinic acid; Phosphoribosyl pyrophosphate; Adenosine triphosphate; Glutamine
Warburg Effect	7	5,04E-14	4,23E-12	1,44E-12	D-Glucose; Glutamic acid; Lactic acid; Pyruvic acid; Succinic acid; Adenosine triphosphate; Glutamine
Citric Acid Cycle	3	7,66E-14	6,36E-12	1,65E-12	Pyruvic acid; Succinic acid; Adenosine triphosphate
Ketone Body Metabolism	3	7,11E-13	5,83E-11	1,22E-11	3-Hydroxybutyric acid; Acetoacetic acid; Succinic acid
Arginine and Proline Metabolism	7	9,29E-13	7,53E-11	1,33E-11	Glycine; Glutamic acid; Proline; L-Aspartic acid; Succinic acid; L-Arginine; Adenosine triphosphate
Ammonia Recycling	8	1,91E-11	1,52E-09	2,31E-10	Glycine; Glutamic acid; Histidine; Serine; L-Aspartic acid; Pyruvic acid; Adenosine triphosphate; Glutamine

Butyrate Metabolism	3	2,15E-11	1,69E-09	2,31E-10	Acetoacetic acid; Succinic acid; Adenosine triphosphate
Betaine Metabolism	5	4,19E-11	3,27E-09	4,00E-10	Betaine; Choline; Adenosine triphosphate; Methionine; Homocysteine
Glycine and Serine Metabolism	12	9,22E-11	7,10E-10	7,93E-10	2-Ketobutyric acid; Betaine; Glycine; Glutamic acid; Pyruvic acid; Sarcosine; L-Arginine; Adenosine triphosphate; Methionine; Homocysteine
Urea Cycle	6	1,11E-10	8,47E-09	8,72E-10	Glutamic acid; L-Aspartic acid; Pyruvic acid; L-Arginine; Adenosine triphosphate; Glutamine
Carnitine Synthesis	4	2,08E-10	1,56E-08	1,49E-09	L-Carnitine; Glycine; Lysine; Succinic acid
Oxidation of Branched Chain Fatty Acids	3	2,58E-11	1,91E-08	1,71E-09	L-Carnitine; Succinic acid; Adenosine triphosphate
Glycolysis	3	8,64E-10	6,22E-08	4,64E-09	D-Glucose; Pyruvic acid; Adenosine triphosphate
Transfer of Acetyl Groups into Mitochondria	3	8,64E-10	6,22E-08	4,64E-09	D-Glucose; Pyruvic acid; Adenosine triphosphate
Gluconeogenesis	4	1,96E-09	1,33E-11	8,85E-09	D-Glucose; Lactic acid; Pyruvic acid; Adenosine triphosphate
Cysteine Metabolism	3	3,96E-09	2,57E-07	1,55E-08	Glutamic acid; Pyruvic acid; Adenosine triphosphate
Glucose-Alanine Cycle	3	6,44E-09	4,12E-07	2,31E-08	D-Glucose; Glutamic acid; Pyruvic acid
Alanine Metabolism	4	6,45E-09	4,12E-07	2,31E-08	Glycine; Glutamic acid; L-Alanine; Pyruvic acid; Adenosine triphosphate
Pyruvate Metabolism	5	1,21E-08	7,41E-07	4,02E-08	Acetic acid; Glutathione; Lactic acid; Pyruvic acid; Adenosine triphosphate
Aspartate Metabolism	7	1,81E-08	1,09E-06	5,77E-08	Acetic acid, Glutamic acid; L-Aspartic acid; L-Arginine; Adenosine triphosphate; Glutamine; N-Acetyl-L-aspartic acid
Nicotinate and Nicotinamide Metabolism	3	4,17E-08	2,46E-06	1,28E-07	Glutamic acid; Adenosine triphosphate; Glutamine
Valine, Leucine and Isoleucine Degradation	8	6,10E-08	3,54E-06	1,81E-07	Acetoacetic acid; Glutamic acid; Isoleucine; Methylmalonic acid; Succinic acid; Adenosine triphosphate; Leucine; L-Valine
Tryptophan Metabolism	4	7,06E-08	3,95E-06	1,96E-08	Formic acid; Glutamic acid; Adenosine triphosphate; L-Tryptophan
Methionine Metabolism	9	7,93E-08	4,36E-06	2,13E-07	2-Ketobutyric acid; Betaine; Choline; Glycine; Serine; Sarcosine; Adenosine triphosphate; Methionine; Homocysteine
Purine Metabolism	5	1,06E-07	5,74E-06	2,77E-07	Glycine; Glutamic acid; L-Aspartic acid; Adenosine triphosphate; Glutamine
Homocysteine Degradation	3	1,40E-06	7,12E-05	3,34E-06	2-Ketobutyric acid; Serine; Homocysteine
Phosphatidylethanolamine Biosynthesis	3	2,20E-06	1,01E-04	4,62E-06	Choline; Serine; Adenosine triphosphate
Tyrosine Metabolism	4	2,79E-06	1,23E-04	5,58E-06	Acetoacetic acid; Glutamic acid; L-Tyrosine; L-Aspartic acid
Fatty Acid Biosynthesis	3	5,72E-06	2,46E-04	1,12E-05	Acetic acid; Acetoacetic acid; 3-Hydroxybutyric acid

Sphingolipid Metabolism	4	7,82E-06	3,28E-04	1,47E-05	D-Glucose; Serine; Uridine diphosphate glucose; Adenosine triphosphate
Glutathione Metabolism	5	8,50E-06	3,40E-04	1,56E-05	Glycine; Glutathione; Glutamic acid; Pyroglutamic acid; Adenosine triphosphate
Folate Metabolism	3	1,20E-05	4,69E-04	2,16E-05	Formic acid; Glutamic acid; Adenosine triphosphate
Selenoamino Acid Metabolism	3	1,75E-05	6,65E-04	3,07E-05	2-Ketobutyric acid; Serine; Adenosine triphosphate
Phenylalanine and Tyrosine Metabolism	5	3,01E-05	1,11E-03	5,17E-05	Acetoacetic acid; Glutamic acid; L-Tyrosine; Phenylalanine; Adenosine triphosphate
Propanoate Metabolism	6	1,20E-04	4,32E-03	2,02E-04	2-Ketobutyric acid; 2-Hydroxybutyric acid; Glutamic acid; Methylmalonic acid; Adenosine triphosphate; L-Valine

Chapter III

Metabolomic approach to evaluate the protective effect of NGF in AD cellular model

3.1 The role of NGF in Alzheimer's disease

Nerve Growth Factor (NGF) is one of the main neurotrophic factors, first identified in the 1950s by Rita Levi-Montalcini, a discovery that earned her the Nobel Prize in Physiology or Medicine in 1986.[1] NGF regulates neuronal viability, plasticity and growth, binding to two receptors: the low-affinity NGF receptor (p75) and the high-affinity NGF receptor (TrkA), which are both expressed in basal forebrain cholinergic neurons and are known to innervate the hippocampal structure. [2]

NGF is synthesized as an unprocessed precursor form, proNGF, which undergoes post-translational processing to produce the mature protein.[3] NGF appears to act via retrograde signaling: it is released by target cells and initiates signaling pathways that propagate retrogradely along the axon. [4]

Several pieces of evidence demonstrate a strong link between NGF and the cholinergic system in the hippocampus. Indeed, injecting NGF in the cerebrospinal fluid induces an increase in choline acetyltransferase activity in the hippocampus. [5] Furthermore, NGF has been shown to protect basal forebrain cholinergic neurons after axonal damage of hippocampal projecting fibres. [6]

Alterations in the brain NGF metabolic pathway have been reported, especially in basal forebrain cholinergic neurons of patients affected with Alzheimer's disease (AD). Among the various hypotheses proposed to explain AD pathogenesis, the NGF hypothesis stands out.[7] This theory is supported by the well-established and tightly regulated relationship between cholinergic neurons and NGF signaling, suggesting that disruptions in NGF availability or signaling may contribute to the degeneration of these neuronal populations.

Actually, cognitive deficits in AD are associated with cholinergic neuron degeneration, and the basal forebrain cholinergic system remains the only brain region

that depends on NGF during postnatal development. Several dysfunctions in NGF signaling, transport, maturation, and degradation characterize AD brains.[8] Even if cortical NGF mRNA levels remain normal in AD, the level of the immature form of the growth factor called proNGF is upregulated in basal forebrain tissue.[9] Consistently, the enzymes involved in its maturation (tPA, plasminogen, and plasmin protein) are dramatically decreased in postmortem AD brains. Moreover, analysis of the main NGF-degrading protease, MMP-9, revealed a marked increase in its activity compared with control cases. [10]

All these effects together contribute to inducing a low level of the mature form of NGF – that is, the one active – and an accumulation of the inactive proNGF.

Based on these premises, the neuroprotective and regenerative effects of NGF on cholinergic neurons have been extensively investigated, yielding positive outcomes in both animal models of AD and clinical studies. [11]

Despite the neuroprotective effects of NGF on neuronal degeneration, its therapeutic application is constrained by two significant limitations: its poor permeability across the blood–brain barrier (BBB) and the dose-dependent induction of pain as a significant side effect. [12, 13]

For this reason, advanced delivery systems have been explored to enhance NGF concentration in the brain and to address its pharmacokinetic limitations. These approaches range from early methods such as intracerebral infusion to more modern delivery technologies, including nasal and intraocular administration routes. In addition, gene- and cell-mediated NGF-based therapies, as well as NGF release from polymer-encapsulated cells, have emerged as promising strategies to improve targeted delivery and therapeutic efficacy. [11, 14]

To address the second limitation, a NGF mutant, named CHF6467 has been develop. CHF6467 sequence included two mutations compared to wild type NGF: P61SR100E. R100E has been introduced to improve the tolerability of NGF in clinical use, since this mutation confer a reduction in pain side effect; P61S mutation was introduced purely as a marker of the recombinant form, to allow CHF6467 to be distinguishable in the presence of wild type NGF. [15]

NGF has a well-established role in the prevention and control of AD; however, the precise molecular mechanisms underlying its neuroprotective effects remain only partially understood. Experimental studies in murine models have shown that

elimination of NGF via transgenic expression of anti-NGF antibodies results in severe deficits in basal forebrain cholinergic neurons. [16] Moreover, NGF depletion has been associated with the induction of AD-like pathological features, including amyloid-β (Aβ) aggregation, tau hyperphosphorylation, and synaptic dysfunction. In contrast, NGF supplementation has demonstrated beneficial effects, including modulation of Aβ pathology and alleviation of memory impairment in AD mouse models. [7, 17] These findings support the hypothesis that NGF may act as a suppressor of Aβ-induced neurotoxicity. Nevertheless, the exact mechanisms by which NGF exerts its protective influence remain incompletely characterized. A comprehensive investigation of NGF's role in cellular processes could uncover previously unrecognized aspects of its mechanism of action and open new avenues for its therapeutic use.

3.2 Aim of the study

The implication of NGF dysregulation in AD is well established, and its therapeutic potential has been demonstrated in both preclinical models and clinical studies. These findings underscore the relevance of NGF as a pharmacological intervention in AD. [11, 18]

Given the rising prevalence of AD and projections for continued growth in the coming years, the development of effective therapeutic strategies is of critical importance. Although the limitation related to pain side effects cannot be overlooked, the availability of a "painless" mutant provides a means to overcome this issue. [15]

In this context, elucidating the mechanisms underlying the beneficial effects of CHF6467 – hereafter referred to simply as NGF – in AD is crucial for the development of innovative pharmacological strategies. Identification of previously unrecognized biological pathways underlying its action may serve as a starting point for clearify its effect and develop new drug candidates. From this perspective, metabolomics has recently emerged as a powerful tool capable of providing a comprehensive view of the biochemical pathways associated with disease or treatment, particularly unforeseen biological responses. [19, 20]

Considering the importance of amyloid-β peptide as a pathological hallmark of Alzheimer's disease (AD), and in light of the results presented in Chapter II – where Aβ1-42 treatment in our cellular model induced dysregulation comparable to that

observed in patients and animal models – we applied a metabolomic approach to investigate the effects of NGF on SH-SY5Y cells in the presence of Aβ peptide.

We consider metabolomics a technique highly suitable for comprehensively assessing the global impact of NGF. It enables an unbiased investigation into its mechanism of action, ensuring that the analysis remains broad, rigorous, and free from restrictive assumptions.

The experimental workflow is illustrated in **Figure 3.1**. We demonstrated that NGF can protect SH-SY5Y cells from Aβ(1–42)-induced toxicity when cells are pretreated for 24 hours. To elucidate the site and nature of NGF's action, we compared the metabolic profiles of SH-SY5Y cells treated with NGF and Aβ(1–42) to those exposed only to Aβ(1–42) and to untreated control cells. This allowed us to evaluate NGF's ability to counteract Aβ -induced metabolic dysregulation.

To further investigate NGF's mode of action, we focused on the early biochemical changes induced during the pretreatment phase. This strategy enabled a comprehensive evaluation of the initial molecular events that may underlie NGF's protective effect against Aβ(1–42) toxicity.

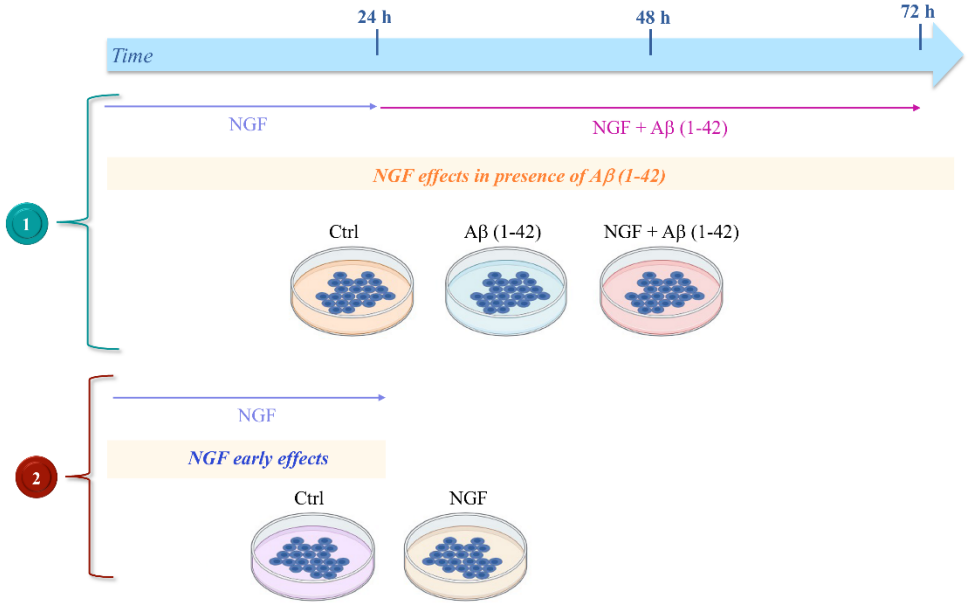

Figure 3.1 *Experimental workflow. NMR metabolomics was the approach used to evaluate the mechanism of action of NGF in presence of a pathological insult, i.e. amyloid peptide. Then, we evaluated early biochemical changes induced during the pretreatment phase. Figure created using BioRender, https://www.biorender.com/.*

It is important to emphasize that the untargeted metabolic profiling applied in this study offers a static representation of cellular status at the end of the treatment period.

Consequently, it does not reflect dynamic metabolic fluxes occurring throughout the biological system. Nevertheless, the quantitative data obtained provide a robust basis for future mechanistic studies exploring the impact of NGF exposure on neuronal cells, both in the presence and absence of pathological insults.

3.3 Results

3.3.1 NGF protects SH-SY5Y cells from Aβ(1–42) toxicity

The NGF mutant CHF6467 was expressed in *E. coli* as proNGF using a method newly established, during my PhD, by downscaling and adapting an industrial protocol. The expression and purification procedures, currently under patent application, are detailed in the Materials and Methods section. All subsequent experiments were performed using the mutant CHF6467, hereafter referred to simply as NGF.

To evaluate the protective effect of NGF on SH-SY5Y neuroblastoma cells, a cell viability assay was performed. The results confirmed that NGF exerts a protective effect against Aβ(1–42)-induced toxicity. As shown in **Figure 3.2**, SH-SY5Y cells exposed to Aβ(1–42) (50 μM) exhibited a survival rate of 50.12 ± 3.91%. In contrast, co-treatment with NGF at concentrations of 200 μg/ml and 100 μg/mL preserved cell viability, increasing survival to 71.1 ± 0.18% and 75.56 ± 5.14%, respectively.

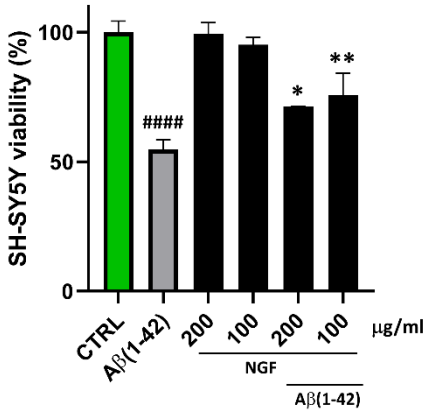

Figure 3.2 *Neuroprotective effect of NGF against Aβ(1–42)-induced cytotoxicity. Cell viability was examined by the CCK-8 assay. SH-SY5Y cells were exposed to NGF (100 μg/mL and 200 μg/mL) for 24 h before administration of Aβ(1- 42) recombinant monomer 50 μM for an additional 48 h. The viability variations were calculated as the percentage of viable cells in treated cultures compared to untreated ones (CTRL). Results are shown as mean ± standard deviation (SD) from three independent experiments.* $^{\#\#\#\#}$ *denote $p < 0.0001$ vs. Ctrl; *, ** denote respectively $p < 0.05$ and $p < 0.01$ vs. Aβ(1–42).*

3.3.2 NGF modulation of amyloid altered pathways

Based on the interesting outcomes of the nicotine study – presented in the Chapter II – we conducted a combined metabolomic analysis of the intracellular and extracellular compartments to evaluate the protective mechanisms induced by NGF in the context of AD. Quantitative data on metabolites were derived from the study of 1D ^{1}H NOESY NMR spectra, acquired from both the endometabolome and the exometabolome. [21]

In more details, we performed a sparse Partial Least Squares Discriminant Analysis (sPLS-DA) to compare the metabolomic profiles of three distinct cell groups: (i) cells treated with NGF followed by incubation with Aβ(1–42) (Abeta_NGF); (ii) cells incubated with Aβ(1–42) alone (Abeta); and (iii) untreated control cells (CTRL). The resulting score scatter plot revealed a clear separation between the metabolic profile of Abeta cells – representing the pathological condition – and both the control and Abeta_NGF groups (**Figure 3.3A**). The validity of the model was evaluated through cross-validation, yielding Q^2 values of 0.65 and 0.90 for PC1 and PC2, respectively. Additional validation was performed using ROC curve analysis (**Figure S1**). These results indicate a significant effect of NGF on reverting the metabolic alterations caused by Aβ(1–42).

The metabolites contributing most significantly to this clustering are illustrated in the alluvial plot (**Figure 3.3B**), which highlights compounds with Variable Importance in Projection (VIP) scores > 1 that exhibit differential abundance across intra- and extracellular compartments among the three experimental conditions.

The alluvial plot reveals that the cells pretreated with NGF before incubation with Aβ(1–42) have low intracellular concentrations of 1-methylguanine, acetylcholine, glutamate, methionine, and UDP-N-acetylglycine, while high concentrations of fucose and GABA. In contrast, the exometabolome of this group of cells has the highest concentrations of glutamine, ketoleucine, and pyruvate, while showing low concentrations of 3-hydroxybutyrate, isoleucine, leucine, and proline. Our analysis highlights that the exchange between the two cellular compartments is particularly important for some metabolites: acetate, arginine, glycine, histidine, and lactate, whose concentrations show to change in the endo and exometabolome.

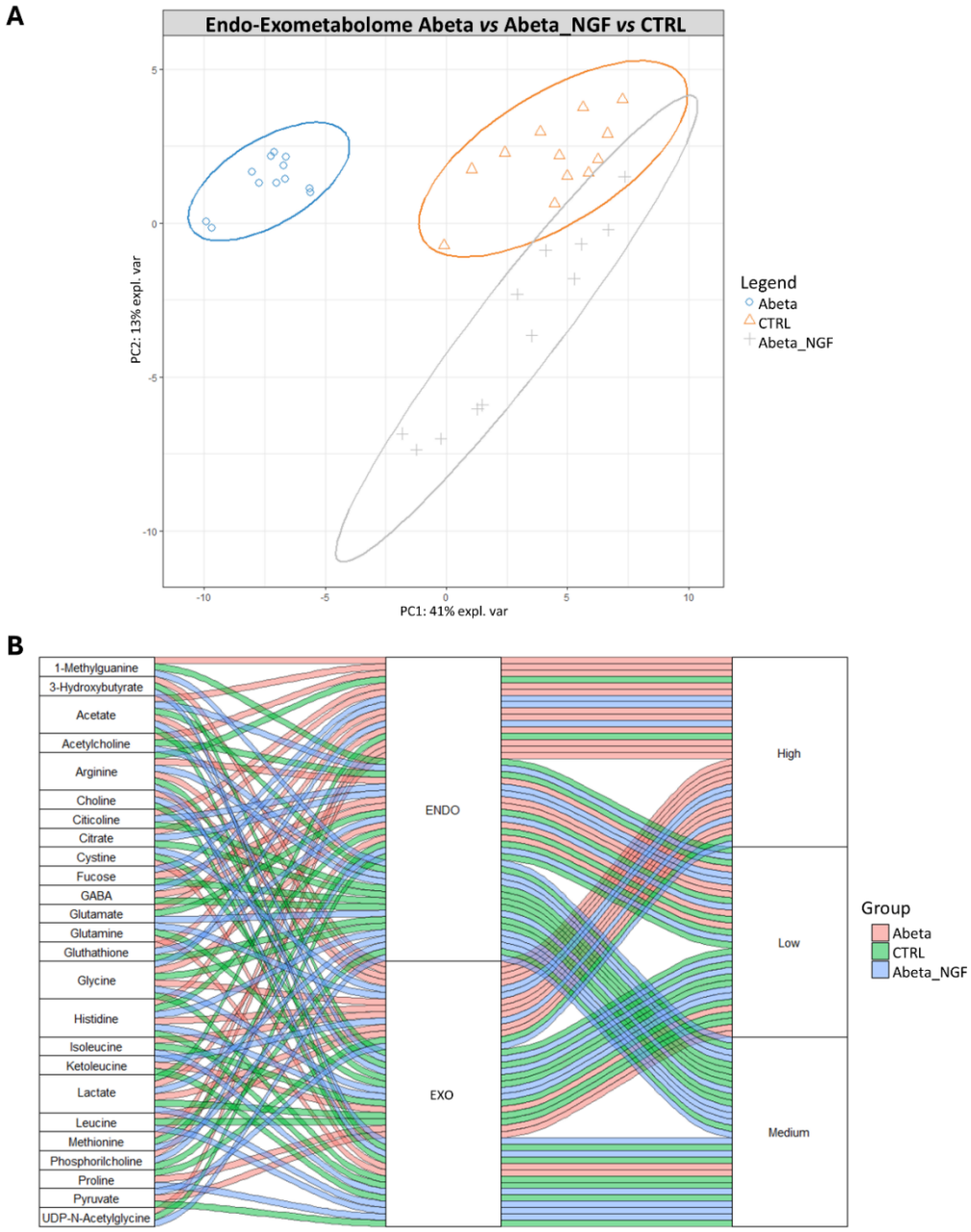

Figure 3.3 *(**A**) sPLS-DA score scatter plots related to the combined matrices of endo and exometabolome of SH-SY5Y cells treated with Aβ(1–42) in blue (Abeta) vs. cells pretreated with NGF before being incubated with Aβ(1–42) in grey (Abeta_NGF) vs. control cells in orange (CTRL). The cluster analyses are reported in the Cartesian space described by the principal components PC1:41% and PC2:13%. sPLS-DA was evaluated using cross-validation (CV) analysis. CV tests performed according to the sPLS-DA statistical protocol show significant cluster separation (0.63 and 0.86 accuracy values on PC1 and PC2, respectively, with positive Q^2 indices of 0.65 and 0.90, respectively). (**B**) Alluvial plot reporting metabolites discriminating clusters analysed in sPLS-DA and classified according to VIP value. The first column reports the discriminating metabolites, the second column is the cellular compartment, and the third column is the concentration change. The maximum concentrations in the comparison between the three clusters are indicated as "High", the intermediate as "Medium", and the minimum as "Low". The lines connect the metabolite, the cell compartment where it is discriminating and the column representing quantitative variation. Each line is reported in pink if the metabolite has the variation in the clusters of*

cells incubated with Aβ(1–42); in blue if the variation is typical of cells pretreated with NGF before being incubated with Aβ(1–42), and in green if the variation is typical of control cells.

The **Figure 3.4** presents heatmaps illustrating the average concentrations of both intracellular and extracellular metabolites across the three experimental cell groups. This analysis reveals that the metabolomic profiles of neuroblastoma cells treated with NGF and Aβ(1–42) closely cluster with those of untreated control cells, both for the endometabolome and the exometabolome. This clustering reflects a high degree of similarity in metabolic signatures between Abeta_NGF-treated cells and healthy controls, suggesting that NGF administration can report the metabolic conditions of Aβ(1–42)- exposed cells to those of untreated cells.

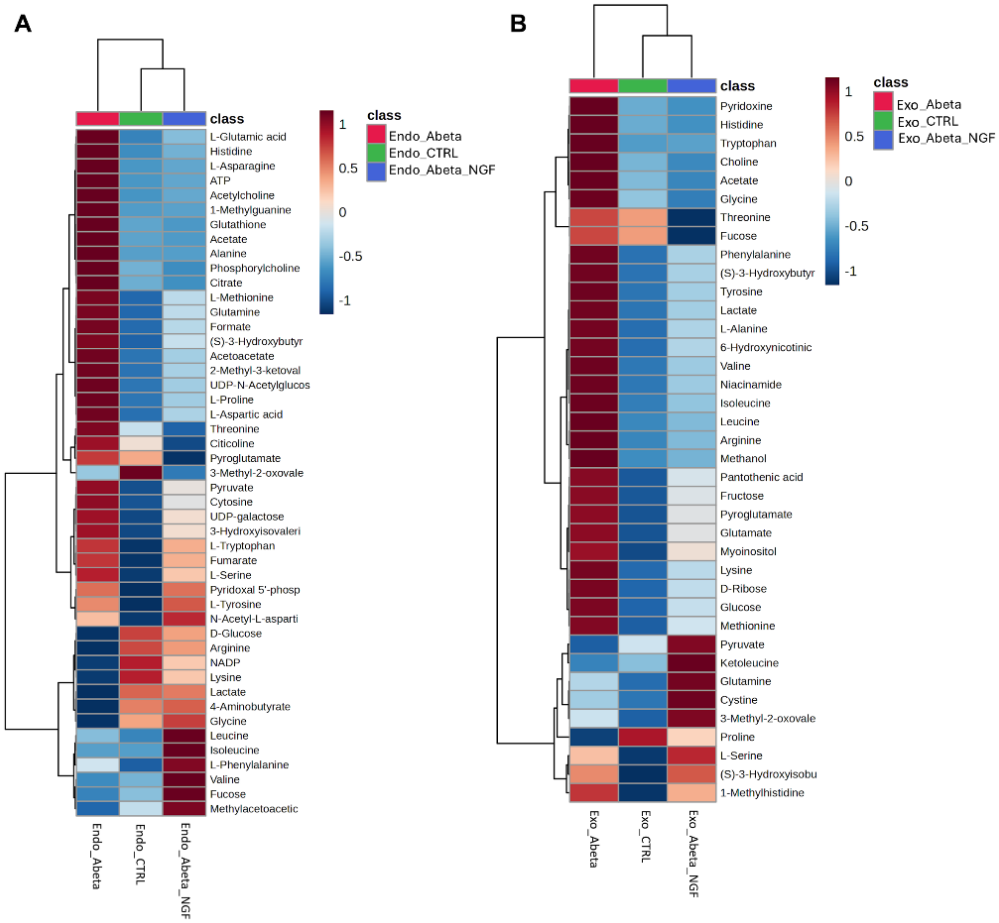

Figure 3.4 *Heatmaps showing changed metabolites in i) SH-SY5Y cells treated with Aβ(1–42), ii) SH-SY5Y cells treated with both Aβ(1–42) and NGF, and iii) untreated SH-SY5Y cells, for exo- (**A**) and endometabolome (**B**). The color of each section corresponds to a concentration value of each metabolite calculated by a normalized concentration matrix (red, up-regulated; blue, down-regulated).*

Table 3.1 presents the results of the *Pathway Enrichment Analysis*, conducted to interpret the NMR-based metabolomic data and identify the specific biochemical pathways modulated by NGF in the presence of Aβ(1–42). The analysis demonstrates modulation of several amino acid-related pathways, including glutamate, alanine, methionine, betaine, glycine and serine, aspartate, and arginine and proline metabolism. In addition to these, lipid-associated processes such as *carnitine synthesis, phospholipid and phosphatidylcholine biosynthesis*, and *sphingolipid metabolism* also appear to be affected. Furthermore, sugar-related pathways – including *amino sugar metabolism, gluconeogenesis, the glucose–alanine cycle, and glycolysis* – emerge as significantly modulated. Finally, the analysis also revealed alterations in *spermidine and spermine metabolism*, as well as in *glutathione metabolism*.

Table 3.1 *Enrichment pathway analysis: pathway discriminating Aβ(1–42)-treated cells and cells exposed to both NGF and Aβ(1–42). For each pathway is reported raw p-value, Holm p, FDR value and metabolites involved. Only pathways with hits >1 and both raw p-values and Holm-adjusted p-values <0.05 were considered significant.*

Pathway	***Hits***	***Raw p***	***Holm p***	***FDR***	***Metabolites***
Glutamate Metabolism	1	8,54E-14	7,86E-12	7,86E-12	Acetoacetic acid; Glutamic acid; Isoleucine; 3-Methyl-2-oxovaleric acid; Adenosine triphosphate; Leucine; Valine; Pyridoxal 5'-phosphate
Alanine Metabolism	6	1,99E-13	1.81E-14	9,15E-11	Glycine; Glutamic acid; L-Alanine; Pyruvic acid; Pyridoxal 5'-phosphate; ATP
Spermidine and Spermine Biosynthesis	3	1,99E-12	1,69E-09	2,28E-10	Methionine; ATP; Pyridoxal 5'-phosphate
Methionine Metabolism	5	9,33E-12	8,30E-10	1,73E-10	Pyridoxal 5'-phosphate; ATP; Methionine; Glycine; Serine
Carnitine Synthesis	3	9,40E-12	8,30E-10	1,73E-10	Glycine; Lysine; Pyridoxal 5'-phosphate
Betaine Metabolism	2	1,57E-11	1,36E-09	2,26E-10	Methionine; ATP
Glycine and Serine Metabolism	10	1,72E-11	1,48E-09	2,26E-10	Glutamic acid; L-Alanine; L-Threonine; Serine; Glycine; Methionine; Pyruvic acid; ATP; Pyridoxal 5'-phosphate;
Amino Sugar Metabolism	6	2,45E-11	2,06E-10	2,51E-10	Uridine diphosphate-N-acetylglucosamine; Acetic acid;

					Glutamic acid; Glutamine; ATP; Pyruvic acid
Phospholipid Biosynthesis	3	1,59E-10	1,32E-08	1,46E-09	Phosphorylcholine; Acetylcholine
Phosphatidylcholine Biosynthesis	2	7,25E-10	5,94E-09	6,06E-09	Phosphorylcholine; Acetylcholine; Citicoline
Gluconeogenesis	4	4,85E-09	3,88E-07	3,43E-08	Glucose; Lactic acid; Pyruvic acid; ATP
Glutathione Metabolism	7	8,03E-09	6,35E-08	4,71E-08	Glycine; Glutathione; Glutamic acid; L-Alanine; NADP; Pyroglutamic acid; Adenosine triphosphate
Aspartate Metabolism	10	1,57E-08	1,19E-06	8,50E-08	Fumaric acid; Glutamic acid; L-Asparagine; Acetic acid; Fumaric acid; Asparagine; Aspartate; NAA; Pyridoxal 5'-phosphate; ATP
Glucose-Alanine Cycle	6	5,71E-08	4,17E-06	2,63E-07	D-Glucose; Glutamic acid; L-Alanine; NADP; Pyruvic acid; Pyridoxal 5'-phosphate
Arginine and Proline Metabolism	9	2,46E-07	1,77E-05	1,05E-06	Fumaric acid; Glutamic acid; Proline; L-Aspartic acid; Glycine; NADP; Arginine; Pyridoxal 5'-phosphate; ATP
Sphingolipid Metabolism	6	2,50E-07	1,78E-05	1,05E-06	ATP; Glucose; Serine; Phosphorylcholine; Pyridoxal 5'-phosphate; Glucose
Glycolysis	3	4,38E-07	3,07E-05	1,75E-06	Glucose; Pyruvic acid; ATP

3.3.3 NGF effects

To identify early biochemical changes that could underlie NGF's protective effect against Aβ(1–42) toxicity, we analysed the metabolomic profiles of SH-SY5Y neuroblastoma cells subjected only to the pretreatment with NGF (100 μg/mL for 24 hours). The metabolic signature of NGF-treated cells was compared with that of untreated controls using sPLS-DA (**Figure 3.5A**). The score plot reveals a clear metabolic shift induced by NGF, affecting both intracellular and extracellular compartments. The performance of the model was evaluated by cross-validation, yielding positive 0.94 and 0.85 Q^2 indices for PC1 and PC2, respectively. Model robustness was further confirmed using using ROC curve analysis (**Figure S2**).

The alluvial plot, in **Figure 3.5B**, illustrates the metabolites responsible for this separation, highlighting those with VIP scores > 1. NGF treatment increased intracellular levels of citicoline, citrate, fumarate, GABA, and serine, while reducing acetylcholine and N-acetylaspartate (NAA) levels. In the extracellular space, NGF exposure decreased aspartate, cystine, and formate concentrations and increased glycine, isoleucine, and serine levels.

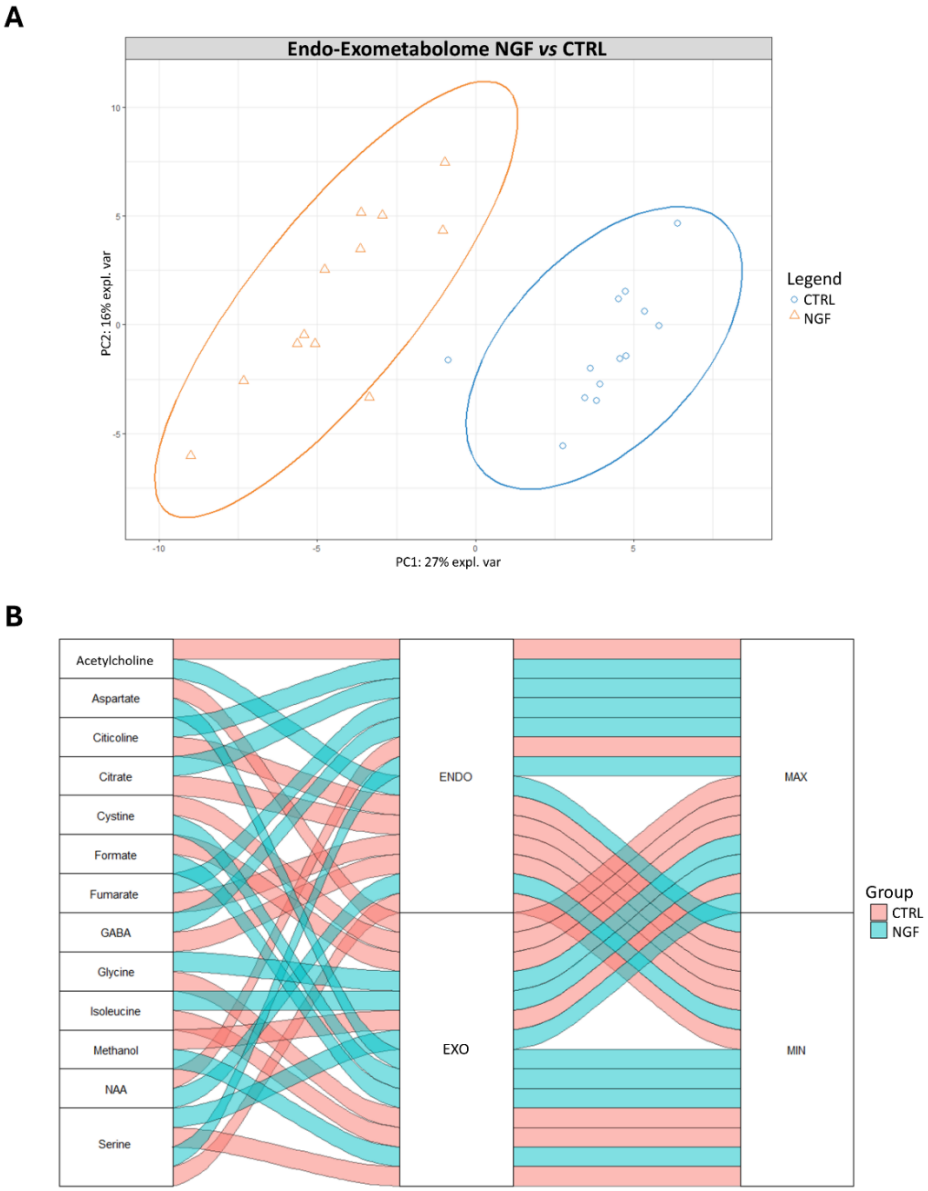

Figure 3.5 *(A) sPLS-DA score scatter plots related to the metabolomic profile of combined cellular compartments related to SH-SY5Y treated with NGF for 24 h (NGF) vs. control cells (CTRL). The cluster analyses are reported in the Cartesian space described by the principal components PC1:27% and PC2:16%. sPLS-DA was evaluated using cross-validation (CV) analysis. CV tests performed according to the sPLS-DA statistical protocol show a significant cluster separation (0.96 and 1.0 accuracy values on PC1 and PC2, with positive 0.94 and 0.85*

*Q^2 indices, respectively). (**B**) Alluvial plot reporting metabolites discriminating clusters analyzed in sPLS-DA and classified according to VIP value. The first column reports the discriminating metabolites, the second column is the cellular compartment, and the third column is the concentration change. The maximum concentrations in the comparison between the two clusters are indicated with "Max", and the minimum with "Min". The lines connect the metabolite, the cell compartment where it is discriminating and the column representing quantitative variation. Each line is reported in green if the metabolite has the variation in the clusters of cells incubated with NGF; in pink if the variation is typical of control cells.*

To investigate the relationship between intra- and extracellular metabolites, a Cluster Image Map and a Relevance Network Graph were constructed, revealing fumarate as the most interconnected metabolite (**Figures 3.6A, B**). Its intracellular increase was positively correlated with extracellular serine, isoleucine, glycine, and methylamine, and negatively correlated with proline, cystine, arginine, and formate.

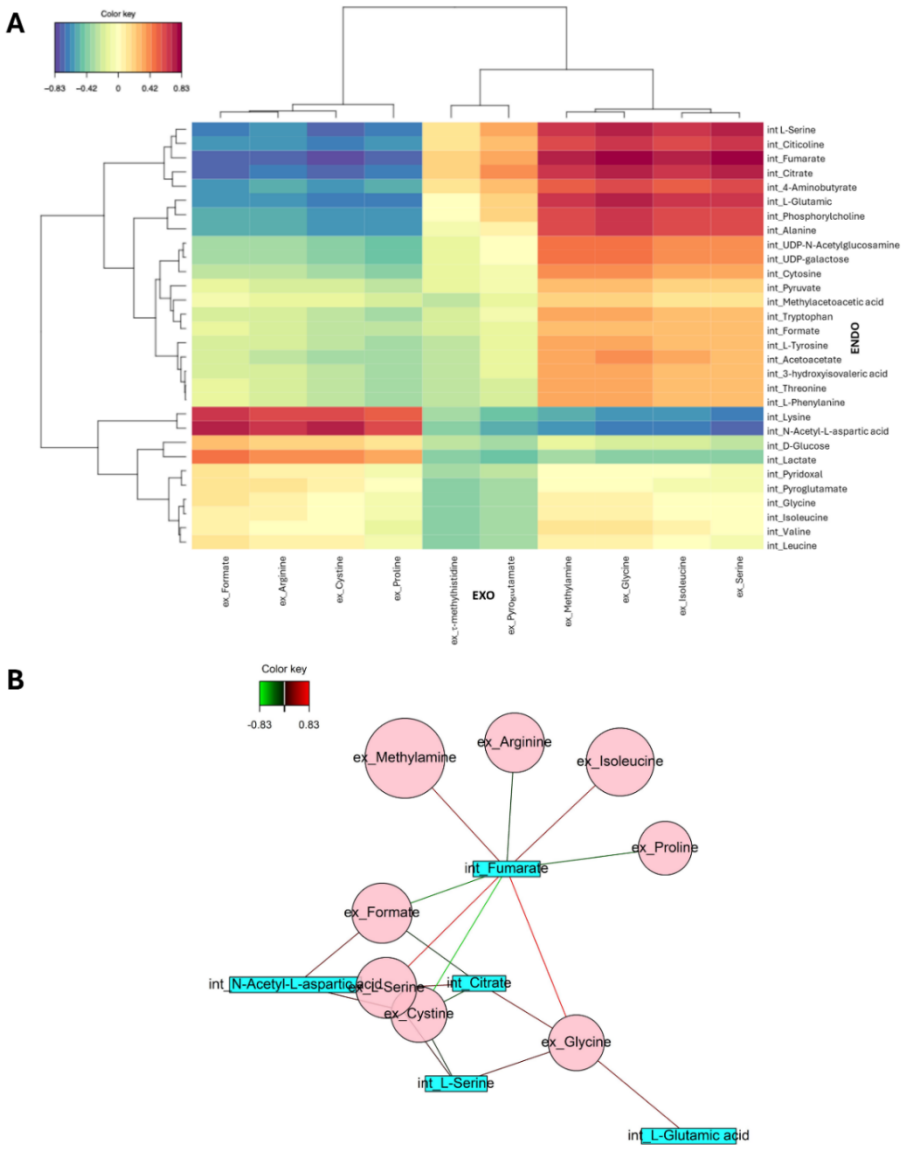

Figure 3.6 *(A) Cluster Image Map: visualization of the relationships between intracellular metabolites (columns) and extracellular metabolites (rows). Linear correlation was conducted*

*using the Pearson coefficient. Negative correlations are shown in shades of blue, while positive correlations are depicted in red. (**B**) Relevance Network Graph: connections between intracellular and extracellular metabolites in SH-SY5Y exposed to NGF compared to control cells are shown. Extracellular metabolites are represented by pink circles, intracellular metabolites by blue rectangles. Larger circle sizes indicate stronger correlations and a greater contribution of the metabolite to cluster differentiation. Green lines represent indirect correlations, while red lines indicate direct correlations.*

To further explore the biochemical pathways affected by NGF in line with the observed metabolite changes, we performed a pathway enrichment analysis of the intracellular metabolite dataset **(Table 3.2**).

Table 3.2 *Enrichment pathway analysis: pathway discriminating NGF-treated cells and control cells. For each pathway is reported raw p-value, Holm p, FDR value and metabolites involved. Only pathways with hits >1 and both raw p-values and Holm-adjusted p-values <0.05 were considered significant.*

Pathway	***Hits***	***Raw p***	***Holm p***	***FDR***	***Metabolites***
Phospholipid Biosynthesis	3	2,45E-09	2,26E-07	2,26E-07	Acetylcholine; Phosphorylcholine; Citicoline
Aspartate Metabolism	10	3,08E-08	2,80E-06	1,42E-06	Fumaric acid; Glutamic acid; L-Asparagine; Acetic acid; L-Aspartic acid; Arginine; ATP; NAA; Pyridoxal5-phosphate
Mitochondrial Electron Transport Chain	2	1,57E-07	1,42E-05	3,11E-06	Fumaric acid; ATP
Citric Acid Cycle	4	1,76E-07	1,57E-02	3,11E-06	Citric acid; Fumaric acid; Pyruvic acid; ATP
Arginine and Proline Metabolism	9	1,95E-07	1,71E-05	3,11E-06	Glycine; Fumaric acid; Glutamic acid; Proline; L-Aspartic acid; NADP; Pyridoxal 5'-phosphate;
Phenylalanine and Tyrosine Metabolism	7	3,08E-07	2,62E-05	3,55E-06	Acetoacetic acid; Fumaric acid; Glutamic acid; L-Tyrosine; Phenylalanine; ATP; Pyridoxal 5'-phosphate
Biotin Metabolism	2	3,81E-07	3,20E-05	3,89E-06	Lysine; ATP
Tyrosine Metabolism	7	4,69E-07	3,89E-05	4,31E-06	Fumaric acid; Glutamic acid; L-Tyrosine; L-Aspartic acid; Acetoacetic acid; Pyridoxal 5'-phosphate
Propanoate Metabolism	4	6,06E-07	4,97E-05	5,07E-06	Glutamic acid; ATP; Valine; Pyridoxal 5'-phosphate
Selenoamino Acid Metabolism	4	2,44E-06	1,96E-04	1,73E-05	L-Alanine; Serine; Pyridoxal 5'-phosphate; ATP

Phosphatidylethanolamine Biosynthesis	2	3,81E-06	2,97E-04	2,34E-05	ATP; Serine
Lysine Degradation	4	9,12E-06	6,77E-04	2,89E-05	Glutamic acid; Lysine; Pyridoxal 5'-phosphate; ATP
Phosphatidylcholine Biosynthesis	2	2,09E-05	1,31E-03	6,40E-05	ATP; Phosphorylcholine
Homocysteine Degradation	2	2,36E-05	1,46E-03	7,01E-05	ATP; Acetoacetate
Butyrate Metabolism	2	3,10E-05	1,89E-03	8,90E-05	gamma-Aminobutyric acid; Glycine; Glutathione; Glutamic acid; L-Alanine; L-Aspartic acid; NADP; Pyruvic acid; ATP; Glutamine; Pyridoxal 5'-phosphate
Glutamate Metabolism	11	4,29E-05	2,53E-03	1,16E-04	Acetoacetic acid; Glutamic acid; Isoleucine; 3-Methyl-2-oxovaleric acid; Adenosine triphosphate; Leucine; Valine; Pyridoxal 5'-phosphate
Valine, Leucine and Isoleucine Degradation	8	1,12E-04	6,19E-03	2,72E-04	Acetoacetic acid; Glutamic acid; Isoleucine 3-Methyl-2-oxovaleric acid; Adenosine triphosphate Leucine; Valine; Pyridoxal 5'-phosphate
Purine Metabolism	7	2,21E-04	1,92E-02	3,11E-06	Glycine; Fumaric acid; Glutamic acid; Adenosine triphosphate; L-Aspartic acid; NADP; Glutamine
Urea Cycle	9	2,36E-04	2,03E-05	3,11E-06	Fumaric acid; Glutamic acid; L-Alanine; L-Aspartic acid; Pyridoxal 5'-phosphate; Glutamine
Carnitine Synthesis	3	2,68E-04	1,42E-02	6,17E-04	Glycine; Lysine; Pyridoxal 5'-phosphate
Ammonia Recycling	10	3,92E-04	2,00E-02	8,58E-04	Glycine; Glutamic acid; L-Asparagine; Histidine; Serine; L-Aspartic acid; Glutamine; Pyridoxal 5'-phosphate
Glycine and Serine Metabolism	10	4,35E-04	2,18E-02	9,31E-04	Glutamic acid; L-Alanine; L-Threonine; Serine; Glycine; Methionine; Pyruvic acid; ATP; Pyridoxal 5'-phosphate;
Histidine Metabolism	5	4,51E-04	2,21E-02	9,43E-04	Glutamic acid; Histidine; ATP; Pyridoxal 5'-phosphate; NADP

The most prominently altered pathway was phospholipid biosynthesis, including *phosphatidylethanolamine and phosphatidylcholine biosynthesis*. Several amino acid-related pathways were also affected, including *arginine and proline metabolism, valine, leucine, and isoleucine degradation, glycine and serine metabolism, selenoamino acid metabolism,* and *lysine degradation*. Alterations in neurotransmission-related processes were suggested by changes in the metabolism of aspartate, glutamate, phenylalanine, and tyrosine. Additionally, pathways associated with cellular energy regulation were affected, including the *citric acid cycle, electron transport chain, biotin metabolism, propionate metabolism,* the *urea cycle,* and *carnitine metabolism*.

3.4 Discussion

3.4.1 The multifaced action of NGF in precence of Aβ(1–42)

Alterations in NGF-related cellular processes have been observed in the cholinergic neurons of patients with AD, suggesting a role of NGF in the progression of disease. [7] In line with these findings, studies in murine models have demonstrated that NGF depletion exacerbates Aβ aggregation and synaptic impairment. On the other hand, NGF supplementation attenuates AD-related neuropathology and enhances cognitive function. [7, 16, 17] Collectively, these data support the hypothesis that NGF may act as a suppressor of Aβ-induced neurotoxicity. Furthermore, NGF administration has demonstrated therapeutic potential in human subjects, despite certain limitations related to its pharmacokinetic properties. [11-13]

Given NGF's therapeutic relevance in AD, we aimed to elucidate its mechanism of action using an untargeted metabolomics approach. Accordingly, we treated SH-SY5Y neuroblastoma cells with NGF in the presence of amyloid-β (Aβ) and performed comprehensive profiling of intracellular and extracellular metabolites.

Preliminarily, we conducted a viability assay to confirm NGF's protective effect against Aβ-induced toxicity in SH-SY5Y cells. Subsequently, we performed comparative analysis of the metabolomic profiles, providing deeper insight into the biological mechanisms underlying NGF's neuroprotective action, potentially supporting its broader application in AD therapy and contributing to the development of more effective treatment strategies.

Interestingly, our data demonstrate that NGF is capable of reversing the metabolic alterations induced by Aβ(1–42). This effect is clearly evident in the sPLS-DA score plot, which shows a proximity of the ellipses, including control cell samples, to those exposed to both Aβ(1–42) and NGF. Further confirmation emerges from the heatmaps, which reveal a clustering of these two experimental groups, distinct from the Aβ(1–42)-treated cells.

Pathway enrichment analysis comparing the metabolomic profiles of cells treated with Aβ(1–42) in the absence and in the presence of NGF reveal the biochemical processes modulated by NGF in a pathological context resembling AD.

Elevated levels of Aβ are known to impair neuronal glutamate uptake at the synaptic level. Consequently, glutamate accumulates in the extracellular space, leading to overstimulation of NMDA receptors. This phenomenon is also observable in our cellular model and is consistent with observations reported in AD models and in the brains of AD patients. [22] Shun *et al.* demonstrated that rat cortical neurons are protected from glutamate toxicity when treated with human or mouse NGF, and observed a similar protective effect against NMDA- and kainate-induced neuronal damage. [23]

In line with these findings, our results suggest that NGF can protect against glutamate-induced neurotoxicity by regulating the glutamate pathway and by lowering glutamate concentrations. Moreover, the reduction in glutamate levels is accompanied by decreased glycine release, a co-agonist required for full NMDA receptor activation (as shown by the alluvial plot and heatmaps).

The combined effect reinforces the hypothesis that NGF may mitigate excitotoxic conditions by modulating key components of glutamatergic signaling.

Another modulated pathway is arginine and proline metabolism, consistent with the reduced concentrations of these amino acids. Arginine participates in several metabolic processes, and its alteration can influence a variety of cellular functions. For instance, arginine is a precursor for nitric oxide (NO) synthesis, and NO production in neurons can exert either neurotoxic or neuroprotective effects. [24] The altered arginine levels may also reflect changes in the metabolism of spermine and spermidine, for which arginine serves as a precursor. [25]

NGF appears to modulate phospholipid metabolism and the synthesis of its precursors in the presence of amyloid-β peptide. This observation suggests that NGF

may play a role in preserving membrane homeostasis, a process frequently compromised in neurodegenerative conditions such as AD. In particular, NGF could help counteract the loss of membrane integrity and the impairment of transmembrane transport mechanisms, which are commonly associated with amyloid toxicity and neurodegenerative diseases.

As demonstrated in the previous chapter, exposure of SH-SY5Y cells to the β-amyloid peptide induces hypoglycemia and an increase in 3-hydroxybutyrate levels. This may reflect a compensatory response to bioenergetic stress and mitochondrial dysfunction, as well as an attempt to buffer oxidative damage. In particular, 3-hydroxybutyrate is known to exert antioxidant effects by scavenging reactive oxygen species (ROS) and modulating redox-sensitive signaling pathways. [26, 27] The concurrent increase in glutathione levels further supports the presence of oxidative stress, likely representing an adaptive upregulation of the cellular antioxidant defense system when cells are exposed to Aβ(1-42). Interestingly, this metabolic profile may indicate that cells are actively responding to amyloid-induced toxicity by shifting toward alternative energy substrates and enhancing redox buffering capacity.

In contrast, when cells were pretreated with NGF before Aβ exposure, a significant reduction in ketone bodies and glutathione was observed. This suggests that NGF may exert a protective effect by preventing the onset of oxidative stress, thereby reducing the need for compensatory antioxidant mechanisms and alternative energy pathways. The observed increase in pyruvate levels under NGF treatment further supports this interpretation, pointing to a restoration of glycolytic flux and improved mitochondrial function.

NGF also modulated glucose-related metabolic pathways, including *glycolysis, gluconeogenesis,* the *glucose–alanine cycle,* and *alanine metabolism*. Such regulation implies that NGF not only counteracts amyloid-induced metabolic reprogramming but also promotes a more physiologically balanced and efficient energy profile. Taken togheter, these findings highlight NGF's potential as an early metabolic modulator, capable of preserving neuronal homeostasis and mitigating the bioenergetic and oxidative disturbances typically associated with neurodegeneration.

3.4.2 NGF acts as an early metabolic modulator

To investigate the metabolic effects underlying NGF's protective action against amyloid-β (Aβ) toxicity, we focused on its activity during the pretreatment phase. Specifically, we compared the metabolomic profiles of SH-SY5Y neuroblastoma cells pre-exposed to NGF (100 μg/mL for 24 hours) with those treated with vehicle alone, aiming to identify early metabolic shifts that may contribute to NGF-mediated neuroprotection.

The Relevance Network Graph highlights a key role for fumarate within the NGF-induced metabolomic landscape. The alluvial plot shows a significant increase in tricarboxylic acid (TCA) cycle intermediates, such as citrate and fumarate, and this is further supported by pathway enrichment analysis. This pattern indicates an upregulation of cellular energy metabolism, typically associated with conditions requiring elevated energy production. In line with this, our data suggest modulation of the electron transport chain, in which reduced coenzymes generated by the Krebs cycle sustain oxidative phosphorylation and ultimately drive ATP synthesis. These findings align with previous studies in PC12 cells, which reported that NGF treatment enhances glucose metabolism, particularly by increasing flux through the TCA cycle. Indeed, NGF induced a two-fold increase in pyruvate levels and TCA cycle intermediates in pheochromocytoma cells, indicating a metabolic shift toward mitochondrial oxidative metabolism. [28]

Fatty acid metabolism is also upregulated, as evidenced by increased carnitine synthesis. Carnitine is an essential biomolecule required for the transport of long-chain fatty acyl-CoAs into the mitochondria, where they are degraded via β-oxidation. Additionally, L-carnitine and its acetylated derivatives have recently gained attention as dietary supplements due to their neuroprotective properties. These compounds have shown potential benefits in various conditions involving central and peripheral nervous system injury, including hypoxia-ischemia and AD. [29] Thus, the modulation of this pathway may reflect an altered energy demand – consistent with the previously described changes in sugar metabolism – as well as a cellular response aimed at promoting neuroprotection.

Taken together, the observed molecular changes indicate a heightened cellular energy requirement. These results support the notion that NGF exerts its

neuroprotective effects against Aβ(1–42) toxicity, in part, by modulating energy-related metabolic pathways initiated during the pretreatment phase.

The observed increase in citicoline, accompanied by a reduction in acetylcholine levels, confirms NGF's ability to modulate phospholipid metabolism even before Aβ(1–42) exposure. This shift suggests a diversion of choline utilization away from acetylcholine synthesis and toward the biosynthesis of membrane components, potentially supporting enhanced membrane stability and structural remodeling.

Consistent with this, pathway analysis revealed that NGF influences the biosynthesis of phosphatidylethanolamine and phosphatidylcholine. These processes are likely involved in NGF's role in neurite outgrowth, as the expansion of neuronal projections requires substantial membrane synthesis. Accordingly, NGF may induce an upregulation of phospholipid biosynthesis to provide the structural building blocks necessary to support neurite elongation. Such mechanisms likely help prepare cells to counteract the membrane-disruptive effects of amyloid-β.

Finally, NGF modulates neurotransmission-related molecules, including glutamate, aspartate, glycine, GABA, and serine – all mediators of glutamate receptor signaling. Following treatment, intracellular GABA levels show a marked reduction, further supported by alterations in glutamate metabolism. These findings suggest an indirect role for NGF in regulating neurotransmitter production. Notably, a close interplay between brain neurotrophic factors and the glutamate–GABA system was already proposed as early as 1991. [30]

3.5 Conclusions

In conclusion, our analysis confirms that NGF exerts a protective effect against Aβ(1-42)-induced toxicity in neuronal-like cells, and this neuroprotection is mediated through the modulation of several key biochemical pathways:

i) NGF promotes the synthesis of crucial intermediates required for phospholipid biosynthesis, which are fundamental components of the cellular membrane. This is particularly relevant given that membrane integrity is often compromised in neurodegenerative conditions, partly due to amyloid peptide toxicity.

ii) NGF regulates cellular energy demands and optimizes the utilization of bioenergetic substrates, thereby supporting metabolic homeostasis under stress conditions.
iii) NGF influences neurotransmitter dynamics, particularly by attenuating glutamate-induced excitotoxicity by modulating its synthesis and release.

These findings underscore the multifaceted role of NGF in maintaining neuronal viability and highlight its therapeutic potential in counteracting the molecular mechanisms underlying neurodegeneration.

3.6 Materials and methods

3.6.1 Chemicals

Dulbecco's Modified Eagle's Medium (DMEM), L-glutamine, penicillin and streptomycin, fetal bovine serum (FBS), CCK-8 were purchased from Sigma-Aldrich (St. Louis, MI, USA).

3.6.2 Production of CHF6467

CHF6467 was expressed in *Escherichia coli* as a pro-protein, pro-human mutant NGF (pro-hmNGF). [31] The method for expressing and purifying NGF was developed – during my PhD – from an *E. coli* culture, adapting and scaling down an industrial process to generate the target protein from its precursor. The most effective steps were chosen and incorporated into the protocol presented here.

CHF6467 sequence included two mutations compared to wild type NGF: P61SR100E. P61S mutation was introduced purely as a marker of the recombinant form, to allow CHF6467 to be distinguishable in the presence of wild type NGF; R100E has been introduced to improve the tolerability of NGF in clinical use, since this mutation confer a reduction in pain side effect. [15]

CHF6467 was obtained after transformation of *E.coli* BL21(DE3) cells with pET11a-hproNGF P61SR100E.

The individual colonies were taken from a stock solution, stored at a temperature of − 80 °C, and added to 50 mL of preinoculum, where 100 μg/mL ampicillin and 30 μg/mL chloramphenicol were previously added for selective control. The bacteria were incubated in a thermostatic incubator under constant stirring at 37 °C overnight.

The following day, 10 mL of the culture was transferred to 500 mL LB medium, added with ampicillin (100 μg/mL) and chloramphenicol (30 μg/mL). When cell density had reached an OD_{600} of 0.6 at 37 °C, gene expression was induced by the addition of 1 mM isopropyl-D-thiogalactoside (IPTG).

The cells were collected after six hours of induction and centrifuged to remove the supernatant. Collected cells, including bodies (IB), within pro-hmNGF were resuspended in 50 mM Tris, 1 mM EDTA, pH 7.0, and homogenized.

Subsequently, the resulting pellet was weighted and resuspended in lysis buffer (6M guanidine hydrochloride, 2M urea, 1.0 mM EDTA, 50 mM TRIS, pH 8.0), keeping a constant ratio of 2.5mL of buffer per gram of IB.

After the dissolution of IB, dithiothreitol (DTT) was added to a final concentration of 50 mM, and the resulting solution was stirred overnight to break the disulphide bridges of pro-hmNGF.

At the end of reduction, the pH was lowered to 3.5 by adding HCl, and the mixture was filtered through a 0.65 μm positively charged glass fiber filter (Sartopure® GF Plus Sartoscale 25).

To allow the refolding step, DTT was removed by constant-volume diafiltration using a solution containing 50 mM Tris, 2 M urea, 6 M guanidine hydrochloride, 1 mM EDTA, pH 3.5, and was eventually concentrated. The buffer exchange was performed against at least seven concentrate volumes of reduction buffer. Diafiltration and concentration were performed using an Amicon® Stirred Cell with 10 kDa Ultrafiltration Discs in polyethersulfone (Biomax).

For refolding of pro-NGF, the resulting solution was added to the refolding buffer (50 mM Tris, 1 M L-arginine HCl, 0.1 M NaCl, 0.35 M NaOH, 5 mM EDTA, 5 mM GSH, 1.0 mM GSSG, pH 9.5) in a 1:50 ratio between the protein solution and the refolding buffer, respectively. The dropping of the protein solution was allowed by a syringe pump with a constant flow of 2μL/min at 4°C. The refolding buffer was continuously stirred during the dropping. After the protein addition, the solution was stirred for an additional 8 hours.

Afterward, the pH was lowered to 7.5 by the addition of HCl, and subsequently the solution was concentrated.

The buffer was exchanged with 1 M arginine HCl and 20 mM sodium phosphate, pH 7.4, using constant-volume diafiltration. The buffer exchange was performed

against at least four concentrate volumes of refolding buffer. The concentration and diafiltration were performed using an Amicon® Stirred Cell with 10 kDa Ultrafiltration Discs in polyethersulfone (Biomax).

The collected retentate was diluted with 10 mM sodium phosphate, pH 7.3, to a conductivity of < 25 mS/cm. To remove the precipitate formed during this step, the product was filtered using a 0.65 µm positively charged glass fiber filter (Sartopure® GF Plus Sartoscale 25).

Before performing the trypsin cleavage, $CaCl_2$ was added to a final concentration of 20 mM, and the pH was adjusted to 7.0 using NaOH. Thus, trypsin was added to the pro-hmNGF solution to a concentration of 1% (w/w). The reaction was constantly stirred for 4 hours at 4°C. This time proved to be the most efficient for cleavage, while for shorter time intervals the amount of pro-hmNGF left was greater, reducing the yield of this step (**Figure 3.7A**).

Trypsin protease activity was stopped by adding Phenylmethanesulfonyl Fluoride (PMSF) to a final concentration of 1 mM and aprotinin (BPTI) to 2 µg/mL.

After trypsin cleavage, the pH of the solution was adjusted to 5.5-6.0 by the addition of HCl, and the solution was filtered through a 0.65 µm positively charged glass fiber filter (Sartopure® GF Plus Sartoscale 25).

Immediately after, the protein was purified with a CaptoMMC column at 1 mL/min using an AKTA purifier system. The column was equilibrated with 350 mM Arg-HCl, 20 mM phosphate buffer, pH 6.0. After the loading of the sample, the system was washed with the same buffer. The protein was eluted using the elution buffer (350 mM Arg-HCl, 50 mM phosphate, pH 9.5).

The eluate of CHF6467 was then dialyzed against phosphate buffer at pH 6.0 to reduce the arginine concentration.

Figure 3.7B shows the final product CHF6467 compared to reference CHF6467 on SDS-PAGE gel stained with Coomassie blue. The CHF6467 identification was further checked via Electro-Spray Mass Spectroscopy (Vanquish Flex UHPLC system interfaced with Orbitrap Exploris 120 and a heated electrospray ionization source HESI-II, Thermo Fisher Scientific, Milan, Italy).

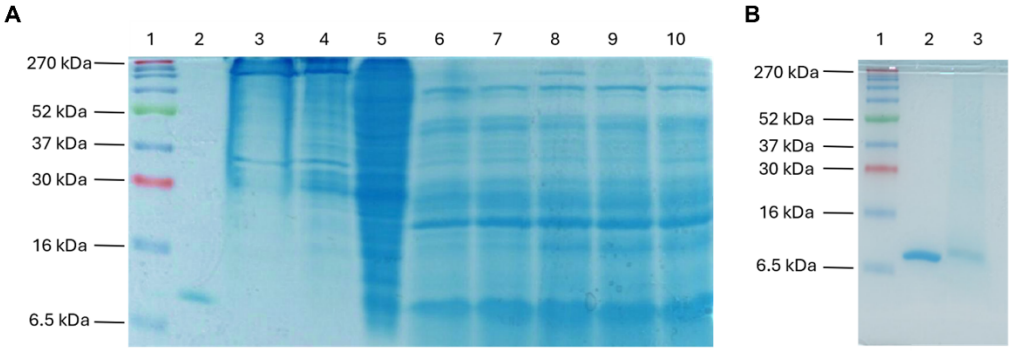

Figure 3.7 *(A) SDS-PAGE with the samples of the time-course of the proteolysis of pro-hmNGF with trypsin. Lane 1: molecular weight marker; lane 2: reference CHF6467; lane 3: pro-hmNGF after refolding; lane 4: pro-hmNGFafter diluition; lane 5: pro-hmNGF before adding trypsin; lane 6: 30 minutes trypsin incubation; lane 7: 1 hour trypsin incubation; line 8: 2 hours trypsin incubation; line 9: 3 hours trypsin incubation; line 10: 4 hours trypsin incubation. (**B**) SDS-PAGE analysis comparing reference CHF6467 with produced CHF6467. Lane 1 = MW marker; lane 2 = reference CHF6467; lane 3 = produced CHF6467 after the purification process.*

3.6.3 Cell Culture

The human neuroblastoma line SH-SY5Y was purchased from American Type Culture Collection (ATCC, Rockville, MD, USA). Cells were cultured in Dulbecco's Modified Eagle Medium (DMEM, 4500 mg/mL glucose) supplemented with 10% (v/v) FBS, 2 mM L-glutamine, 100 U/mL penicillin, and 0.1 mg/mL streptomycin. Cells were maintained in a humidified incubator at 37 °C with 5% CO_2 and passaged every 2 days.

3.6.4 Cell Viability Assay

Cell viability was assessed by measuring mitochondrial metabolic activity using the Cell Counting Kit-8 (CCK-8, Cat. CK04, Dojindo Laboratories, Rockville, MD, USA), following the manufacturer's instructions. Briefly, to evaluate NGF's ability to protect SH-SY5Y cells from Aβ(1–42) toxicity, 8×10^3 cells/well were plated in 96-well plates for 24 h, then NGF at 100 µg/mL or 200 µg/mL was added for 24 h. Next, Aβ(1–42) peptide 50 µM was added for 48 h.

The CCK-8 reagent was then diluted in cell medium (10%) and incubated for 1 hour. Absorbance was measured at 450 nm with a microplate reader (Multiskan Go, Thermo Scientific, Waltham, MA, USA).

Cell viability was calculated as the percentage of viable cells relative to the untreated control. Data are presented as mean ± standard deviation (SD) from three independent experiments. Statistical analysis was performed using one-way ANOVA followed by Dunnett's multiple comparisons test, using GraphPad Prism version 8.0 (GraphPad Software, San Diego, CA, USA). Statistical significance was set at $p < 0.05$. Symbols indicate significance levels as described: $^{####}$ denote $p < 0.0001$ *vs.* CTRL; *, ** denote respectively $p < 0.05$ and $p < 0.01$ *vs.* Aβ(1–42).

3.6.5 ^{1}H NMR Metabolomics

3.6.5.1 Exposure of SH-SY5Y cells to NGF and Aβ(1–42)

To prepare metabolomic samples, cells were plated in 60 mm culture dishes and allowed to adhere overnight.

For co-administration, cells were pretreated with NGF (100 μg/mL) and, after 24 h, Aβ(1–42) was added for an additional 48 hours at a sub-toxic concentration (5 μM). Cells exposed only to Aβ(1–42) peptide at the same concentration and incubation time were used for the comparison. For the control group, cells were treated only with the vehicle for the same duration.

3.6.5.2 Sample collection and intracellular metabolites extraction

After treatments, both culture media and cell pellet were collected for the metabolomics analysis targeting the exometabolome and endometabolome, respectively. Specifically, the medium was transferred to microcentrifuge tubes and centrifuged at 1000× g for 10 min. The same procedure was applied to cell-free medium incubated under identical conditions. The resulting supernatants were transferred to fresh microcentrifuge tubes and stored at −80 °C until NMR analysis. After media removal, cell dishes were washed with cold PBS (pH 7.4) to remove media residues and cells were collected by scraping in methanol. To extract intracellular metabolites from cell pellet, homogenization was followed by biphasic extraction method using methanol, chloroform, and water in a 1:1:1 ratio. [32] Samples were centrifuged at 6000 rpm for 10 min at 4 °C to separate the polar and apolar phases. Polar extracts from cell pellet were dried under vacuum with a SP-Genevac EZ-2 4.0 concentrator while lipophilic extracts were dried with nitrogen flow for later analysis. All extracts were stored at −80 °C before NMR testing.

3.6.5.3 NMR Sample Preparation

Lyophilized cell extracts were reconstituted in 200 µL of buffer (50 mM Na_2HPO_4, 1 mM trimethylsilyl propionic-2,2,3,3-d_4 acid sodium salt (TSP-d_4), 10% of D_2O). TSP-d_4 was used as an internal standard for the alignment and quantification of NMR signals. For growth media analysis, 100 µL of cell medium was mixed with 100 µL of the same buffer used for the lyophilized extracts. The resulting samples were transferred into 3 mm NMR tubes for ^1H NMR acquisition.

3.6.5.4 NMR Data Acquisition and Processing

1D ^1H NMR spectra were recorded on a Bruker Ascend™ 600 MHz spectrometer equipped with a 5 mm triple resonance Z gradient TXI probe (Bruker Co, Rheinstetten, Germany) at 298 K. One-dimensional NOESY NMR spectra were recorded with 20 k points, 12 ppm spectral width, 1.36s acquisition time, 5 s relaxation delay, 10 ms of mixing time and 128 scans. [33] Topspin version 3.0 (Bruker Biospin) was used for spectrometer control and data processing. Spectra analysis followed an untargeted metabolomic approach, with each metabolite identified prior to statistical testing using Chenomx NMR-Suite v10.1 (Chenomx NMR suite, v10.1, Edmonton, AB, Canada). Quantitative analysis of the 1D-NMR spectra was performed with NMRProcFlow ver 1.4.10. [34]

3.6.5.5 Statistical analysis

The resulting quantification matrix was normalised to the sum of quantified metabolites, log-transformed, Pareto-scaled, and analysed using the open-source tool Metaboanalyst 6.0 and the MixOmics R package, as explained in Chapter 2. [35, 36] Univariate analysis was performed separately on the exometabolome and endometabolome of the groups, using a T-Test and Fold Change, and the results were displayed in a Volcano plot. [37]

To enhance data accuracy and gain biological insights, multivariate statistical analysis (MVA) was first applied to the exometabolome and endometabolome concentration matrices, followed by analysis of the combined data sets.

To analyze the combined endo- and exometabolome, we employed the mixOmics R package using a P-integration approach. To ensure greater precision in the combined analysis and to mitigate the influence of inherent variability between the matrices, the

batch effect was further eliminated using the R *limma* package. [38] MVA was conducted on combined matrices of endo- and exo-metabolites using the supervised sparse Partial Least Squares (sPLS), also known as the projection to latent space method. [39] In this integrated approach, sPLS analysis is effective when the total number of variables in the combined matrices exceeds the number of samples analysed, as demonstrated in this study. The sPLS was conducted with an LASSO penalty on the loading vectors to reduce the number of original variables used to construct the latent variables. [40] A sample plot illustrates the clustering of samples' metabolomic profiles. In the graph, each sample appears as a point located based on its projection onto the selected latent components of the data. Leave-one-out cross-validation is conducted to validate the model, using R^2, Q^2, and accuracy metrics. [41] Furthermore, sPLS models were additionally validated using ROC curve analysis. [42]

Variable correlations are displayed using a circular correlation plot, where all vectors are plotted inside a unit circle with a radius of 1. Each vector's position reflects its correlation with the components; stronger associations produce vectors that extend further from the center. Additionally, variables with vectors close to each other are highly correlated. [35] The contribution of each variable is shown in a bar graph. The contribution graph based on loadings for variable separation has been color-coded to show the maximum value between two, indicating the clusters where the metabolite has the highest concentration. To comprehensively depict the quantitative changes in metabolites, we created heatmaps using normalised data, average group concentrations, and Euclidean distance. [43]

Correlational analysis between intra- and extracellular metabolites using the Cluster Image Map was performed by applying the Pearson correlation coefficient. The same statistical approach was employed to construct the cluster image map. The Pearson correlation coefficient (r) quantifies both the strength and direction of the relationship between two quantitative variables. Its values range from –1 to +1, with significance increasing as the coefficient approaches either extreme. A negative value indicates an inverse correlation, while a positive value reflects a direct correlation. [44]

The Relevance Network Graph also incorporates metabolite centrality, which reflects the extent to which individual metabolites contribute to the discrimination of metabolic profiles. Only metabolites with a Pearson correlation coefficient cutoff of 0.70 and a high degree were visualized, based on the number of variables present in

the joint matrix of the exometabolome and endometabolome. The degree of a node refers to the number of connections it maintains within the network – serving as a measure of centrality based on direct link count. [45]

The enrichment pathway tool was used to conduct pathway analysis with Metaboanalyst 6.0. KEGG pathways were selected based on lower false discovery rates (FDR), with p-values less than 0.05, and a hit value (the number of metabolites in the pathway) greater than 1. [46]

Bibliography

1. Levi-Montalcini, R., Growth Control of Nerve Cells by a Protein Factor and Its Antiserum: Discovery of this factor may provide new leads to understanding of some neurogenetic processes. *Science* **1964,** *143* (3602), 105-110.
2. Chao, M. V.; Hempstead, B. L., p75 and Trk: a two-receptor system. *Trends in neurosciences* **1995,** *18* (7), 321-326.
3. Shooter, E. M., Early days of the nerve growth factor proteins. *Annual review of neuroscience* **2001,** *24* (1), 601-629.
4. Ehlers, M. D.; Kaplan, D. R.; Price, D. L.; Koliatsos, V. E., NGF-stimulated retrograde transport of trkA in the mammalian nervous system. *The Journal of Cell Biology* **1995,** *130* (1), 149-156.
5. Vantini, G.; Fusco, M.; Schiavo, N.; Gradkowska, M.; Zaremba, M.; Leon, A.; Oderfeld-Nowak, B., Nerve growth factor induces a dose-dependent and long-lasting increase of choline acetyltransferase activity in the septal area and hippocampus of uninjured rats. *Acta neurobiologiae experimentalis* **1990,** *50* (4-5), 323-332.
6. Hefti, F., Nerve growth factor promotes survival of septal cholinergic neurons after fimbrial transections. *Journal of Neuroscience* **1986,** *6* (8), 2155-2162.
7. Iulita, M. F.; Cuello, A. C., Nerve growth factor metabolic dysfunction in Alzheimer's disease and Down syndrome. *Trends in pharmacological sciences* **2014,** *35* (7), 338-348.
8. Pentz, R.; Iulita, M. F.; Ducatenzeiler, A.; Bennett, D. A.; Cuello, A. C., The human brain NGF metabolic pathway is impaired in the pre-clinical and clinical continuum of Alzheimers disease. *Molecular psychiatry* **2021,** *26* (10), 6023-6037.
9. Fahnestock, M.; Michalski, B.; Xu, B.; Coughlin, M. D., The precursor pro-nerve growth factor is the predominant form of nerve growth factor in brain and is increased in Alzheimer's disease. *Molecular and Cellular Neuroscience* **2001,** *18* (2), 210-220.
10. Bruno, M. A.; Leon, W. C.; Fragoso, G.; Mushynski, W. E.; Almazan, G.; Cuello, A. C., Amyloid β-induced nerve growth factor dysmetabolism in Alzheimer disease. *Journal of Neuropathology & Experimental Neurology* **2009,** *68* (8), 857-869.
11. Amadoro, G.; Latina, V.; Balzamino, B. O.; Squitti, R.; Varano, M.; Calissano, P.; Micera, A., Nerve growth factor-based therapy in Alzheimer's disease and age-related macular degeneration. *Frontiers in Neuroscience* **2021,** *15*, 735928.
12. Faustino, C.; Rijo, P.; Reis, C. P., Nanotechnological strategies for nerve growth factor delivery: Therapeutic implications in Alzheimer's disease. *Pharmacological research* **2017,** *120*, 68-87.
13. Mitra, S.; Behbahani, H.; Eriksdotter, M., Innovative therapy for Alzheimer's disease-with focus on biodelivery of NGF. *Frontiers in neuroscience* **2019,** *13*, 38.
14. Eriksdotter Jönhagen, M.; Nordberg, A.; Amberla, K.; Bäckman, L.; Ebendal, T.; Meyerson, B.; Olson, L.; Seiger, Å.; Shigeta, M.; Theodorsson, E., Intracerebroventricular infusion of nerve growth factor in three patients with Alzheimer's disease. *Dementia and geriatric cognitive disorders* **1998,** *9* (5), 246-257.
15. Malerba, F.; Paoletti, F.; Bruni Ercole, B.; Materazzi, S.; Nassini, R.; Coppi, E.; Patacchini, R.; Capsoni, S.; Lamba, D.; Cattaneo, A., Functional characterization of human ProNGF and NGF mutants: identification of NGF P61SR100E as a "painless" lead investigational candidate for therapeutic applications. *PLoS One* **2015,** *10* (9), e0136425.
16. Ruberti, F.; Capsoni, S.; Comparini, A.; Di Daniel, E.; Franzot, J.; Gonfloni, S.; Rossi, G.; Berardi, N.; Cattaneo, A., Phenotypic knockout of nerve growth factor in adult transgenic mice reveals severe deficits in basal forebrain cholinergic neurons, cell death in the spleen, and skeletal muscle dystrophy. *Journal of Neuroscience* **2000,** *20* (7), 2589-2601.
17. Zhang, Y.-w.; Chen, Y.; Liu, Y.; Zhao, Y.; Liao, F.-F.; Xu, H., APP regulates NGF receptor trafficking and NGF-mediated neuronal differentiation and survival. *PloS one* **2013,** *8* (11), e80571.

18. Covaceuszach, S.; Capsoni, S.; Ugolini, G.; Spirito, F.; Vignone, D.; Cattaneo, A., Development of a non invasive NGF-based therapy for Alzheimer's disease. *Current Alzheimer Research* **2009,** *6* (2), 158-170.
19. Alarcon-Barrera, J. C.; Kostidis, S.; Ondo-Mendez, A.; Giera, M., Recent advances in metabolomics analysis for early drug development. *Drug discovery today* **2022,** *27* (6), 1763-1773.
20. Zampieri, M., From the metabolic profiling of drug response to drug mode of action. *Current Opinion in Systems Biology* **2018,** *10*, 26-33.
21. Wang, K.-C.; Wang, S.-Y.; Kuo, C.-h.; Tseng, Y. J. J. A. C., Distribution-based classification method for baseline correction of metabolomic 1D proton nuclear magnetic resonance spectra. **2013,** *85* (2), 1231-1239.
22. Li, S.; Hong, S.; Shepardson, N. E.; Walsh, D. M.; Shankar, G. M.; Selkoe, D., Soluble oligomers of amyloid β protein facilitate hippocampal long-term depression by disrupting neuronal glutamate uptake. *Neuron* **2009,** *62* (6), 788-801.
23. Shimohama, S.; Ogawa, N.; Tamura, Y.; Akaike, A.; Tsukahara, T.; Iwata, H.; Kimura, J., Protective effect of nerve growth factor against glutamate-induced neurotoxicity in cultured cortical neurons. *Brain research* **1993,** *632* (1-2), 296-302.
24. Wu, G.; Meininger, C. J.; McNeal, C. J.; Bazer, F. W.; Rhoads, J. M., Role of L-arginine in nitric oxide synthesis and health in humans. In *Amino acids in nutrition and health*, Springer: 2021; pp 167-187.
25. Morris Jr, S. M., Arginine: beyond protein. *The American journal of clinical nutrition* **2006,** *83* (2), 508S-512S.
26. Kong, G.; Huang, Z.; Ji, W.; Wang, X.; Liu, J.; Wu, X.; Huang, Z.; Li, R.; Zhu, Q., The ketone metabolite β-hydroxybutyrate attenuates oxidative stress in spinal cord injury by suppression of class I histone deacetylases. *Journal of neurotrauma* **2017,** *34* (18), 2645-2655.
27. Achanta, L. B.; Rae, C. D., β-Hydroxybutyrate in the brain: one molecule, multiple mechanisms. *Neurochemical research* **2017,** *42* (1), 35-49.
28. Goglia, I.; Węglarz-Tomczak, E.; Gioia, C.; Liu, Y.; Virtuoso, A.; Bonanomi, M.; Gaglio, D.; Salmistraro, N.; De Luca, C.; Papa, M., Fusion–fission–mitophagy cycling and metabolic reprogramming coordinate nerve growth factor (NGF)-dependent neuronal differentiation. *The FEBS Journal* **2024,** *291* (13), 2811-2835.
29. Ferreira, G. C.; McKenna, M. C., L-carnitine and acetyl-L-carnitine roles and neuroprotection in developing brain. *Neurochemical research* **2017,** *42* (6), 1661-1675.
30. Zafra, F.; Castren, E.; Thoenen, H.; Lindholm, D., Interplay between glutamate and gamma-aminobutyric acid transmitter systems in the physiological regulation of brain-derived neurotrophic factor and nerve growth factor synthesis in hippocampal neurons. *Proceedings of the National Academy of Sciences* **1991,** *88* (22), 10037-10041.
31. Rattenholl, A.; Lilie, H.; Grossmann, A.; Stern, A.; Schwarz, E.; Rudolph, R., The pro-sequence facilitates folding of human nerve growth factor from Escherichia coli inclusion bodies. *European Journal of Biochemistry* **2001,** *268* (11), 3296-3303.
32. Beckonert, O.; Keun, H. C.; Ebbels, T. M. D.; Bundy, J.; Holmes, E.; Lindon, J. C.; Nicholson, J. K., Metabolic profiling, metabolomic and metabonomic procedures for NMR spectroscopy of urine, plasma, serum and tissue extracts. *Nature protocols* **2007,** *2* (11), 2692.
33. McKay, R. T., How the 1D-NOESY suppresses solvent signal in metabonomics NMR spectroscopy: an examination of the pulse sequence components and evolution. *Concepts in Magnetic Resonance Part A* **2011,** *38* (5), 197-220.
34. Jacob, D.; Deborde, C.; Lefebvre, M.; Maucourt, M.; Moing, A., NMRProcFlow: a graphical and interactive tool dedicated to 1D spectra processing for NMR-based metabolomics. *Metabolomics* **2017,** *13* (4), 36.
35. Rohart, F.; Gautier, B.; Singh, A.; Lê Cao, K.-A., mixOmics: An R package for 'omics feature selection and multiple data integration. *PLoS computational biology* **2017,** *13* (11), e1005752.

36. Pang, Z.; Lu, Y.; Zhou, G.; Hui, F.; Xu, L.; Viau, C.; Spigelman, A. F.; MacDonald, P. E.; Wishart, D. S.; Li, S., MetaboAnalyst 6.0: towards a unified platform for metabolomics data processing, analysis and interpretation. *Nucleic acids research* **2024,** *52* (W1), W398-W406.
37. Kumar, N.; Hoque, M. A.; Sugimoto, M. J. B. b., Robust volcano plot: identification of differential metabolites in the presence of outliers. **2018,** *19*, 1-11.
38. Ritchie, M. E.; Phipson, B.; Wu, D. I.; Hu, Y.; Law, C. W.; Shi, W.; Smyth, G. K., limma powers differential expression analyses for RNA-sequencing and microarray studies. *Nucleic acids research* **2015,** *43* (7), e47-e47.
39. Abdi, H., Partial least squares regression and projection on latent structure regression (PLS Regression). *Wiley interdisciplinary reviews: computational statistics* **2010,** *2* (1), 97-106.
40. Lê Cao, K.-A.; Rossouw, D.; Robert-Granié, C.; Besse, P., A sparse PLS for variable selection when integrating omics data. *Statistical applications in genetics and molecular biology* **2008,** *7* (1).
41. Wong, T.-T., Performance evaluation of classification algorithms by k-fold and leave-one-out cross validation. *Pattern recognition* **2015,** *48* (9), 2839-2846.
42. Vanderlooy, S.; Hüllermeier, E., A critical analysis of variants of the AUC. *Machine Learning* **2008,** *72* (3), 247-262.
43. Tiessen, A.; Cubedo-Ruiz, E. A.; Winkler, R., Improved representation of biological information by using correlation as distance function for heatmap cluster analysis. *American Journal of Plant Sciences* **2017,** *8* (3), 502-516.
44. Benesty, J.; Chen, J.; Huang, Y.; Cohen, I., Pearson correlation coefficient. In *Noise reduction in speech processing*, Springer: 2009; pp 1-4.
45. Lê Cao, K.-A.; Welham, Z. M., *Multivariate data integration using R: methods and applications with the mixOmics package*. Chapman and Hall/CRC: 2021.
46. Pang, Z.; Lu, Y.; Zhou, G.; Hui, F.; Xu, L.; Viau, C.; Spigelman, Aliya F.; MacDonald, Patrick E.; Wishart, David S.; Li, S.; Xia, J., MetaboAnalyst 6.0: towards a unified platform for metabolomics data processing, analysis and interpretation. *Nucleic Acids Research* **2024,** *52* (W1), W398-W406.

Appendix

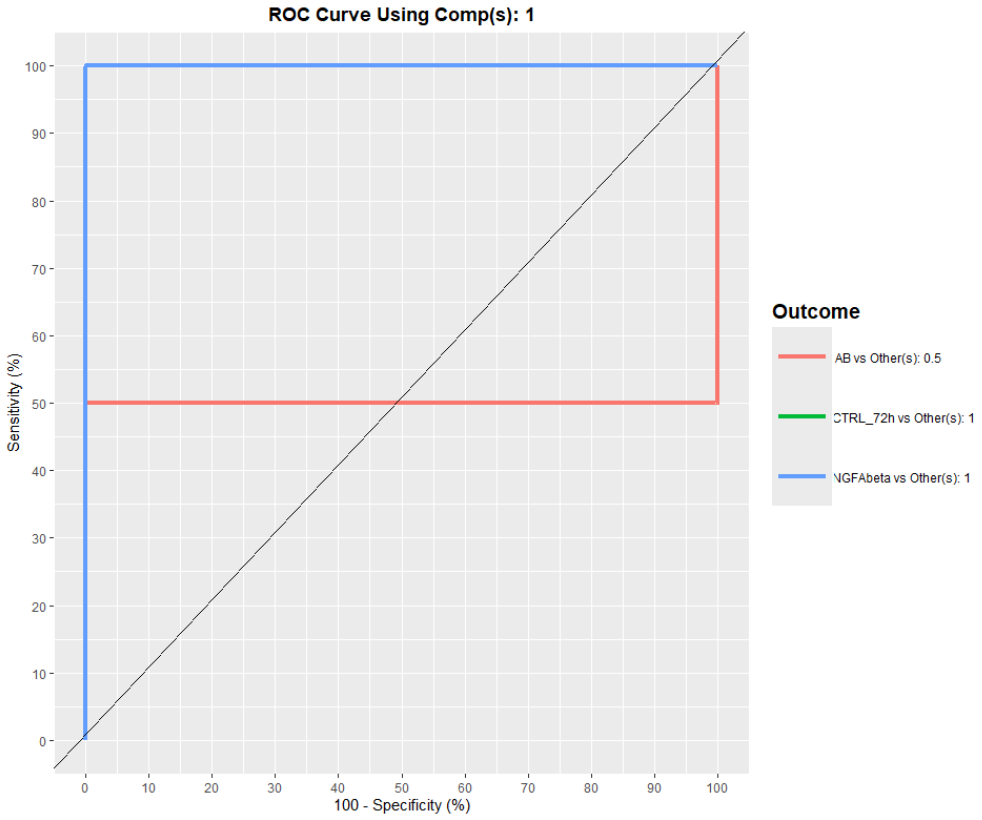

Outcome	AUC Component 1	*p-value*
Aβ vs Others	0.50	0.003
CTRL_72h vs Others	1	1.25E-11
NGFAbeta vs Others	1	1.48E-09

Figure S1. *Performance evaluations of the sPLS-DA model based on ^{1}H-NMR data were performed using ROC curve analysis on the combined exo and endometabolome profiles of NGFAbeta and Aβ versus CTRL_72h. The ROC curve values for the first and second components with the relative p-value are given in Table.*

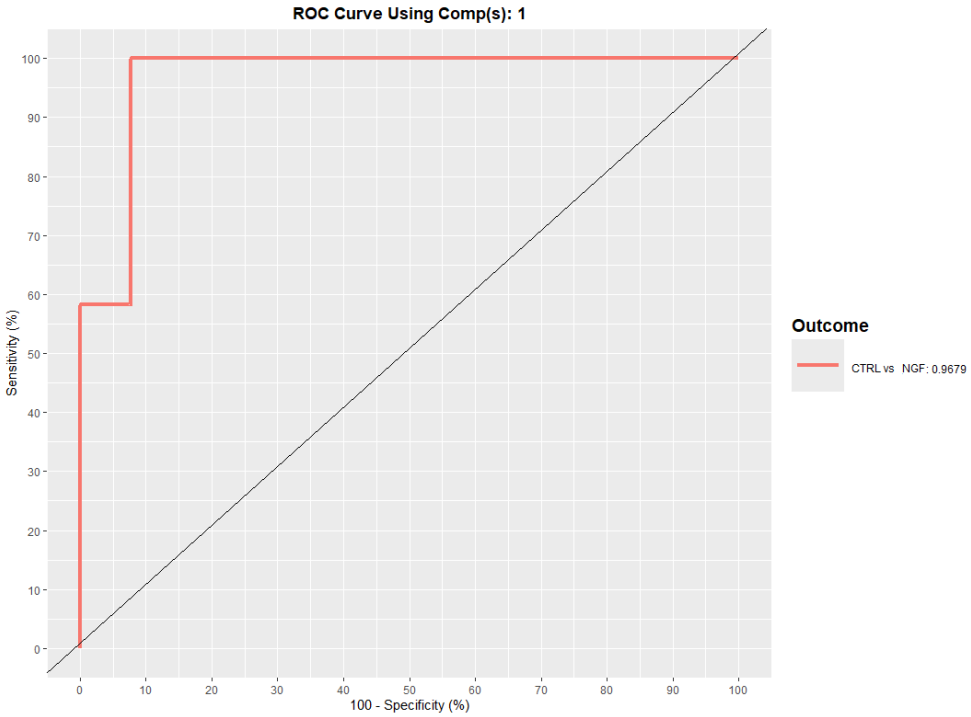

AUC Component 1	*p-value*
0.97	1.25E-10
AUC Component 2	***p-value***
0.96	1.15E-09

Figure S2. *Performance evaluations of the sPLS-DA model based on ^{1}H-NMR data were performed using ROC curve analysis on the combined exo and endometabolome profiles of NGF-24h versus CTRL. The ROC curve values for the first and second components with the relative p-value are given in Table.*

Chapter IV

Exploring D-aspartic acid role in the brain by hyperpolarization-NMR

4.1 D-amino acid in mammalian brain

For a long time, D-amino acids were believed to exist exclusively in microorganisms and plants. However, in recent decades, growing evidence – supported by increasingly sensitive analytical techniques – has revealed their presence in mammals as well. Among the free D-amino acids identified in mammals, D-serine (D-Ser) and D-aspartate (D-Asp) are the most abundant within the central nervous system (CNS). [1]

The role of D-Ser is well characterized: it acts as a physiological co-agonist of NMDA receptors (NMDARs) at central excitatory synapses. Changes in cerebral D-Ser levels modulate NMDAR signaling, thereby influencing glutamatergic transmission and, ultimately, key neuronal processes and behaviors. [2, 3] Abnormal concentrations of D-Ser in the brain and cerebrospinal fluid (CSF) have been associated with various neurological and psychiatric disorders, including post-traumatic stress disorder, traumatic brain injury, amyotrophic lateral sclerosis (ALS), Alzheimer's disease (AD), and schizophrenia. [4-7]

In contrast, the biological relevance of endogenous free D-Asp in the mammalian CNS remains comparatively less well defined. Accordingly, recent research has begun to investigate its potential role in glutamatergic signaling and brain function.

In living organisms, D-aspartate levels are regulated by both biosynthetic and degradative pathways. Early studies supported the existence of a specific mammalian aspartate racemase capable of converting L-aspartate into D-aspartate within the brain.[8] Still, its existence has not yet been conclusively demonstrated. [9, 10] Additionally, recent findings suggest that serine racemase (SR) – the enzyme responsible for D-Ser production [11] – may also contribute to D-Asp generation in specific brain regions. [12, 13]

Regarding the catabolic pathway, it is well established that D-aspartate oxidase (DDO or DASPO), a flavin adenine dinucleotide (FAD)-dependent enzyme, degrades D-Asp within peroxisomes, producing α-oxaloacetate, hydrogen peroxide (H_2O_2), and ammonium ions (NH_4^+) as byproducts. DDO is inactive toward basic and neutral D-amino acids, including D-serine, which are instead metabolized by distinct flavoenzymes homologous to DDO. [14, 15]

4.2 The time-dependency of D-Asp

Although current knowledge regarding D-Asp is still evolving, one well-established aspect is its distinct temporal and spatial distribution within the organism. D-Asp is highly concentrated in the brain during fetal development, but its levels decline sharply immediately after birth, suggesting a tightly regulated role in early neurodevelopment.

This developmental pattern is closely associated with the expression and the activity of DDO, the enzyme responsible for oxidizing D-Asp into oxaloacetate (**Figure 4.1A**). During the prenatal period, D-Asp levels are elevated while DDO activity remains low. Conversely, in the postnatal phase, DDO expression and activity increase markedly, leading to a rapid reduction in D-Asp concentrations (**Figure 4.1B**). This inverse relationship supports the hypothesis that D-Asp plays a critical role in brain maturation and underscores the need to downregulate its levels once key developmental processes have been completed. [16]

The mechanisms underlying DDO expression have also been investigated, revealing transcriptional regulation, as evidenced by a significant increase in *Ddo* mRNA levels during postnatal development. Notably, this transcriptional activation appears to be finely modulated by epigenetic mechanisms, specifically through progressive demethylation of the *Ddo* gene in the brain, within the promoter region. [17-19]

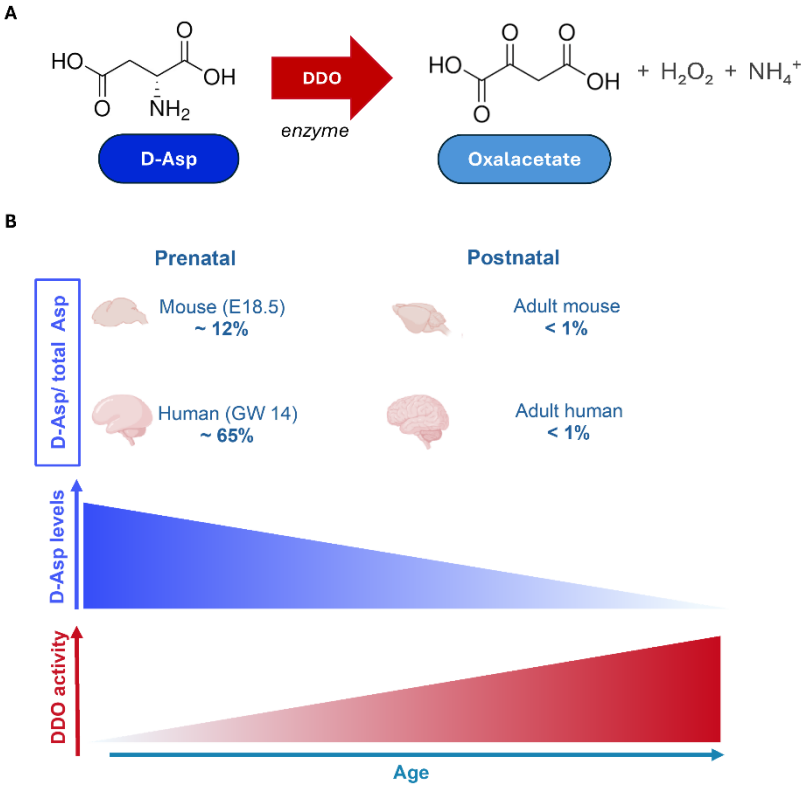

Figure 4.1 *(**A**) The reaction catalyzed by D-aspartate oxidase (DDO) converts D-aspartate (D-Asp) into oxaloacetate, generating hydrogen peroxide and ammonium as byproducts. (**B**) Temporal relationship between cerebral D-Asp levels and DDO enzymatic activity. D-Asp concentration peaks during the prenatal phase of mammalian brain development. However, the proportion of D-Asp relative to total aspartate (D-Asp/total Asp ratio) varies across species. Notably, in the embryonic human brain, D-Asp constitutes approximately 65% of total Asp, compared to only ~12% in the embryonic mouse brain (upper panel). Postnatally, D-Asp levels progressively decline (middle panel), and its relative abundance remains low in both species. This reduction is driven by increased DDO activity during postnatal life (lower panel). Abbreviations: E18.5, embryonic day 18.5; GW14, gestational week 14. Adapted from* [16].

4.3 Pharmacological and functional properties of D-Asp

Free D-Asp in mammals was first identified in rats and humans in the late 1980s. [20] Already at that time, early studies demonstrated that D-Asp was capable of binding to the L-glutamate site on the ionotropic NMDAR. [21] This was later confirmed by subsequent experiments using both competitive and noncompetitive NMDAR antagonists, which showed that these antagonists blocked the inward current induced by D-Asp. [22, 23] Interestingly, residual D-Asp-dependent inward currents persisted even after the application of high doses of these antagonists, leading to the hypothesis that this D-amino acid might also act on other receptor types. [22, 24] This suggestion was

subsequently confirmed, demonstrating that D-Asp functions not only as an agonist of NMDARs, but also of the metabotropic glutamate receptor 5 (mGluR5). [25]

Moreover, microdialysis experiments conducted in the prefrontal cortex (PFC) of freely moving mice revealed that D-Asp is present at nanomolar concentrations in the extracellular space and that its release occurs via Ca^{2+}-dependent mechanisms. [17, 26] Supporting these *in vivo* findings, previous *in vitro* studies showed that D-Asp can be stored in secretory granules, released through vesicular Ca^{2+}-mediated exocytosis, and taken up by both nerve terminals and glial cells *via* a Na^{+}/K^{+}-dependent L-glutamate/L-aspartate transporter system, which recognizes L-Glu as well as both Asp enantiomers. [27-29]

Beyond its direct action on postsynaptic NMDAR and mGluR5 receptors, recent research has shown that exogenous administration of D-Asp induces a significant extracellular release of L-glutamate in the PFC of freely moving mice. This effect is mediated through the stimulation of presynaptic NMDA, AMPA, and mGluR5 receptors. [26]

The influence of D-Asp signaling on NMDAR-mediated transmission has been demonstrated in various rodent models characterized by elevated endogenous D-Asp levels, achieved either through genetic ablation of the *Ddo* gene (*Ddo*$^{-/-}$ mice) or via chronic oral administration of D-Asp. Persistent elevation of D-Asp induces pronounced NMDAR-dependent excitotoxicity, severe neuroinflammation, and neuronal cell death, which, in turn, exacerbates early synaptic plasticity deterioration and accelerates cognitive decline during aging. [17, 24, 30] However, short-term D-Asp treatment has been shown to reverse the age-related decay of long-term potentiation (LTP) observed in untreated aged mice. [22]

Taken together, these findings suggest that D-Asp upregulation may exert either detrimental or beneficial effects on NMDAR-related aging processes, depending on the timing and duration of D-Asp deregulation. In line with this evidence, DDO enzymatic activity appears to play a physiological role in maintaining D-Asp levels below a critical “danger threshold”, thereby preventing the potentially toxic consequences of prolonged D-Asp stimulation on NMDAR-mediated signaling. [16]

It is well established that glutamatergic neurotransmission is involved in several neurodevelopmental processes – including neurogenesis, proliferation, migration, differentiation, and apoptosis/survival – primarily through early activation of

NMDARs and mGluR5 receptors. [31-33] Based on D-Asp's ability to stimulate these L-glutamate receptor subtypes, a recent study has, for the first time, described the impact of embryonic D-Asp depletion on adult brain morphology and behavior, using a novel genetic mouse model characterized by non-physiological, prenatal-onset *Ddo* gene expression. [18] In this *Ddo* knock-in model, premature cerebral expression of *Ddo* was accompanied by a corresponding increase in DDO enzymatic activity, resulting in the early removal of cerebral D-Asp during the initial stages of brain development. These mice were found to be viable and fertile, and to exhibit enhanced spatial memory performance. Significantly, *Ddo* overexpression did not directly or indirectly affect the prenatal or postnatal metabolism of other amino acids involved in NMDAR signaling, such as L-glutamate, L-aspartate, D-serine, and L-serine. Furthermore, no major neuroanatomical alterations were observed in the overall adult brain architecture, including neuronal and myelin distribution, in *Ddo* knock-in mice. In this animal model, D-Asp removal is associated with alterations in the number of parvalbumin-positive cortical interneurons and in memory abilities. [18]

4.4 Aim of the study

D-Asp has gained increasing attention as a significant endogenous amino acid with neurotransmitter-like activity, implicated in key neurological processes such as brain development, memory formation, and cognitive function. Unlike classical neurotransmitters – whose roles have been extensively characterized – D-Asp remains relatively underexplored due to its more recent identification.

A previous study demonstrated the value of employing a metabolomic approach to investigate the impact of prenatal D-Asp depletion in brain tissues from murine models. Specifically, the research groups of Prof. Anna Maria D'Ursi and Prof. Alessandro Usiello utilized a genetically modified mouse model with constitutive activation of DDO from the zygotic stage, resulting in abnormally low levels of D-Asp in the prenatal phase. By comparing the cerebral metabolic profiles of *Ddo* knock-in and wild-type mice at both prenatal and early postnatal stages, they revealed several dysregulations, including significant alterations in amino acid pathways associated with D-Asp deficiency. [34]

To expand this investigation, we aimed to include adult stages, specific brain sub-regions, and conditions of D-Asp excess, while also enabling chiral resolution. For this

purpose, we adopted an innovative NMR technique based on non-hydrogenative parahydrogen-induced hyperpolarization (nhPHIP). nhPHIP enhances the detection of low-abundance metabolites in complex biological matrices, such as brain extracts, and, crucially, allows direct assessment of amino acid chirality without chemical derivatization. This is particularly advantageous given the limitations of derivatization, including incomplete reaction efficiency, potential racemization, and increased sample preparation complexity.

This approach is especially relevant to our objectives, as many amino acids – including D-Asp – play direct or modulatory roles in neurotransmission. The ability to distinguish between enantiomers is essential, given that D- and L-forms of amino acids often exhibit markedly different biological activities.

To explore the neurochemical consequences in adulthood of prenatal D-Asp depletion and sustained postnatal D-Asp accumulation, we subdivided the workflow as shown in **Figure 4.2A**:

- First, we genetically engineer the *Ddo* gene to create a mammalian model of the brain with altered levels of D-Asp. This has been possible thanks to the collaboration with prof Usiello from Vanvitelli University of Caserta, Italy, and his expertise in animal models of D-Asp alterations.

  Specifically, we obtained four brain regions – the cerebellum, cortex, hippocampus, and striatum – and spinal cord from three experimental groups (**Figure 4.2B**):

  1. Wild-type mice, which show physiological DDO expression and low D-Asp levels in adulthood;
  2. *Ddo* Knock-in mice, in which DDO expression begins from the zygotic phase and is maintained after birth;
  3. *Ddo* Knock-out mice, in which DDO is not expressed in adulthood, leading to sustained postnatal D-Asp accumulation.
- Then, we performed NMR nhPHIP experiments on mouse brain extracts to obtain qualitative and quantitative information about cerebral amino acids. The spectra have been recorded at the Magnetic Resonance Research Center of Radboud University during the international research period of my PhD, under the supervision of Dr. Marco Tessari.

- Finally, biostatistical analyses of the metabolomic data derived from spectral profiling were conducted to evaluate the long-term neurochemical impact of early prenatal D-Asp depletion and sustained postnatal accumulation.

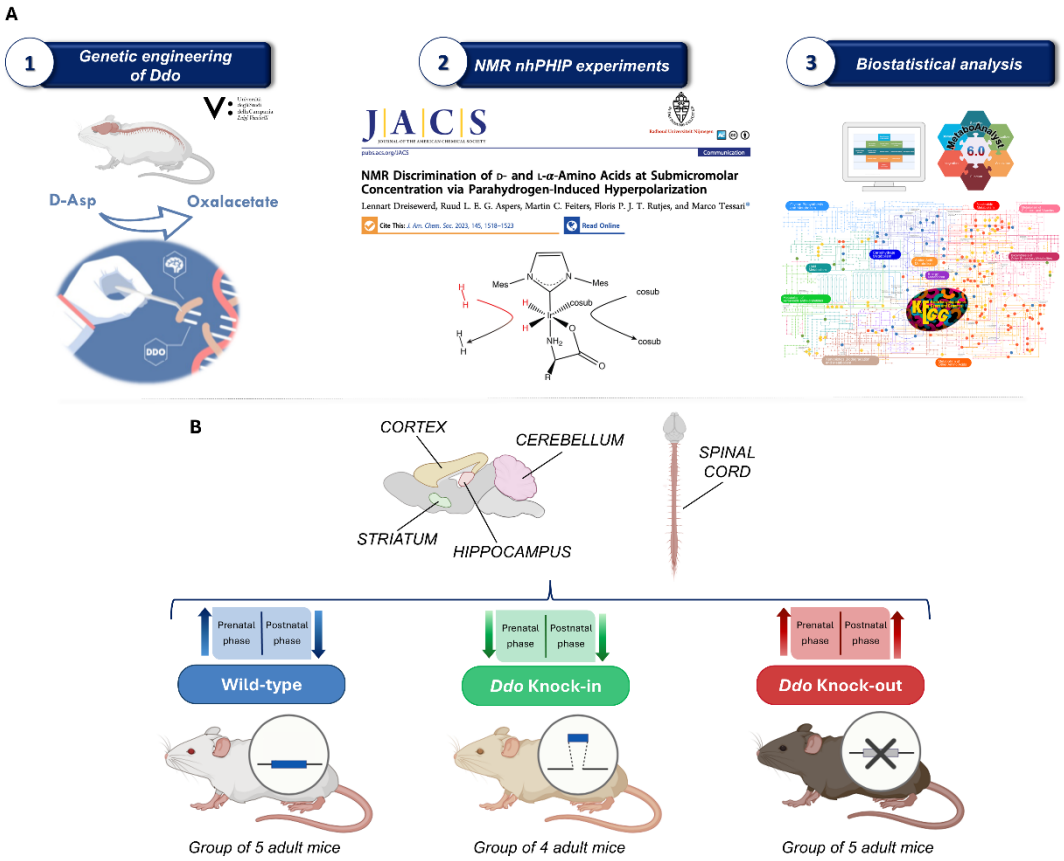

Figure 4.2 *(A) Experimental workflow designed to investigate the neurochemical consequences in adulthood of prenatal D-Asp depletion and sustained postnatal D-Asp accumulation. First, murine models with altered D-Asp levels were generated. Next, non-hydrogenative parahydrogen-induced polarization (nhPHIP) NMR spectroscopy was employed to detect and characterize amino acid content in the murine brain. Finally, biostatistical analysis using MetaboAnalyst was performed to assess the impact of altered D-Asp concentrations on cerebral biochemical pathways. (**B**) The murine brain subregions analyzed include the hippocampus, cortex, cerebellum, striatum, and spinal cord. Tissues were collected from three groups of mice: (i) wild-type, (ii) Ddo knock-in, and (iii) Ddo knock-out mice. Figure created using BioRender, https://www.biorender.com/.*

The application of nhPHIP in this study highlights the potential of hyperpolarized NMR techniques for targeted metabolomics, particularly in investigating stereospecific alterations in amino acid metabolism within neurological contexts. This approach not only enhances analytical resolution but also opens new avenues for

exploring the pharmacological and physiological relevance of D-amino acids in biological samples, including tissue extracts and human biofluids.

4.5 Results

4.5.1 Targeted metabolomic profiling of amino acids in the mouse brain via nhPHIP

To analyze the neurochemical consequences of early prenatal depletion of D-Asp or sustained D-Asp accumulation in the adult brain, the hippocampus, cortex, cerebellum, striatum, and spinal cord were collected from 4 *Ddo* knock-in adult mice, 5 *Ddo* knock-out adult mice, and 5 wild-type adult mice.

A targeted metabolomic approach was employed to investigate alterations in amino acid metabolites that function as neurotransmitters or serve as precursors and modulators of neurotransmission. Advanced NMR experiments based on nhPHIP were performed on polar extracts from selected brain regions to facilitate the targeted metabolomic analysis.

In this experiment, the sample was supplemented with a specific set of reagents: an iridium–heterocyclic carbene catalyst (Ir–IMes) and a chiral substrate (*S*-nicotine). In the presence of parahydrogen (p-H_2), which was continuously bubbled into the solution within NMR tubes, these components facilitated the formation of diastereoisomeric complexes (**Figure 4.3**). These complexes enabled the differentiation of amino acids, including the assessment of their chirality.

Under the specific conditions used for sample preparation (see Materials and Methods), only metabolites with an α-amino acid structure produced detectable NMR signals. More specifically, once formed, the complexes generated characteristic signals observable in 2D nhPHIP zero-quantum (ZQ) spectra. I had the opportunity to acquire these spectra at the Magnetic Resonance Research Center of Radboud University (the Netherlands) under the supervision of Dr. Marco Tessari during the international research period of my PhD.

Figure 4.3 shows a representative example of a 2D nhPHIP ZQ spectrum acquired from the hippocampus of a wild-type mouse. Almost all amino acids – except for proline and its derivatives – produced a pair of doublet signals in the region between –27 and –29 ppm. This specific chemical shift does not originate from the hydrogen atoms of the amino acids themselves, but rather from the hydrides produced by p-H_2

association with the complex. These signals are susceptible to the amino acid side chain, enabling fine discrimination based on molecular structure and, thanks to the presence of the chiral cosubstrate *S*-nicotine, also on stereochemical configuration. The assignment (**Figure 4.3**) was based on spectra of individual amino acids previously recorded under identical conditions (e.g., same pH, same water content, which can affect chemical shift) by Dr. Tessari's research group and published in [35].

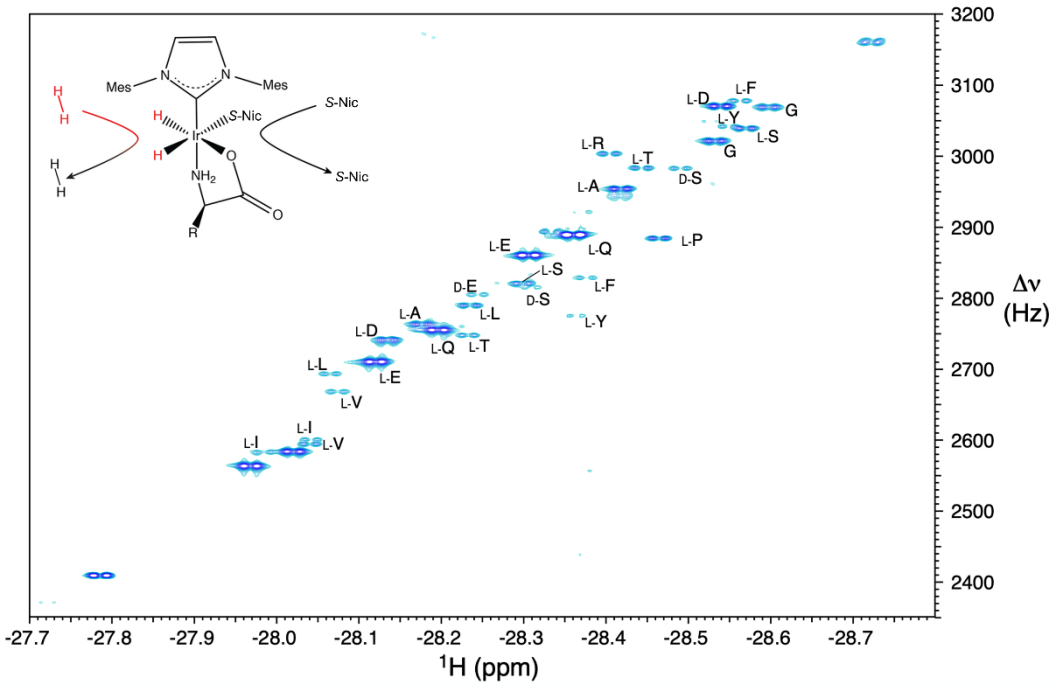

Figure 4.3 *2D nhPHIP zero quantum (ZQ) spectrum of hippocampus polar extract from wild-type mouse. The spectrum was acquired at 10 °C and at a ^{1}H resonance frequency of 600 MHz. The signal assignment is indicated in one letter code. In the upper left corner, a transient complex formed upon association of a α-amino acid deriving from brain extracts, p-H_2, and an additional ligand (cosubstrate), represented by S-nicotine (S-Nic), to an iridium–heterocyclic carbene catalyst.*

4.5.2 Ddo Knock-in

To investigate the neurochemical alterations occurring in adulthood as a consequence of prenatal DDO expression – and the resulting low levels of D-aspartate during fetal development – we performed a biostatistical analysis of quantitative and qualitative data on amino acid content across brain regions, derived from 2D nhPHIP ZQ spectral analysis.

Figure 4.4 presents the score plots from the PLS-DA analysis performed to compare the amino acid profiles of *Ddo* knock-in mice (red points) and wild-type mice

(green points). The supervised analysis was conducted on quantitative matrices derived from the hippocampus (**Figure 4.4A**), cortex (**Figure 4.4B**), cerebellum (**Figure 4.4C**), striatum (**Figure 4.4D**), and spinal cord (**Figure 4.4E**).

Model performance was evaluated using Q^2, R^2, and classification accuracy, with the corresponding values reported in the tables below each score plot. All metrics fell below the thresholds typically considered significant, indicating no substantial differences between the two groups.[36] These findings suggest that the adult cerebral amino acid composition of mice subjected to prenatal D-Asp depletion closely resembles that of mice with physiologically high D-Asp levels during brain development.

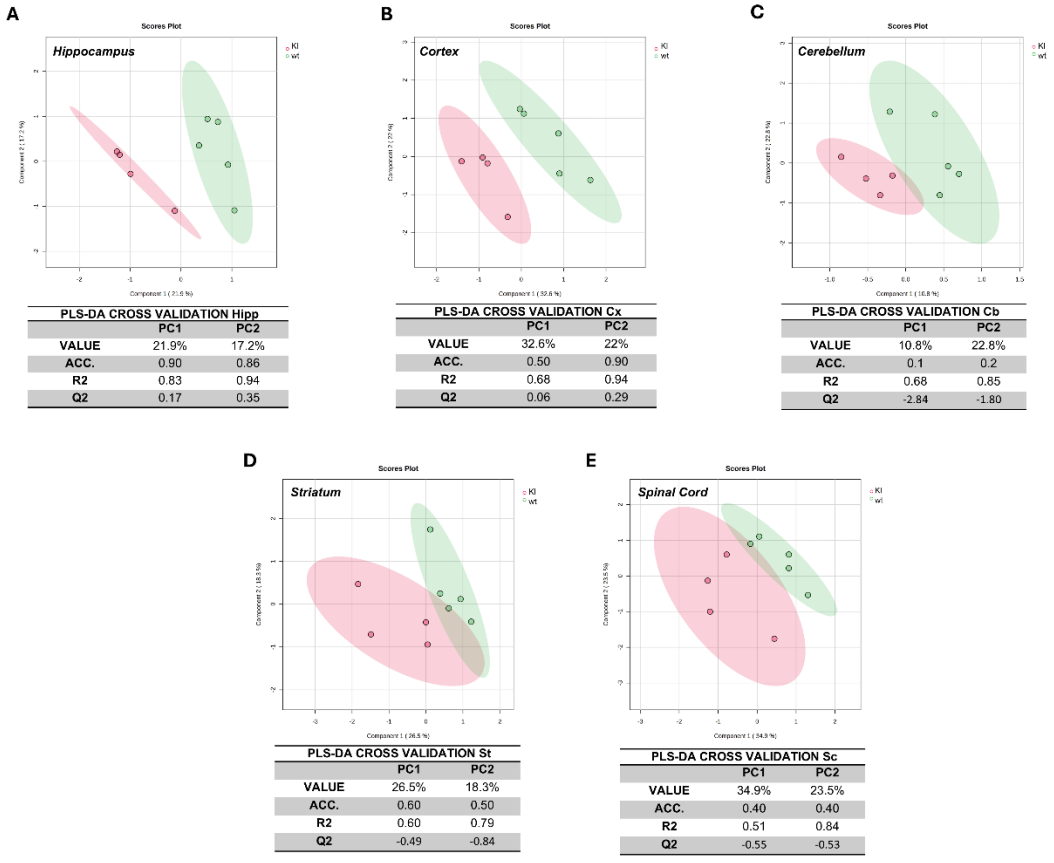

PLS-DA CROSS VALIDATION Hipp

	PC1	PC2
VALUE	21.9%	17.2%
ACC.	0.90	0.86
R2	0.83	0.94
Q2	0.17	0.35

PLS-DA CROSS VALIDATION Cx

	PC1	PC2
VALUE	32.6%	22%
ACC.	0.50	0.90
R2	0.68	0.94
Q2	0.06	0.29

PLS-DA CROSS VALIDATION Cb

	PC1	PC2
VALUE	10.8%	22.8%
ACC.	0.1	0.2
R2	0.68	0.85
Q2	-2.84	-1.80

PLS-DA CROSS VALIDATION St

	PC1	PC2
VALUE	26.5%	18.3%
ACC.	0.60	0.50
R2	0.60	0.79
Q2	-0.49	-0.84

PLS-DA CROSS VALIDATION Sc

	PC1	PC2
VALUE	34.9%	23.5%
ACC.	0.40	0.40
R2	0.51	0.84
Q2	-0.55	-0.53

Figure 4.4 *PLS-DA score plots of the amino acid metabolomic profiles comparing Ddo Knock-in (KI, red) and Wild-Type (wt, green) mice across five brain regions: hippocampus (**A**), cortex (**B**), cerebellum (**C**), striatum (**D**), and spinal cord (**E**). The tables below each plot report cross-validation results, including the explained variance for each component, as well as accuracy, R^2, and Q^2 values.*

4.5.3 Ddo Knock-out

The sustained accumulation of D-Asp in adulthood was assessed using genetically modified mice in which the *Ddo* gene was silenced, thereby preventing its metabolization. Similar to the comparison presented in the previous paragraph, a PLS-DA analysis was performed to compare *Ddo* knock-out mice and wild-type mice.

The PLS-DA score scatter plot for the comparison between *Ddo* knock-out mice's hippocampus and wild-type mice's hippocampus is illustrated in **Figure 4.5A**. The graph shows a clear separation between the two clusters, whose differences in amino acid content were confirmed by cross-validation analysis (Q^2 = 0.98 and 0.97, respectively, on PC1 and PC2). To identify specific metabolites responsible for discriminating the metabolomic changes induced by D-Asp accumulation in the hippocampus of *Ddo* knock-out mice, a Variable Importance in the Projection (VIP) score analysis was performed (**Figure 4.5B**). As expected, the study revealed an increase in D-aspartate as the primary discriminating metabolite. Additionally, it highlighted reduced levels of several amino acids, including L-isoleucine, L-phenylalanine, L-leucine, L-arginine, L-tryptophan, L-tyrosine, L-proline, L-valine, and glycine. These findings were further supported by univariate statistical analysis conducted via volcano plot, which confirmed the same trends in concentration changes (**Figure 4.5C**).

Note that in the VIP analysis and in volcano plot, each amino acid typically appears twice, distinguished by the labels 1 and 2. This duplication arises because all amino acids – except proline and its derivatives – produce a pair of doublet signals in the spectral region between –27 and –29 ppm, and both signals were incorporated into the matrix used for the biostatistical analysis.

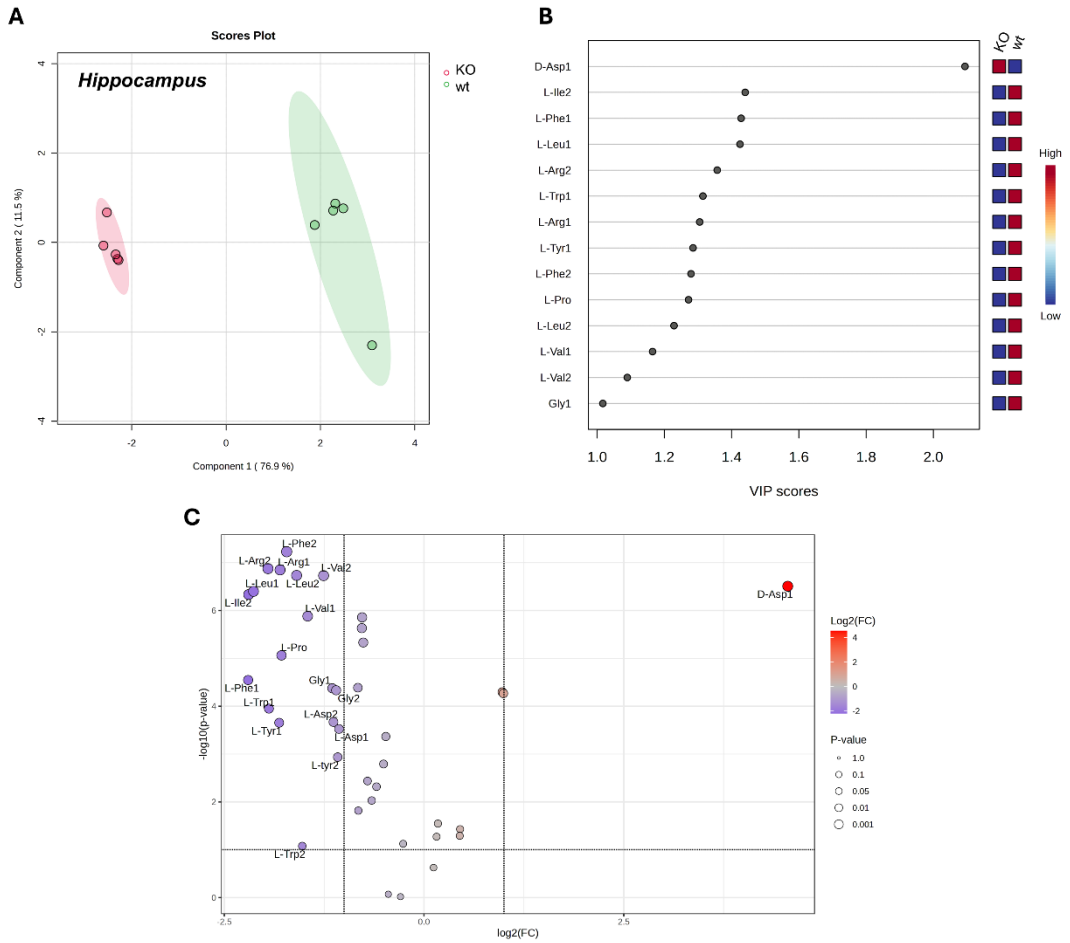

Figure 4.5 *(**A**) PLS-DA score plot of amino acid metabolomic profiles from the hippocampus, comparing Ddo knock-out (KO, red) and wild-type (wt, green) mice. Cluster separation is shown in Cartesian space defined by principal components PC1 (76.9%) and PC2 (11.5%). Model performance was evaluated using cross-validation (CV) based on the PLS-DA statistical protocol, revealing significant separation between groups (accuracy = 1.0 on both PC1 and PC2; Q^2 = 0.98 and 0.97, respectively). (**B**) VIP score plot of metabolites contributing to group discrimination. (**C**) Volcano plot showing metabolic changes in the hippocampus of Ddo knock-out and wild-type mice. Each point represents a metabolite, plotted according to p-value and fold-change thresholds (<0.05 and ±2.0, respectively). Red points indicate upregulated metabolites; blue points indicate downregulated metabolites.*

Subsequently, the same analysis was repeated on cortical samples, revealing distinct clustering of the metabolomic profiles between *Ddo* knock-out and wild-type mice (**Figure 4.6A**) (Q^2 = 0.95 and 0.97, respectively, on PC1 and PC2). VIP score analysis confirmed the expected increase in D-aspartate as a consequence of *Ddo* gene silencing, along with elevated hydroxyproline levels and reduced concentrations of several amino acids, including the three aromatic L-amino acids, L-leucine, L-isoleucine, L-proline, glycine, L-arginine, and L-valine (**Figure 4.6B**). These variations – particularly in branched-chain amino acids (BCAAs), aromatic amino

acids (ArAAs), L-arginine, and L-lysine – were further validated by univariate statistical analysis using a volcano plot representation (**Figure 4.6C**).

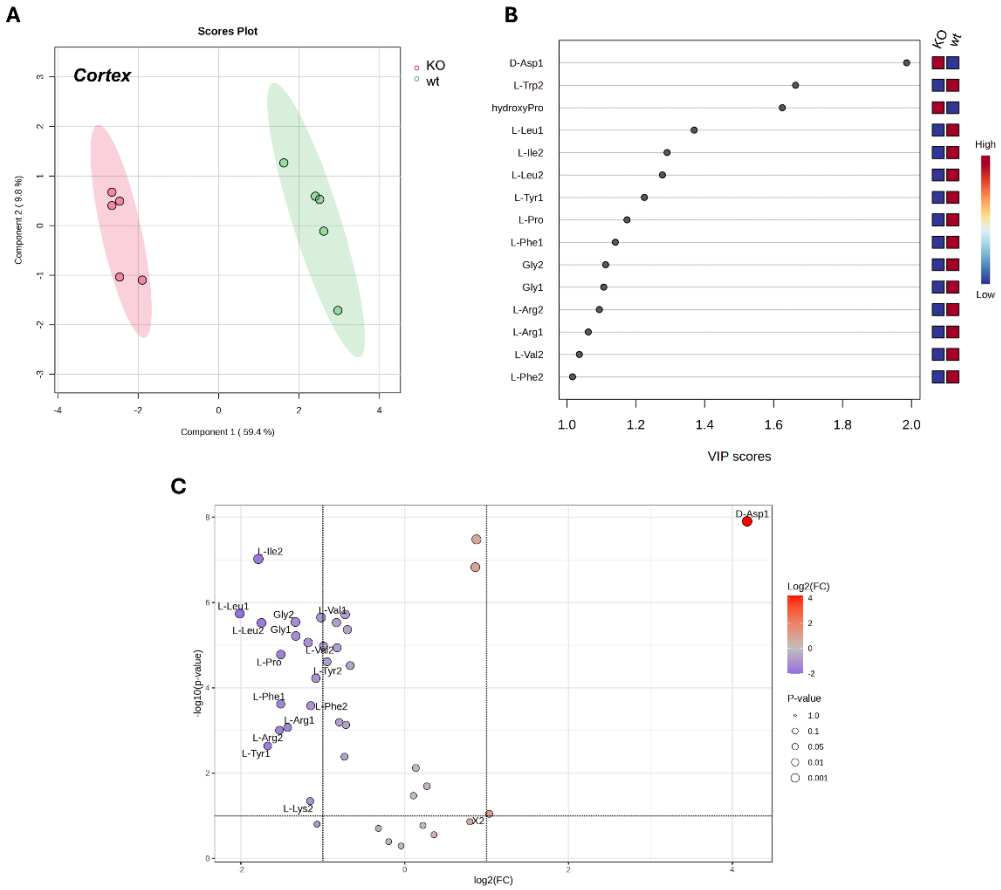

Figure 4.6 *(**A**) PLS-DA score plot of amino acid metabolomic profiles from the cortex, comparing Ddo knock-out (KO, red) and wild-type (wt, green) mice. Cluster separation is shown in Cartesian space defined by principal components PC1 (59.4%) and PC2 (9.8%). Model performance was evaluated using cross-validation (CV) based on the PLS-DA statistical protocol, revealing significant separation between groups (accuracy = 1.0 on both PC1 and PC2; Q^2 = 0.95 and 0.97, respectively). (**B**) VIP score plot of metabolites contributing to group discrimination. (**C**) Volcano plot showing metabolic changes in the cortex of Ddo knock-out and wild-type mice. Each point represents a metabolite, plotted according to p-value and fold-change thresholds (<0.05 and ±2.0, respectively). Red points indicate upregulated metabolites; blue points indicate downregulated metabolites.*

To investigate the metabolic effects induced by D-Asp in the cerebellum, we repeated the PLS-DA analysis on NMR nhPHIP 2D ZQ data obtained from cerebellar extracts of *Ddo* knock-out and wild-type mice (**Figure 4.7A**). Once again, the supervised statistical method revealed a significantly different amino acid profile between the two groups, with Q^2 values of 0.94 and 0.93 for PC1 and PC2, respectively. VIP score analysis confirmed elevated D-aspartate concentration and additionally revealed increased levels of L-glutamate. Conversely, reduced

concentrations were observed for several amino acids, including L-leucine, L-arginine, L-tryptophan, L-phenylalanine, glycine, L-isoleucine, L-tyrosine, L-valine, L-lysine, and L-proline (**Figure 4.7B**). These trends were supported by univariate statistical analysis (**Figure 4.7C**), which showed consistent variations in amino acid levels within the cerebellum.

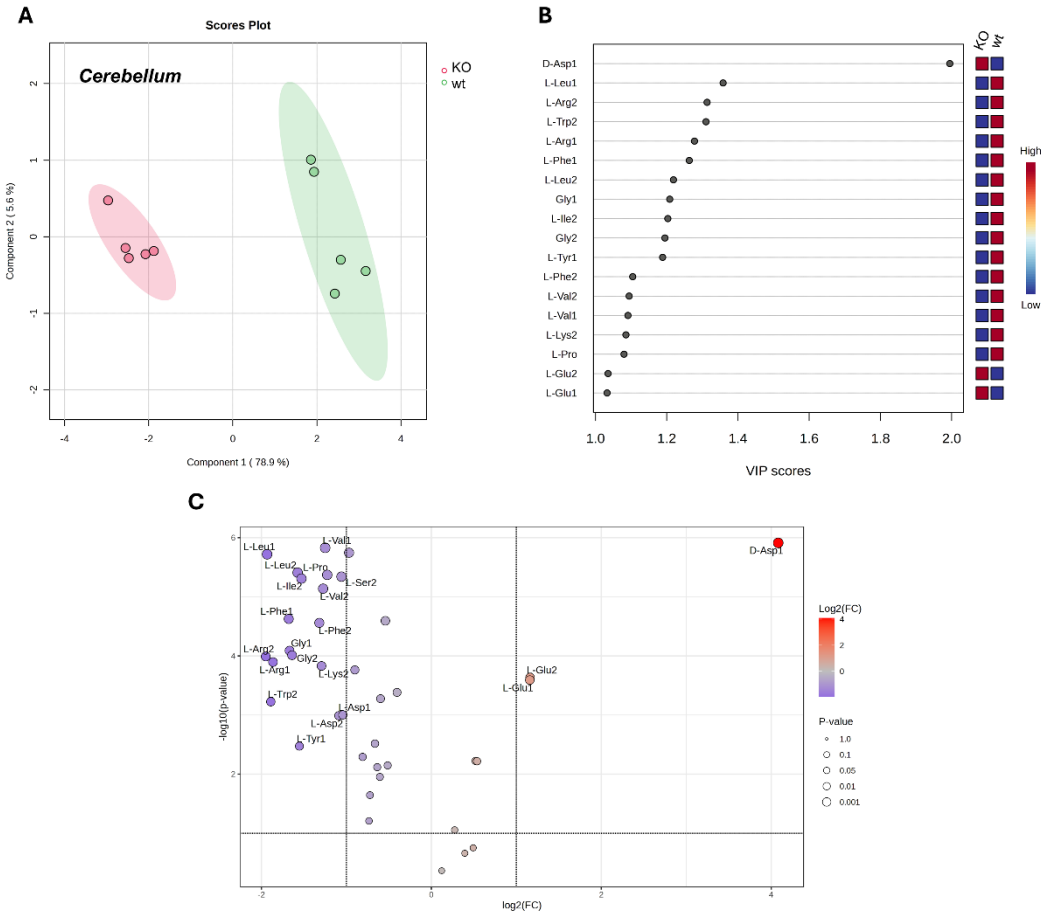

Figure 4.7 *(**A**) PLS-DA score plot of amino acid metabolomic profiles from the cerebellum, comparing Ddo knock-out (KO, red) and wild-type (wt, green) mice. Cluster separation is shown in Cartesian space defined by principal components PC1 (78.9%) and PC2 (5.6%). Model performance was evaluated using cross-validation (CV) based on the PLS-DA statistical protocol, revealing significant separation between groups (accuracy = 1.0 on both PC1 and PC2; Q^2 = 0.94 and 0.93, respectively). (**B**) VIP score plot of metabolites contributing to group discrimination. (**C**) Volcano plot showing metabolic changes in the cerebellum of Ddo knock-out and wild-type mice. Each point represents a metabolite, plotted according to p-value and fold-change thresholds (<0.05 and ±2.0, respectively). Red points indicate upregulated metabolites; blue points indicate downregulated metabolites.*

The same targeted metabolomic approach was applied to investigate the impact of D-Asp accumulation on striatal amino acid composition. Comparison of striatal metabolomic fingerprints between *Ddo* knock-out and wild-type mice revealed a significant difference between the two groups, with Q^2 values of 0.89 for both PC1

and PC2 (**Figure 4.8A**), confirming consistent alterations across all four analyzed brain regions. In line with the findings in the cerebellum, VIP score analysis indicated elevated concentrations of D-aspartate and L-glutamate in the striatum of *Ddo* knock-out mice. In contrast, reduced levels were observed for several amino acids, including L-arginine, L-leucine, L-phenylalanine, L-isoleucine, glycine, L-proline, L-aspartate, L-alanine, L-tyrosine, and L-lysine (**Figure 4.8B**). These variations were largely confirmed by univariate statistical analysis, as illustrated in the volcano plot (**Figure 4.8C**).

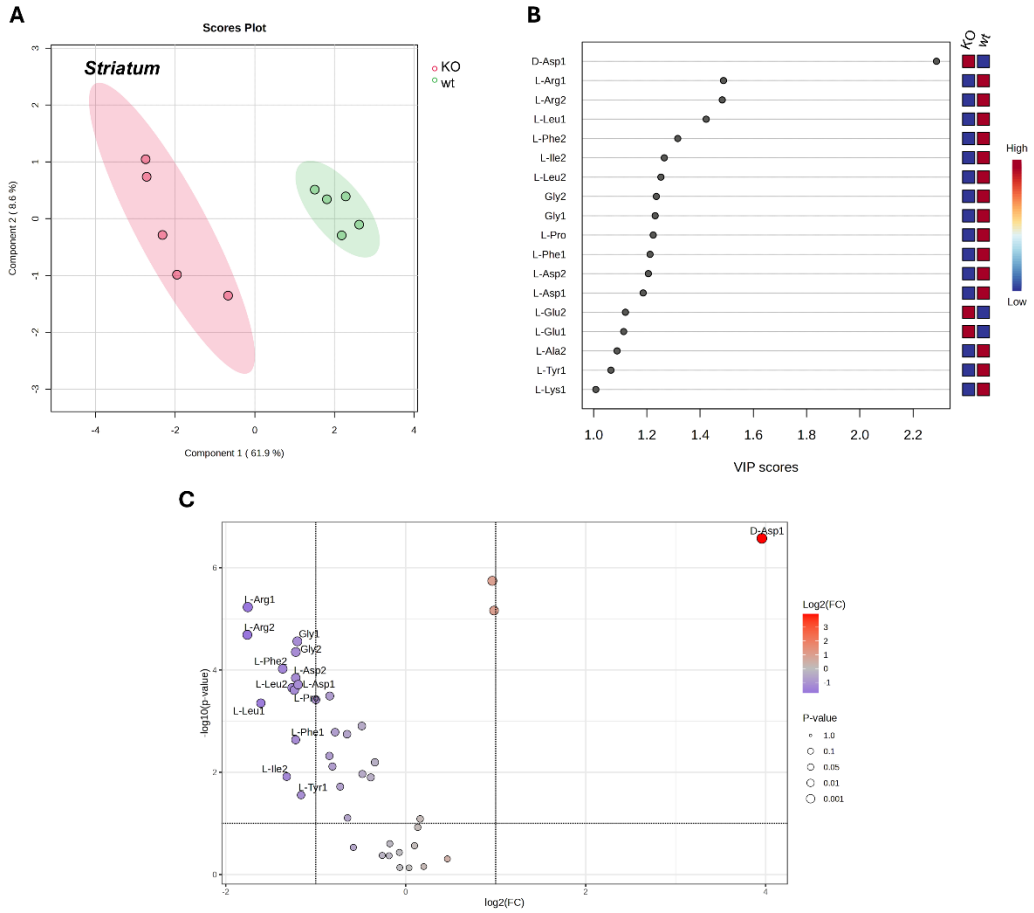

Figure 4.8 *(**A**) PLS-DA score plot of amino acid metabolomic profiles from the striatum, comparing Ddo knock-out (KO, red) and wild-type (wt, green) mice. Cluster separation is shown in Cartesian space defined by principal components PC1 (61.9%) and PC2 (8.6%). Model performance was evaluated using cross-validation (CV) based on the PLS-DA statistical protocol, revealing significant separation between groups (accuracy = 1.0 and Q^2 = 0.89 on both PC1 and PC2). (**B**) VIP score plot of metabolites contributing to group discrimination. (**C**) Volcano plot showing metabolic changes in the striatum of Ddo knock-out and wild-type mice. Each point represents a metabolite, plotted according to p-value and fold-change thresholds (<0.05 and ±2.0, respectively). Red points indicate upregulated metabolites; blue points indicate downregulated metabolites.*

To conclude, we analyzed polar extracts from the spinal cord to investigate the consequences of elevated D-aspartate levels in the central nervous system outside the brain. PLS-DA analysis performed on the spinal cord metabolomic matrix from *Ddo* knock-out and wild-type mice revealed a significant impact on amino acid composition (**Figure 4.9A**), with Q^2 values of 0.93 for both PC1 and PC2. Similar to the four brain regions previously examined, the spinal cord was characterized by increased levels of D-aspartate and reduced concentrations of BCAAs, ArAAs, L-arginine, L-proline. Notably, L-serine levels were also reduced in the spinal cord, a variation not observed in the other brain regions analyzed (**Figure 4.9B**). These findings were further confirmed by univariate statistical analysis (**Figure 4.9C**).

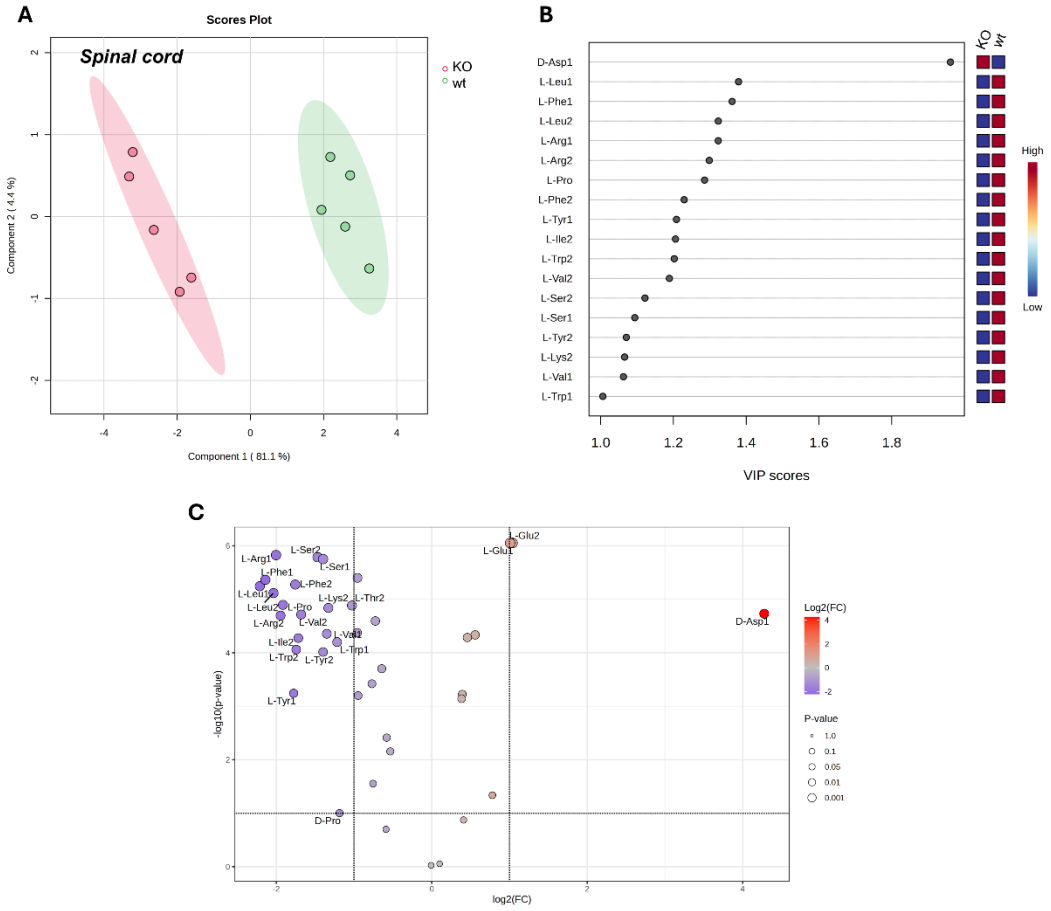

Figure 4.9 *(**A**) PLS-DA score plot of amino acid metabolomic profiles from the spinal cord, comparing Ddo knock-out (KO, red) and wild-type (wt, green) mice. Cluster separation is shown in Cartesian space defined by principal components PC1 (81.1%) and PC2 (4.4%). Model performance was evaluated using cross-validation (CV) based on the PLS-DA statistical protocol, revealing significant separation between groups (accuracy = 1.0 and Q^2 = 0.93 on both PC1 and PC2). (**B**) VIP score plot of metabolites contributing to group discrimination. (**C**) Volcano plot showing metabolic changes in the spinal cord of Ddo knock-out and wild-type mice. Each point represents a metabolite, plotted according to p-value and fold-change thresholds (<0.05 and ±2.0, respectively). Red points indicate upregulated metabolites; blue points indicate downregulated metabolites.*

4.5.3.1 Biochemical pathways altered in Ddo knock-out mice

We subsequently used enrichment analyses to identify the distinct biochemical pathways modulated by D-Asp in the hippocampus, cortex, cerebellum, striatum and spinal cord.

Metabolomic data derived from NMR nhPHIP 2D ZQ spectra of *Ddo* knock-out and wild-type mice were used to perform pathway enrichment analysis using the *Kyoto Encyclopedia of Genes and Genomes* (KEGG) database. In accordance with the observed variations in amino acid concentrations in the hippocampus, the analysis revealed dysregulation not only in D-amino acid metabolism but also in *valine, leucine, and isoleucine biosynthesis* and their *degradation* pathways. Additional amino acid-related alterations included *alanine, aspartate, and glutamate metabolism*; *glycine, serine, and threonine metabolism*; *phenylalanine metabolism*; *phenylalanine, tyrosine, and tryptophan biosynthesis*; *arginine biosynthesis*; and *histidine metabolism*. Furthermore, disruptions were observed in *pantothenate and CoA biosynthesis*, *glyoxylate and dicarboxylate metabolism*, *porphyrin metabolism*, and *nitrogen metabolism* (**Figure 4.10A**).

The same analysis was performed for the remaining three brain regions and the spinal cord, confirming alterations not only in D-amino acid metabolism and several L-amino acid pathways, but also in energy-related and redox-associated biochemical routes (**Figures 4.10B–E**).

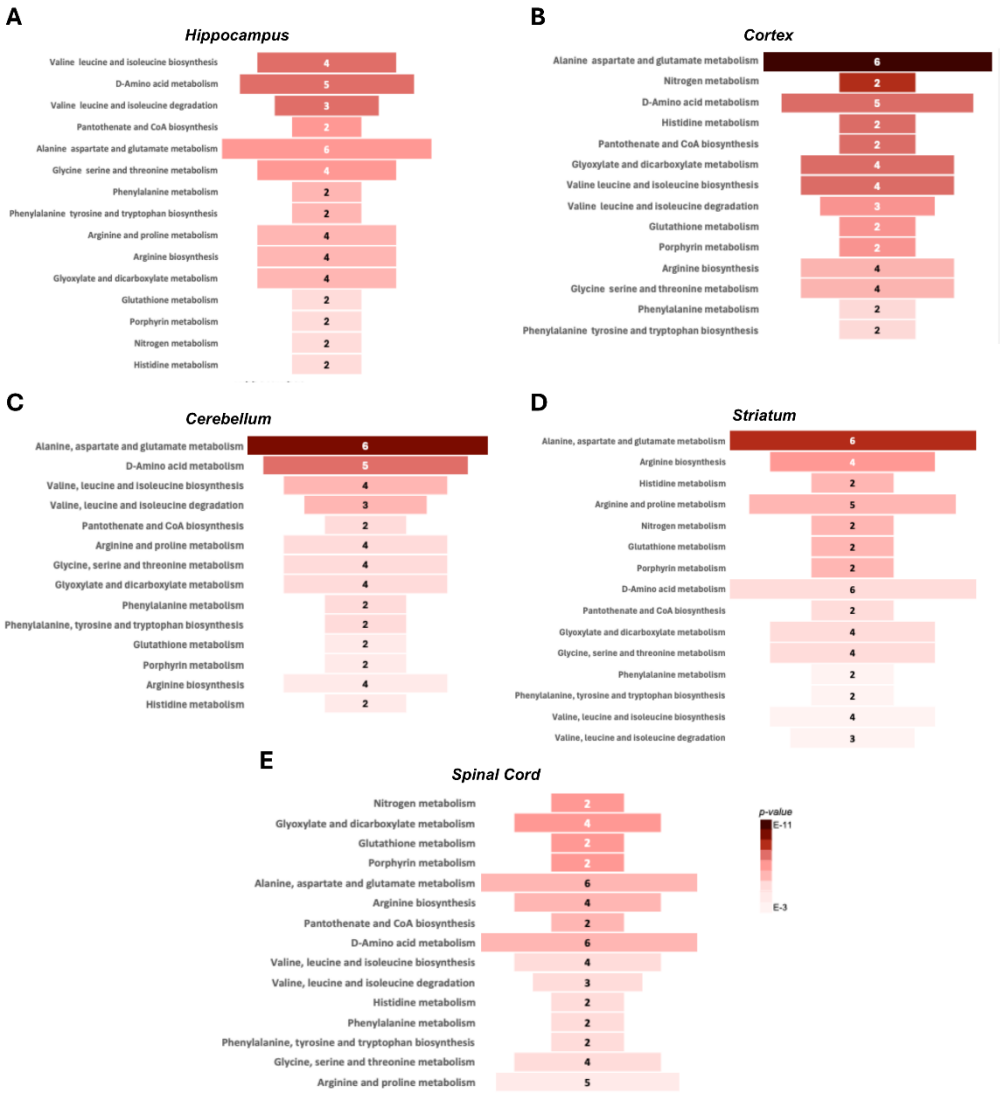

Figure 4.10 *Enrichment pathways analysis for the five brain regions: hippocampus (**A**), cortex (**B**), cerebellum (**C**), striatum (**D**), spinal cord (**E**). The discriminative pathways are ranked according to p-value and number of hits reported in the bars. Only pathways reporting a p-value <0.05 and a number of hits (metabolites involved in the biochemical pathway) >2 are considered significant.*

4.5.3.2 Comparative analyses of Ddo knock-out amino acidic dysregulation in the five subregions

To obtain a comprehensive overview of the effects of elevated D-aspartate concentrations in the central nervous system and to compare the dysregulation observed across the five analyzed regions, we performed comparative analyses.

As a first step, we constructed a Venn diagram highlighting the amino acids responsible for the differentiation of the *Ddo* knock-out metabolomic fingerprint. This representation identifies the key metabolites whose concentrations were significantly altered by *Ddo* gene silencing (**Figure 4.11A**).

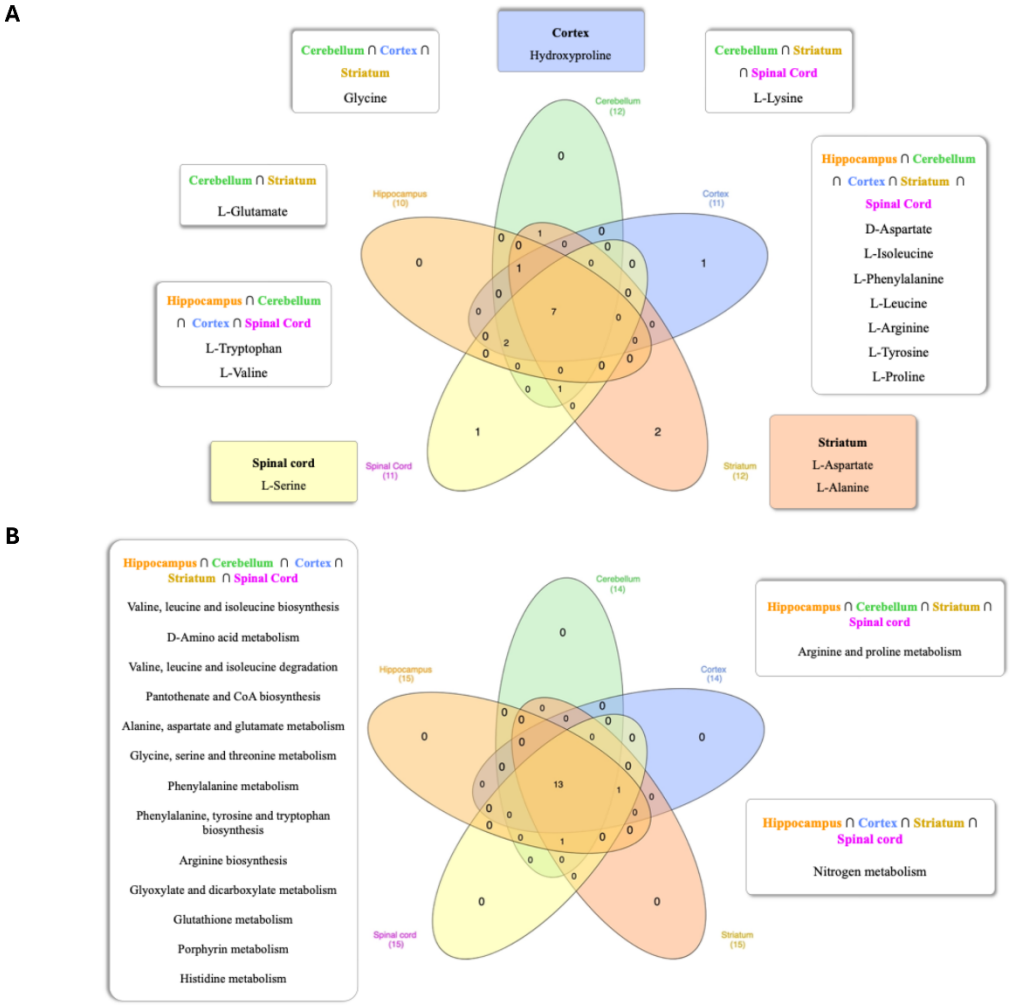

Figure 4.11 *(A) Venn diagram showing the amino acids with VIP > 1 identified in the comparison of hippocampus, cortex, cerebellum, striatum, and spinal cord from Ddo knock-out mice. (**B**) Venn diagram illustrating the disrupted biochemical pathways emerging from the same regional comparison in Ddo knock-out mice. Created with InteractiVenn, https://www.interactivenn.net/*

The diagram shows that several amino acids are commonly altered across all five regions, including D-aspartate, L-isoleucine, L-phenylalanine, L-leucine, L-arginine, L-tyrosine, and L-proline. In contrast, L-tryptophan and L-valine were consistently affected in all regions except the striatum.

Some metabolites appear to be specific to individual anatomical regions: hydroxyproline reduction was observed exclusively in the cortex. At the same time, decreased levels of L-aspartate and L-alanine were unique to the striatum. Similarly, L-serine reduction was found only in the spinal cord.

Additionally, certain alterations were common to different subsets of regions: L-glutamate was elevated in both the cerebellum and striatum; glycine levels were reduced in the cerebellum, cortex, and striatum; and L-lysine showed consistent decreases in the cerebellum, striatum, and spinal cord.

The comparison of altered biochemical pathways was performed using the same approach: a Venn diagram was constructed (**Figure 4.11B**). In this case, no pathway emerged as uniquely associated with a specific brain region. On the contrary, several amino acid-related pathways were commonly affected across multiple areas, including *D-amino acid metabolism*; *valine, leucine, and isoleucine degradation* and *biosynthesis*; *pantothenate and CoA biosynthesis*; *alanine, aspartate, and glutamate metabolism*; *glycine, serine, and threonine metabolism*; *phenylalanine metabolism*; *phenylalanine, tyrosine, and tryptophan biosynthesis*; *arginine biosynthesis*; and *histidine metabolism*.

In addition to these shared pathways, other metabolic routes, such as *glyoxylate and dicarboxylate metabolism, glutathione metabolism*, and *porphyrin metabolism*, were also disrupted. Notably, all regions except the cortex showed alterations in *arginine and proline metabolism*, while *nitrogen metabolism* was affected in all regions except the cerebellum.

4.6 Discussion

Given the intriguing role of D-Asp in brain development, we extended our previous metabolomic analysis – originally conducted on the prenatal whole brain of *Ddo* knock-in mice – to investigate the long-term effects of prenatal D-Asp depletion in adulthood. Grimaldi *et al.* demonstrated that reduced levels of this D-amino acid significantly affected amino acid concentrations and related metabolic pathways across all developmental time points. [34] However, the classical NMR techniques used in that study could not resolve amino acid chirality. Given the critical role of stereochemical resolution in studies involving D-amino acids, the integration of chirality-sensitive methodologies is fundamental to the accuracy of the present metabolomic analysis.

One promising technique is non-hydrogenative parahydrogen-induced polarization (nhPHIP), an emerging NMR method in metabolomics. [35, 37, 38] As a hyperpolarization method, nhPHIP significantly enhances NMR sensitivity, enabling the detection and

quantification of metabolites at low concentrations. Moreover, 2D nhPHIP ZQ experiments introduce a second spectral dimension, allowing for the resolution of amino acids with similar chemical structures that typically overlap in conventional ^{1}H NMR spectra. When a chiral cosubstrate is used during sample preparation, the resulting metal complex can serve as a stereochemical probe, distinguishing between D- and L-amino acids with identical formula and connectivity. [35]

In this study, we focused on specific brain subregions – including the hippocampus, cortex, cerebellum, striatum – and the spinal cord, to assess the broader impact of altered D-Asp levels across the CNS. When comparing amino acid profiles between adult *Ddo* knock-in mice and wild-type controls, we found comparable concentrations of nearly all L- and D-series amino acids. As expected, no significant differences in D-Asp levels were observed across the analyzed regions, consistent with the high physiological activity and expression of the DDO enzyme during the postnatal phase. However, it was not a given that other amino acids would remain unaffected. Our findings align with those of De Rosa *et al.*, who reported no differences in D-serine, L-serine, and L-glutamate – key modulators of NMDA receptor function. Consistent with these neurochemical results, the authors observed no significant neuroanatomical alterations in adult brain architecture, including neuronal and myelin distribution, in *Ddo* knock-in mice. [18]

Taken together, these results support the hypothesis that the amino acid pathway disruptions observed during prenatal and early postnatal development, as reported by Grimaldi *et al.*, are largely compensated in adulthood – when D-Asp no longer plays a central role in the brain. [34] However, further research could be beneficial to confirm this hypothesis.

The opposite scenario – characterized by elevated D-Asp concentrations in adulthood – represents a deviation from the physiological norm, as D-Asp levels are typically low due to the postnatal induction of *Ddo* gene expression and the enzymatic activity of its protein product. Previous studies have shown that the effects of D-Asp in adulthood are not uniform but depend strongly on the duration of exposure, whether due to exogenous administration or genetic modifications such as *Ddo* gene silencing. Specifically, elevated D-Asp levels during early adulthood (2–4 months) have been associated with enhanced cognitive performance and improved memory in murine

models. In contrast, persistent D-Asp elevation into later adulthood (beyond 6 months) has been linked to detrimental outcomes, likely due to chronic overstimulation of L-glutamate receptors, which may exacerbate age-related neurodegeneration. [16]

In this study, our murine models were within this latter age range, and our findings underscore the widespread impact of sustained D-Asp accumulation on amino acid profiles across the entire CNS. Comparative analyses revealed that the amino acid alterations induced by D-Asp accumulation in aged mice were largely consistent across all CNS regions, with no evidence of region-specific dysregulation. Several amino acids identified as significantly altered in individual subregions were also consistently affected in both the brain and spinal cord, suggesting a shared biochemical response to D-Asp elevation. As expected, D-Asp levels were markedly elevated in all analyzed regions, reflecting the *Ddo* gene manipulation and confirming modulation of D-amino acid pathways as a common feature across the CNS.

Among the affected metabolic pathways, *alanine, aspartate, and glutamate metabolism* emerged as the most significantly impacted, particularly in the cortex, cerebellum, and striatum. Notably, L-glutamate levels were elevated in both the cerebellum and striatum. Previous studies have demonstrated that increased D-Asp levels modulate the glutamatergic system. For example, Cristino *et al.* reported that D-Asp enhances glutamate release in both *in vitro* and *in vivo* models. Microdialysis experiments in six-month-old mice showed that elevated D-Asp levels – either through acute injection in freely moving animals or via genetic deletion of the *Ddo* gene – led to increased extracellular concentrations of L-glutamate in the hippocampus and prefrontal cortex, but not in the striatum. [30]

The apparent discrepancy with our findings may be attributed to methodological differences. While Cristino *et al*. employed microdialysis to selectively measure extracellular glutamate, our analysis was based on homogenized tissue, which does not differentiate between intra- and extracellular compartments. Despite this distinction, our results remain consistent with previous evidence indicating that elevated D-Asp levels alter glutamatergic pathways in the adult brain.

In addition to alterations in glutamatergic pathways, our analysis revealed significantly reduced levels of L-arginine and L-proline in *Ddo* knock-out mice compared with wild-type controls. These changes were observed across nearly all anatomical regions examined. In the brain, L-arginine serves as the primary precursor

for nitric oxide (NO), a key physiological regulator involved in cerebral blood flow, memory and cognitive function, the sleep-wake cycle, and olfactory processing. However, in neurodegenerative conditions, excessive NO production can lead to nitroxidative stress, contributing to cellular damage. [39] Consistent with this, dysregulation of *L-arginine and L-proline metabolism* – as well as broader *nitrogen metabolism* – has been reported in the brains of *Ddo* knock-out mice.

L-proline also plays a neuromodulatory role, exerting both excitatory and inhibitory effects, and is involved in energy metabolism and oxidative stress responses. Importantly, L-proline acts as an NMDA receptor agonist, modulating glutamatergic transmission. Abnormal proline levels have been linked to psychiatric disorders, and their reduction in our model aligns with impaired neurotransmission, cognitive deficits, and oxidative stress – hallmarks of neurodegenerative conditions associated with sustained D-Asp elevation. [40]

We also observed alterations in aromatic amino acids, such as phenylalanine and tyrosine, which serve as precursors for catecholamine biosynthesis. These changes suggest a potential disruption in catecholaminergic neurotransmission. Supporting this hypothesis, previous studies have reported that elevated levels of D-Asp following exogenous administration can inhibit dopamine release in the hippocampus, indicating a modulatory role for D-Asp in monoaminergic signaling. [41]

Furthermore, BCAAs were altered in both their biosynthesis and degradation pathways. Reduced BCAA levels have been reported in similar pathological contexts, including AD, which – like *Ddo* knock-out mice – is characterized by sustained excitotoxicity due to NMDA receptor overstimulation. [42] Although the underlying mechanisms remain unclear, these findings suggest a link to neurotransmitter imbalance, as BCAAs serve as nitrogen donors for glutamate and GABA synthesis and can also support the tricarboxylic acid (TCA) cycle as alternative energy substrates.

Additional disruptions were observed in *pantothenate and CoA biosynthesis* pathways, as well as in *glyoxylate and dicarboxylate metabolism*, suggesting an altered neuronal energetic demand. In the brain, CoA is synthesized from pantothenate and plays a central role in energy metabolism, particularly in fatty acid synthesis and β-oxidation, as well as in the TCA cycle. Furthermore, CoA is essential for the biosynthesis of neurotransmitters and steroid hormones. Notably, inborn errors in CoA

biosynthesis have been linked to neurodegenerative disorders in humans, underscoring CoA's critical role in maintaining neuronal health and metabolic homeostasis. [43]

Consistent with the observed energetic alterations, we detected clear signs of mitochondrial dysfunction and persistent oxidative stress, as evidenced by changes in glutathione and porphyrin metabolism. Notably, heme (iron-protoporphyrin IX) plays a central role as a structural component of cytochrome complexes within the electron transport chain. It is essential for catalase activity, which protects cells from H_2O_2-induced oxidative damage. Beyond its role in redox balance, heme functions as a vital cofactor in numerous biological processes, including neuronal survival, differentiation, and synaptic function. Emerging evidence suggests that dysregulation of heme metabolism may contribute significantly to neurodegenerative processes. Indeed, several neurodegenerative disorders have been linked to impaired heme homeostasis, further supporting its critical involvement in the pathogenesis of these conditions. [44]

In conclusion, our analysis highlights the crucial role of D-Asp downregulation in the aging CNS, where its suppression – primarily mediated by DDO activation – emerges as a key physiological mechanism for maintaining neurochemical balance in later life. D-Asp stimulation in the mature brain induces alterations in several amino acids involved in neurotransmission and cognitive functions, such as L-proline and L-glutamate. Additionally, amino acids linked to oxidative stress regulation are significantly affected. In line with these changes, increased production of NO and reactive oxygen species (ROS) is observed, with a notable impact on glutathione metabolism and mitochondrial energy processes. Altogether, these findings outline a pathological framework that overlaps with mechanisms commonly associated with neurodegenerative diseases.

4.7 Conclusions

This study presents, for the first time, the application of a targeted metabolomics approach focused on amino acid dysregulation, employing an emerging NMR technique in metabolomics: non-hydrogenative parahydrogen-induced polarization (nhPHIP). This innovative method enabled us to specifically investigate amino acid imbalances triggered by altered D-Asp levels – modulated through genetic manipulation – while allowing a clear distinction between D- and L-amino acid

enantiomers. Thanks to this advanced technique, we demonstrated that, in adult murine models, the metabolic changes caused by D-Asp depletion appear to be largely compensated. More importantly, we provide the first evidence that persistent D-Asp levels in the adult brain lead to neurodegeneration-like conditions, affecting multiple amino acid pathways and suggesting broader disruption of neurochemical homeostasis.

4.8 Materials and methods

4.8.1 Mouse models and sample collection

Ddo knock-in mice ($Rosa26^{Ddo/+}$) were generated and genotyped by polymerase chain reaction (PCR) as previously described. [18] All experiments were conducted on male wild-type ($Rosa26^{+/+}$) and heterozygous knock-in ($Rosa26^{Ddo/+}$) mice, obtained from the mating of $Rosa26^{+/+}$ and $Rosa26^{Ddo/+}$ animals. These mice were backcrossed for five generations (F5) onto the C57BL/6J genetic background. Adult-phase experiments were performed on 6- to 9-month-old male mice.

Knock-out mice ($Ddo^{-/-}$) were generated as previously reported. [19] Male wild-type ($Ddo^{+/+}$) and homozygous knock-out ($Ddo^{-/-}$) mice, aged approximately 7–8 months, were used in this study. These animals were derived from heterozygous ($Ddo^{+/-}$) matings and similarly backcrossed to the C57BL/6J background for five generations, in accordance with the Banbury Conference guidelines on genetic background in mice (1997). [24] Genotyping was performed by PCR following the protocol described by Errico *et al*. [19]

All animals were group-housed (four to five per cage) under controlled environmental conditions (22 ± 1 °C; 12-hour light/dark cycle) with ad libitum access to food and water. Organs and tissues were collected from mice anaesthetized with 1.5% sevoflurane, and 98.5% O_2 (Oxygen concentrator, Longfei Industry Co, Zhejiang, China). The hippocampus, cortex, cerebellum, striatum, and spinal cord were rapidly removed after cerebral dissection, immediately frozen on dry ice, and stored at −80 °C until use. All procedures were approved by the Institutional Animal Care and Use Committee and conducted in accordance with relevant guidelines.

4.8.2 Chemicals

Reagents were purchased from the suppliers listed below and used as received.

S-Nicotine, piperidine, piperidine hydrochloride, (R)-(+)-α-methylvaline were purchased from Sigma-Aldrich. α-Aminoisobutyric acid was purchased from Janssen Chemica. Methanol was purchased from Fischer Scientific. Ultrapure water (Milli-Q) was produced using a Milli-Q purification system equipped with a Q-Gard® 2 pack and a Quantum® EX cartridge (Millipore).

The catalyst precursor [Ir(COD)(IMes)Cl](Imes = 1,3-bis(2,4,6-trimethylphenyl)imidazole-2-ylidene; COD = cyclooctadiene) was synthesized in-house as previously described. [45] Parahydrogen was generated using a HyperSpin Scientific generator cooled with liquid nitrogen at 77 K, converting thermal hydrogen (purity 5.0, Linde Gas Benelux B.V.) to 51% para-enriched H_2.

4.8.3 nhPHIP NMR experiments

4.8.3.1 Sample preparation for nhPHIP

Brain sub-regions and spinal cord tissues were collected from wt, *Ddo* knock-in, and *Ddo* knock-out mice and processed according to the standard operating procedure.[46] In detail, 15–30 mg of each brain tissue sample was homogenised in 0.45 mL of water and 2 mL of methanol using sonication. The homogenates were then diluted with 3 mL of a chloroform/water solution (2:1, v/v) and vortexed to facilitate extraction. After centrifugation at 10000 × *g* for 2 min at 4 °C, the polar and apolar phases were separated. The polar phase was subsequently dried under vacuum using a SP-Genevac EZ-2 4.0 concentrator. Dried polar extracts were dissolved in methanol to obtain a concentration of approximately 1125 µM, calculated to ensure that a 100 µL aliquot would yield a final amino acid concentration of around 150 µM upon dilution in the NMR tube. This dilution strategy was specifically designed to maintain a total amino acid concentration below 150 µM, thereby minimising potential competitive interactions among amino acids for binding to the catalyst complex. Such competition could otherwise impair quantification accuracy due to differences in binding affinities.

100 µL of tissue extract in methanol was transferred to a vial containing the other reagents needed for the diastereoisomeric complexes formation to have a final concentration of 500 µM Ir-IMes catalyst precursor, 9 mM *S*-nicotine, 10 mM piperidine buffer, 10 µM of each (R)-(+)-α-methylvaline and α-aminoisobutyric acid as internal references for a total volume of 750 µL MeOH/H_2O with 5.4% water content (v/v). The mixture was then vortexed and centrifuged for 5 minutes at 13000

rpm. Subsequently, a sample aliquot of 700 µL was transferred to a Wilmad® quick pressure valve (QPV) NMR tube with 5 mm diameter.

As a quality control measure, nhPHIP samples containing all constituents except tissue extracts were prepared and analyzed as described to assess background signal levels and exclude cross-contamination between successive experiments. To further ensure data integrity, randomised sampling across different experimental groups was avoided.

4.8.3.2 Bubble setup for nhPHIP

The QPV NMR tube containing the sample was sealed with an in-house-built headpiece connected to three PEEK tubing lines. A tailored, in-house-designed hydrogen bubble setup enabled the steps required for complex formation and activation.

Firstly, the sample mixture was flushed with nitrogen to remove dissolved oxygen. Afterwards, *p*-H_2 (5 bar) was bubbled through the sample to activate the catalyst.

The NMR tube was then placed in a 50 °C water bath for 7.5 minutes while maintaining a pressure of 5 bar *p*-H_2, to simultaneously accelerate catalyst precursor activation and promote the attainment of thermodynamic equilibrium, favouring the nhPHIP-active binding mode of α-amino acids. Subsequently, the tube was cooled to 5 °C for 2 minutes and repressurised before transferring the sample to the NMR spectrometer, maintained at 10 °C. [47]

At the beginning of each nhPHIP-NMR transient, the solution was saturated with *p*-H_2 through a four-step process controlled by the spectrometer. First, the pressure inside the NMR tube was reduced from 5 to 4 bar via a relief valve connected to the vent line (0.25 s). Second, *p*-H_2 was bubbled through the solution, restoring the pressure to 5 bar (0.75–1.5 s). This was followed by a brief delay (ca. 300 ms) during which pressure was applied above the liquid surface ("back pressure") to stop bubbling that could interfere with the pulse sequence. Lastly, a final delay (0.7-1.0 s) is applied, allowing the sample to stabilise before the actual pulse sequence begins.

4.8.3.3 nhPHIP NMR acquisition and processing

All hydride nhPHIP NMR experiments were performed at 10 °C on a Bruker Avance III spectrometer operating at 600 MHz ^{1}H resonance frequency, with a HCN

triple-resonance cryo-cooled probe equipped with z-pulsed field gradients. Note that no ^{2}H lock was employed in the acquisition of nhPHIP spectra.

1D nhPHIP hydride signals were acquired with a spectral width of 9500 Hz over an acquisition time of 0.43 s, following 4 dummy scans and using 32 transients. The SEPP (Selective Excitation of Polarization using PASADENA) pulse scheme was employed, centered at approximately –26 ppm, with a total experiment duration of 2 minutes. [48, 49] A Lorentz-to-Gauss apodization function was applied prior to zero-filling to 32k points and Fourier transformation. Phase and baseline corrections were performed manually using nmrPipe.

2D zero-quantum (ZQ) nhPHIP hydride spectra were acquired over approximately 1 hour, with 2 transients per increment and 768 real increments. Spectral widths were set to 9500 Hz in the direct dimension and 2200 Hz in the indirect dimension. To reduce overall acquisition time, signal folding in the indirect dimension was employed. Data processing was performed using nmrPipe, applying Lorentz-to-Gauss apodization in both dimensions, followed by zero-filling to 2048 (t1) × 32768 (t2) points and Fourier transformation. Field drift correction was implemented by aligning the signal prior to the Fourier transformation in the indirect dimension. To suppress t1-noise in the 2D ZQ spectra, particularly near the most intense hydride signals, the method described by Wei *et al.* was applied. [50]

4.8.3.4 2D ZQ nhPHIP NMR spectra analysis

Well-resolved 2D peaks from the hydride region between –27.7 and –28.8 ppm were manually integrated in Topspin 4.4.1 to build the data matrix, which contained the intensity values of each amino acid in every sample.

4.8.4 Statistical analysis

NMR metabolomic data were analysed using both univariate and multivariate statistical approaches. Data matrices derived from nhPHIP-NMR 2D ZQ spectra analysis, were normalized by sum and scaled using the Pareto method. Univariate analysis was performed by combining Student's *t*-test and fold-change evaluation, visualised through Volcano plots. [51]

Subsequently, multivariate analysis was conducted using principal component analysis (PCA) and partial least squares discriminant analysis (PLS-DA) via

MetaboAnalyst 6.0 (http://www.metaboanalyst.ca). PCA was employed to reduce the dataset to a lower-dimensional feature space while preserving most of the variance, whereas PLS-DA was used to maximise separation between experimental groups. PCA performance was assessed using PERMANOVA, while the quality of the PLS-DA model was evaluated using the Q^2 coefficient (based on 5-fold internal cross-validation) and the R^2 coefficient, which represent the predictive and explained variance, respectively. [52]

Loading plots from the PLS-DA analysis were used to identify metabolites that contributed most to group separation, ranked by their variable importance in projection (VIP) scores. Pathway analysis was performed using the Enrichment tool in MetaboAnalyst. KEGG pathways were selected based on false discovery rate (FDR), p-value < 0.05, and a minimum of two metabolite hits per pathway.

Dysregulated biochemical pathways across CNS regions were compared using Venn diagrams generated with InteractiVenn. [53]

Bibliography

1. Hashimoto, A.; Oka, T., Free D-aspartate and D-serine in the mammalian brain and periphery. *Progress in neurobiology* **1997,** *52* (4), 325-353.
2. Coyle, J. T.; Balu, D.; Wolosker, H., D-serine, the shape-shifting NMDA receptor co-agonist. *Neurochemical research* **2020,** *45* (6), 1344-1353.
3. Wolosker, H., The neurobiology of d-serine signaling. *Advances in pharmacology* **2018,** *82*, 325-348.
4. Kondori, N. R.; Paul, P.; Robbins, J. P.; Liu, K.; Hildyard, J. C. W.; Wells, D. J.; De Belleroche, J. S., Focus on the role of D-serine and D-amino acid oxidase in amyotrophic lateral sclerosis/motor neuron disease (ALS). *Frontiers in molecular biosciences* **2018,** *5*, 8.
5. Lin, C.-H.; Lane, H.-Y.; Tsai, G. E., Glutamate signaling in the pathophysiology and therapy of schizophrenia. *Pharmacology Biochemistry and Behavior* **2012,** *100* (4), 665-677.
6. Durrant, A. R.; Heresco-Levy, U., d-serine in neuropsychiatric disorders: New advances. *Advances in Psychiatry* **2014,** *2014* (1), 859735.
7. Lin, C.-H.; Yang, H.-T.; Lane, H.-Y., D-glutamate, D-serine, and D-alanine differ in their roles in cognitive decline in patients with Alzheimer's disease or mild cognitive impairment. *Pharmacology Biochemistry and Behavior* **2019,** *185*, 172760.
8. Kim, P. M.; Duan, X.; Huang, A. S.; Liu, C. Y.; Ming, G.-l.; Song, H.; Snyder, S. H., Aspartate racemase, generating neuronal D-aspartate, regulates adult neurogenesis. *Proceedings of the National Academy of Sciences* **2010,** *107* (7), 3175-3179.
9. Matsuda, S.; Katane, M.; Maeda, K.; Kaneko, Y.; Saitoh, Y.; Miyamoto, T.; Sekine, M.; Homma, H., Biosynthesis of D-aspartate in mammals: the rat and human homologs of mouse aspartate racemase are not responsible for the biosynthesis of D-aspartate. *Amino acids* **2015,** *47* (5), 975-985.
10. Tanaka-Hayashi, A.; Hayashi, S.; Inoue, R.; Ito, T.; Konno, K.; Yoshida, T.; Watanabe, M.; Yoshimura, T.; Mori, H., Is d-aspartate produced by glutamic-oxaloacetic transaminase-1 like 1 (Got1l1): a putative aspartate racemase? *Amino acids* **2015,** *47* (1), 79-86.
11. Wolosker, H.; Sheth, K. N.; Takahashi, M.; Mothet, J.-P.; Brady Jr, R. O.; Ferris, C. D.; Snyder, S. H., Purification of serine racemase: biosynthesis of the neuromodulator D-serine. *Proceedings of the National Academy of Sciences* **1999,** *96* (2), 721-725.
12. Horio, M.; Ishima, T.; Fujita, Y.; Inoue, R.; Mori, H.; Hashimoto, K., Decreased levels of free D-aspartic acid in the forebrain of serine racemase (Srr) knock-out mice. *Neurochemistry international* **2013,** *62* (6), 843-847.
13. Ito, T.; Hayashida, M.; Kobayashi, S.; Muto, N.; Hayashi, A.; Yoshimura, T.; Mori, H., Serine racemase is involved in d-aspartate biosynthesis. *The journal of biochemistry* **2016,** *160* (6), 345-353.
14. D'Aniello, A.; Vetere, A.; Petrucelli, L., Further study on the specificity of D-amino acid oxidase and D-aspartate oxidase and time course for complete oxidation of D-amino acids. *Comparative biochemistry and physiology. B, Comparative biochemistry* **1993,** *105* (3-4), 731-734.
15. Molla, G.; Chaves-Sanjuan, A.; Savinelli, A.; Nardini, M.; Pollegioni, L., Structure and kinetic properties of human d-aspartate oxidase, the enzyme-controlling d-aspartate levels in brain. *The FASEB Journal* **2020,** *34* (1), 1182-1197.
16. Errico, F.; Napolitano, F.; Nistico, R.; Usiello, A., New insights on the role of free D-aspartate in the mammalian brain. *Amino acids* **2012,** *43* (5), 1861-1871.
17. Punzo, D.; Errico, F.; Cristino, L.; Sacchi, S.; Keller, S.; Belardo, C.; Luongo, L.; Nuzzo, T.; Imperatore, R.; Florio, E., Age-related changes in D-aspartate oxidase promoter methylation control extracellular D-aspartate levels and prevent precocious cell death during brain aging. *Journal of Neuroscience* **2016,** *36* (10), 3064-3078.
18. De Rosa, A.; Mastrostefano, F.; Di Maio, A.; Nuzzo, T.; Saitoh, Y.; Katane, M.; Isidori, A. M.; Caputo, V.; Marotta, P.; Falco, G., Prenatal expression of D-aspartate oxidase

causes early cerebral D-aspartate depletion and influences brain morphology and cognitive functions at adulthood. *Amino Acids* **2020,** *52* (4), 597-617.
19. Errico, F.; Pirro, M. T.; Affuso, A.; Spinelli, P.; De Felice, M.; D'Aniello, A.; Di Lauro, R., A physiological mechanism to regulate D-aspartic acid and NMDA levels in mammals revealed by D-aspartate oxidase deficient mice. *Gene* **2006,** *374*, 50-57.
20. Dunlop, D. S.; Neidle, A.; McHale, D.; Dunlop, D. M.; Lajtha, A., The presence of free D-aspartic acid in rodents and man. *Biochemical and biophysical research communications* **1986,** *141* (1), 27-32.
21. Fagg, G. E.; Matus, A., Selective association of N-methyl aspartate and quisqualate types of L-glutamate receptor with brain postsynaptic densities. *Proceedings of the National Academy of Sciences* **1984,** *81* (21), 6876-6880.
22. Errico, F.; Nisticò, R.; Palma, G.; Federici, M.; Affuso, A.; Brilli, E.; Topo, E.; Centonze, D.; Bernardi, G.; Bozzi, Y., Increased levels of d-aspartate in the hippocampus enhance LTP but do not facilitate cognitive flexibility. *Molecular and Cellular Neuroscience* **2008,** *37* (2), 236-246.
23. Krashia, P.; Ledonne, A.; Nobili, A.; Cordella, A.; Errico, F.; Usiello, A.; D'Amelio, M.; Mercuri, N. B.; Guatteo, E.; Carunchio, I., Persistent elevation of D-Aspartate enhances NMDA receptor-mediated responses in mouse substantia nigra pars compacta dopamine neurons. *Neuropharmacology* **2016,** *103*, 69-78.
24. Errico, F.; Nisticò, R.; Napolitano, F.; Oliva, A. B.; Romano, R.; Barbieri, F.; Florio, T.; Russo, C.; Mercuri, N. B.; Usiello, A., Persistent increase of D-aspartate in D-aspartate oxidase mutant mice induces a precocious hippocampal age-dependent synaptic plasticity and spatial memory decay. *Neurobiology of aging* **2011,** *32* (11), 2061-2074.
25. Molinaro, G.; Pietracupa, S.; Di Menna, L.; Pescatori, L.; Usiello, A.; Battaglia, G.; Nicoletti, F.; Bruno, V., D-aspartate activates mGlu receptors coupled to polyphosphoinositide hydrolysis in neonate rat brain slices. *Neuroscience letters* **2010,** *478* (3), 128-130.
26. Sacchi, S.; Novellis, V. D.; Paolone, G.; Nuzzo, T.; Iannotta, M.; Belardo, C.; Squillace, M.; Bolognesi, P.; Rosini, E.; Motta, Z., Olanzapine, but not clozapine, increases glutamate release in the prefrontal cortex of freely moving mice by inhibiting D-aspartate oxidase activity. *Scientific reports* **2017,** *7* (1), 46288.
27. Nakatsuka, S.; Hayashi, M.; Muroyama, A.; Otsuka, M.; Kozaki, S.; Yamada, H.; Moriyama, Y., D-Aspartate is stored in secretory granules and released through a Ca2+-dependent pathway in a subset of rat pheochromocytoma PC12 cells. *Journal of Biological Chemistry* **2001,** *276* (28), 26589-26596.
28. Davies, L. P.; Johnston, G. A. R., Uptake and release of D-and L-aspartate by rat brain slices. *Journal of neurochemistry* **1976,** *26* (5), 1007-1014.
29. Danbolt, N. C., Glutamate uptake. *Progress in neurobiology* **2001,** *65* (1), 1-105.
30. Cristino, L.; Luongo, L.; Squillace, M.; Paolone, G.; Mango, D.; Piccinin, S.; Zianni, E.; Imperatore, R.; Iannotta, M.; Longo, F., d-Aspartate oxidase influences glutamatergic system homeostasis in mammalian brain. *Neurobiology of aging* **2015,** *36* (5), 1890-1902.
31. Jansson, L. C.; Åkerman, K. E., The role of glutamate and its receptors in the proliferation, migration, differentiation and survival of neural progenitor cells. *Journal of neural transmission* **2014,** *121* (8), 819-836.
32. Komuro, H.; Rakic, P., Modulation of neuronal migration by NMDA receptors. *Science* **1993,** *260* (5104), 95-97.
33. Di Giorgi-Gerevini, V.; Melchiorri, D.; Battaglia, G.; Ricci-Vitiani, L.; Ciceroni, C.; Busceti, C. L.; Biagioni, F.; Iacovelli, L.; Canudas, A. M.; Parati, E., Endogenous activation of metabotropic glutamate receptors supports the proliferation and survival of neural progenitor cells. *Cell Death & Differentiation* **2005,** *12* (8), 1124-1133.
34. Grimaldi, M.; Marino, C.; Buonocore, M.; Santoro, A.; Sommella, E.; Merciai, F.; Salviati, E.; De Rosa, A.; Nuzzo, T.; Errico, F., Prenatal and early postnatal cerebral D-

aspartate depletion influences L-amino acid pathways, bioenergetic processes, and developmental brain metabolism. *Journal of Proteome Research* **2020,** *20* (1), 727-739.
35. Dreisewerd, L.; Aspers, R. L. E. G.; Feiters, M. C.; Rutjes, F. P. J. T.; Tessari, M., Nmr discrimination of d-and l-α-amino acids at submicromolar concentration via parahydrogen-induced hyperpolarization. *Journal of the American Chemical Society* **2023,** *145* (3), 1518-1523.
36. Andersson, E. R.; Bayless, A. L.; Brua, R. B.; Casu, F.; Cheng, L. L.; Choo, M.; Edison, A. S.; Eghbalnia, H. R.; Fleischer, C. C.; Gouveia, G. J., Securing the Future of NMR Metabolomics Reproducibility: A Call for Standardized Reporting. *Analytical Chemistry* **2025**.
37. Fraser, R.; Rutjes, F. P. J. T.; Feiters, M. C.; Tessari, M., Analysis of complex mixtures by chemosensing NMR using para-hydrogen-induced hyperpolarization. *Accounts of Chemical Research* **2022,** *55* (13), 1832-1844.
38. Posthumus, T. B.; Engelke, U. F. H.; Aspers, R. L. E. G.; Merx, J.; Boltje, T. J.; Martens, J.; Wevers, R. A.; Feiters, M. C.; Rutjes, F. P. J. T.; Tessari, M., Semi-Targeted Nuclear Magnetic Resonance Metabolomics via Parahydrogen-Induced Hyperpolarization for Enhanced Sensitivity to Metabolic Composition. *Journal of the American Chemical Society* **2025**.
39. Virarkar, M.; Alappat, L.; Bradford, P. G.; Awad, A. B., L-arginine and nitric oxide in CNS function and neurodegenerative diseases. *Critical reviews in food science and nutrition* **2013,** *53* (11), 1157-1167.
40. Carvalho, G. A.; Cavalcanti, D. P.; Parreira, R. C.; Chiareli, R. A.; Leoncini, G. O.; Gomez, R. S.; Ulrich, H.; Caixeta, L.; Oliveira-Lima, O. C.; Pinto, M. C. X., Neurobiology of L-proline: From molecules to behavior. *Neuroscience* **2025**.
41. Pampillo, M.; Scimonelli, T.; Bottino, M. C.; Duvilanski, B. H.; Rettori, V.; Seilicovich, A.; Lasaga, M., The effect of D-aspartate on luteinizing hormone-releasing hormone, α-melanocyte-stimulating hormone, GABA and dopamine release. *Neuroreport* **2002,** *13* (17), 2341-2344.
42. Ikeuchi, T.; Kanda, M.; Kitamura, H.; Morikawa, F.; Toru, S.; Nishimura, C.; Kasuga, K.; Tokutake, T.; Takahashi, T.; Kuroha, Y., Decreased circulating branched-chain amino acids are associated with development of Alzheimer's disease in elderly individuals with mild cognitive impairment. *Frontiers in Nutrition* **2022,** *9*, 1040476.
43. Hayflick, S. J., Defective pantothenate metabolism and neurodegeneration. *Biochemical Society Transactions* **2014,** *42* (4), 1063-1068.
44. Chiabrando, D.; Fiorito, V.; Petrillo, S.; Tolosano, E., Unraveling the role of heme in neurodegeneration. *Frontiers in neuroscience* **2018,** *12*, 712.
45. Kelly Iii, R. A.; Clavier, H.; Giudice, S.; Scott, N. M.; Stevens, E. D.; Bordner, J.; Samardjiev, I.; Hoff, C. D.; Cavallo, L.; Nolan, S. P., Determination of N-heterocyclic carbene (NHC) steric and electronic parameters using the [(NHC) Ir (CO) 2Cl] system. *Organometallics* **2008,** *27* (2), 202-210.
46. Beckonert, O.; Keun, H. C.; Ebbels, T. M. D.; Bundy, J.; Holmes, E.; Lindon, J. C.; Nicholson, J. K., Metabolic profiling, metabolomic and metabonomic procedures for NMR spectroscopy of urine, plasma, serum and tissue extracts. *Nature protocols* **2007,** *2* (11), 2692.
47. Sellies, L.; Aspers, R. L. E. G.; Feiters, M. C.; Rutjes, F. P. J. T.; Tessari, M., Parahydrogen hyperpolarization allows direct NMR detection of α-amino acids in complex (bio) mixtures. *Angewandte Chemie* **2021,** *133* (52), 27160-27165.
48. Sengstschmid, H.; Freeman, R.; Barkemeyer, J.; Bargon, J., A new excitation sequence to observe the PASADENA effect. *Journal of Magnetic Resonance, Series A* **1996,** *120* (2), 249-257.
49. Barkemeyer, J.; Bargon, J.; Sengstschmid, H.; Freeman, R., Heteronuclear polarization transfer using selective pulses during hydrogenation with parahydrogen. *Journal of Magnetic Resonance* **1996,** *120* (1), 129-132.
50. Wei, S.; Ding, Y.; Song, K.; Liu, Z., A robust t1 noise suppression method in NMR spectroscopy. *Magnetic Resonance in Chemistry* **2023,** *61* (8), 473-480.

51. Kumar, N.; Hoque, M. A.; Sugimoto, M. J. B. b., Robust volcano plot: identification of differential metabolites in the presence of outliers. **2018,** *19*, 1-11.
52. Pang, Z.; Lu, Y.; Zhou, G.; Hui, F.; Xu, L.; Viau, C.; Spigelman, Aliya F.; MacDonald, Patrick E.; Wishart, David S.; Li, S.; Xia, J., MetaboAnalyst 6.0: towards a unified platform for metabolomics data processing, analysis and interpretation. *Nucleic Acids Research* **2024,** *52* (W1), W398-W406.
53. Heberle, H.; Meirelles, G. V.; da Silva, F. R.; Telles, G. P.; Minghim, R., InteractiVenn: a web-based tool for the analysis of sets through Venn diagrams. *BMC bioinformatics* **2015,** *16* (1), 169.

General conclusions

This PhD thesis underscores the contemporary relevance of metabolomics – particularly NMR-based metabolomics – which remains the method of choice when an untargeted analytical approach is required. NMR spectroscopy offers several advantages, including straightforward sample preparation, inherent quantitative reliability, high reproducibility, non-destructive data acquisition, and non-selective detection of metabolites.

Owing to its untargeted nature, NMR metabolomics represents a powerful tool for investigating the biological mechanisms of action (MoA) of molecules within the framework of pharmacometabolomics and pharmacodynamics. By moving beyond traditional hypothesis-driven strategies, this approach provides a comprehensive and unbiased overview of treatment-induced metabolic changes, thereby enabling the discovery of unexpected or off-target effects.

Using this strategy, our analyses revealed the multifaceted activity of nicotine and its capacity to restore metabolic profiles toward those characteristic of a healthy phenotype. Nicotine effectively counteracted the broad metabolic dysregulation induced by Aβ(1–42), with principal effects observed in pathways related to neurotransmission, membrane stability, and energy metabolism. Similarly, using the same approach, our results demonstrate that NGF exerts neuroprotective effects by acting as an early modulator of Alzheimer's disease–related metabolic alterations, thereby reducing the cellular stress induced by amyloid toxicity.

These insights, which highlight the multitargeted mechanisms of action of the compounds under investigation, were achievable only through the untargeted metabolomic approach employed. With a single experiment, this methodology enables the characterization of complex biological responses without restricting the analysis to predefined pathways or individual molecular targets.

During my international research period, I further deepened my expertise in NMR spectroscopy by exploring emerging hyperpolarization techniques, particularly non-hydrogenative parahydrogen-induced hyperpolarization (nhPHIP). The work

presented in this thesis demonstrates the applicability of nhPHIP to various biological matrices, including tissue extracts, and its ability to resolve specific metabolic modulations that are otherwise difficult to detect. This targeted approach is especially valuable given the spectral overlap typical of conventional 1D ^{1}H NMR, which can obscure low-abundance but biologically relevant metabolites. Moreover, nhPHIP offers the unique advantage of providing information on the stereochemical configuration of metabolites – such as amino acids – when a chiral co-substrate is employed. This study represents the first metabolomic application of nhPHIP for chiral analysis, enabling the investigation of alterations in brain tissue with unprecedented detail.

Together with recent advances reported over the past five years, the research presented in this thesis may help pave the way for a new era in metabolomics – one characterized not only by increasingly sophisticated statistical tools, but also by technical innovations in sample preparation and NMR instrumentation.

In conclusion, this doctoral work highlights the potential of NMR metabolomics both for elucidating mechanisms of action and for advancing innovative analytical approaches such as nhPHIP, thereby opening new avenues for future applications in pharmacology and neuroscience.